

**ÉCOLE DOCTORALE DES SCIENCES CHIMIQUES**

**L'Institut de chimie et procédés pour l'énergie, l'environnement et la santé**

**THÈSE** présentée par :

**Qian JIANG**

soutenue le : **28 février 2017**

pour obtenir le grade de : **Docteur de l'université de Strasbourg**

Discipline/ Spécialité : Chimie / Catalyse hétérogène

**Synthèse directe de diméthyl éther  
à partir de CO<sub>2</sub>/H<sub>2</sub>**

**THÈSE dirigée par :**

**Mme ROGER Anne-Cécile** Professeur, ICPEES - Université de Strasbourg

**RAPPORTEURS :**

**M. PINARD Ludovic** Maître de conférences, IC2MP - Université de Poitiers

**Mme MASSIANI Pascale** Directeur de recherche, LRS - Institut des Matériaux de Paris Centre

**AUTRES MEMBRES DU JURY :**

**M. LOUIS Benoit** Directeur de recherche, LaSyROC - Université de Strasbourg

**MEMBRE INVITE :**

**Mme PARKHOMENKO Ksenia** Chargée de recherche, ICPEES - Université de Strasbourg  
Co-encadrante



## Acknowledgements

I would like to appreciate all the people I met and all the things I encountered, that's what makes me who I am now. I want to express my great gratitude to all the members who have helped me during my PhD period in ICPEES (Institut de chimie et procédés pour l'énergie, l'environnement et la santé). The China Scholarship Council (CSC) is greatly acknowledged for the financial supporting of my PhD study. It not only provides me the possibility to pursue my PhD degree in France but also gives me the chance to feel the different culture and different lifestyle.

I really want to express my great thanks to my supervisor Ksenia PARKHOMENKO. We work together from the very beginning-prepare the catalysts, make the setup under pressure, calibration for the micro-GC and so on. Before my PhD, I work on the DFT simulation and I don't have any experimental experience in the lab. Thanks to her kindness and enough patience, now I can work on some project on my own even start from building setups even though now I still have some shortcomings to overcome, such as procrastination, carelessness and not so concentrated sometimes. Her attitude to life is also impressive, always optimistic, smiling and very open-minded. Now I really inherit her spirit-enjoy life. I am also very grateful to professor Anne-Cécile ROGER who provides the research condition and also very good atmosphere in the group. Her smart mind and professional instructions are very impressive.

I would like to present my appreciation for Yvan Zimmermann and Marion Vgder for their help in building the setup and helping me solve the problems encountered in the lab. I also want to thank Sébastien Thomas, who is very kind and always ready to help others.

I would like to show my gratitude to Thierry Dintzer for the DFT calculations, Thierry Romero and Corinne Bouillet for the TEM characterization and Séou Sall for NH<sub>3</sub>-TPD.

I would like to thank my colleagues in our group, Laetitia, Kilian, Charlotte, Myriam, Qinqin, Marina, Dimitry, Francesca, Pauline, Valentin, Andrea. A lot of thanks for their

help and accompany. The communications and discussions make me know more about the world and form the habit to see the world or think the international affairs with diversified vision.

A lot of thanks for all my Chinese friends in Strasbourg for their accompany and help in my life, Tianyan, Nan, Jingjie, Yuefeng, Wen, Zhenxin, Wei, Yunjie, Yige, Tianyang, Quan, Shuai...

Above all, thanks to my parents and brother for their forever love and support.

# Content

<i>Résumé</i> .....	1
Chapter 1: Introduction.....	19
1.1 CO <sub>2</sub> utilization.....	21
1.2 DME synthesis from CO <sub>2</sub> /H <sub>2</sub> .....	24
1.3 Catalysts.....	26
1.3.1 Copper based catalyst.....	27
1.3.2 Methanol dehydration to DME catalyst.....	32
1.3.3 Bifunctional catalyst.....	37
1.4 Objectives of the thesis.....	42
1.5 References.....	44
Chapter 2: Experimental techniques.....	55
2.1 Catalysts characterization.....	57
2.1.1 N <sub>2</sub> adsorption/ desorption measurement.....	57
2.1.2 X-ray powder diffraction (XRD).....	57
2.1.3 Thermo-gravimetric analysis (TGA).....	58
2.1.4 Temperature programmed reduction (TPR).....	59
2.1.5 Temperature programmed desorption of NH <sub>3</sub> (NH <sub>3</sub> -TPD).....	60
2.1.6 Temperature programmed desorption of CO <sub>2</sub> (CO <sub>2</sub> -TPD).....	60
2.1.7 Temperature programmed desorption of N <sub>2</sub> O (N <sub>2</sub> O-TPD).....	61
2.1.8 Transmission electron microscopy (TEM).....	62
2.2 Catalytic tests.....	63
2.2.1 Methanol dehydration to DME.....	63
2.2.2 Direct DME synthesis from CO <sub>2</sub> /H <sub>2</sub> .....	67
2.3 References.....	72
Chapter 3: Al-TUD-1 as the catalyst of methanol dehydration to DME.....	75

3.1 Introduction .....	77
3.2 Catalysts preparation .....	77
3.3 Characterization results .....	78
3.3.1 Crystalline phase and morphology .....	78
3.3.2 Textural properties.....	79
3.3.3 Acid properties .....	81
3.4 Catalytic test: Methanol dehydration to DME .....	82
3.4.1 Pure methanol as reactant .....	83
3.4.2 Water/methanol mixture as reactant.....	84
3.5 Conclusions .....	85
3.6 References .....	86
Chapter 4: Bifunctional catalysts prepared by co-precipitation-deposition method.....	89
4.1 Introduction .....	91
4.2 Catalysts preparation .....	91
4.3 The influence of Si/Al ratio.....	94
4.3.1 Characterization.....	94
4.3.2 Catalytic tests.....	111
4.4 The influence of weight ratio between CZZ and Al-TUD-1.....	121
4.4.1 Characterization results .....	121
4.4.2 Direct DME synthesis.....	125
4.5 Conclusions and perspectives .....	127
4.6 References .....	129
Chapter 5: Optimization of the bifunctional catalysts .....	135
5.1 Introduction .....	137
5.2 Catalysts preparation .....	137
5.3 Characterizations and discussions.....	138
5.3.1 Textural properties.....	138
5.3.2 Crystalline structure.....	140
5.3.3 Redox properties.....	143
5.3.4 Basic properties .....	145
5.4 Catalytic results .....	146

5.4.1 Direct DME synthesis.....	146
5.4.2 Methanol dehydration to DME.....	154
5.5 Conclusions and perspectives .....	157
5.6 References .....	159
Chapter 6: General conclusions and perspectives.....	163



## Figures list

Figure 1- 1 Schematic diagram for the greenhouse gas effect.....	21
Figure 1-2 The CO <sub>2</sub> emissions percentages all over the world.....	22
Figure 1- 3 CO <sub>2</sub> applications.....	23
Figure 1-4 Schematic diagram for traditional DME synthesis .....	25
Figure 1- 5 Schematic diagram of the direct DME synthesis on a bifunctional catalyst..	26
Figure 1- 6 (a) Schematic representations of the necessary ingredients for a high-performance methanol synthesis catalyst (b) The role of precursor composition for the Cu dispersion in the final catalyst.....	28
Figure 1-7 CO <sub>2</sub> hydrogenation mechanisms on Cu-ZnO/ZrO <sub>2</sub> and Cu-ZnO/Al <sub>2</sub> O <sub>3</sub> catalysts.....	30
Figure 1-8 Methanol conversion variations for pure methanol and crude methanol.....	34
Figure 1-9 Proposed mechanisms for the formation of DME from methanol dehydration over the sulfated zirconia catalysts at low (pathway I) and high (pathway II) sulfur contents. ....	35
Figure 1-10 3-D TEM reconstruction of TUD-1 .....	36
Figure 1-11 Models for Brønsted and Lewis acid sites .....	37
Figure 1- 12 Schematic model of the variation of Cu species with increasing Si/Al ratio	40
Figure 1-13 TPO profiles of the CuO-ZnO-Al <sub>2</sub> O <sub>3</sub> / $\gamma$ -Al <sub>2</sub> O <sub>3</sub> catalyst after direct DME synthesis.....	41
Figure 1-14 Thesis schematic flow-chart.....	43
Figure 2- 1 Bragg's Law reflection .....	58
Figure 2- 2 N <sub>2</sub> O-TPD profile .....	62
Figure 2- 3 Scheme of the methanol dehydration to DME reaction setup.....	63
Figure 2- 4 Scheme of setup for direct DME synthesis from CO <sub>2</sub> /H <sub>2</sub> .....	68

Figure 3- 1 Catalysts after hydrothermal treatment (a) and after calcination (b) .....	78
Figure 3- 2 XRD patterns of Al-TUD-1 .....	79
Figure 3- 3 TEM image for Si/Al-25 .....	79
Figure 3- 4 N <sub>2</sub> adsorption/ desorption isotherm (a) and pore distribution (b) of Al-TUD-1 .....	80
Figure 3- 5 NH <sub>3</sub> desorption profiles for Al-TUD-1 .....	81
Figure 3- 6 Methanol conversion for Al-TUD-1 .....	83
Figure 3- 7 Catalytic results for Si/Al-25 .....	84
Figure 4- 1 Diagrams for CZZ synthesis by co-precipitation method .....	92
Figure 4- 2 Precursors after drying (a) and catalyst after calcination at 400 °C (b).....	93
Figure 4- 3 N <sub>2</sub> adsorption/ desorption isotherms and pore distribution for CZZ (a), isotherms (b) and pore distributions (c) for bifunctional catalysts .....	95
Figure 4- 4 XRD patterns of fresh (a) and reduced (b) CZZ and bifunctional catalysts CZZ-Si/Al .....	97
Figure 4- 5 TPR profiles for the CZZ and the bifunctional catalysts .....	99
Figure 4- 6 TGA profiles of CZZ and of CZZ-Si/Al-25 .....	102
Figure 4- 7 CO <sub>2</sub> profile from CZZ-Si/Al-25 TGA analysis .....	103
Figure 4- 8 NH <sub>3</sub> -TPD profiles of the bifunctional catalysts .....	104
Figure 4- 9 CO <sub>2</sub> -TPD profiles for CZZ and CZZ-Si/Al-25 .....	105
Figure 4-10 The TEM images of the fresh Al-TUD-1 (a), CZZ-Si/Al-25 (b) and CZZ- Si/Al-100 (c) .....	106
Figure 4- 11 TEM for the reduced CZZ-Si/Al-25 (a) and CZZ-Si/Al-50 (b).....	107
Figure 4- 12 Models for copper (a), pure SiO <sub>2</sub> (b) and Al doped SiO <sub>2</sub> (c).....	108
Figure 4- 13 Different adsorption sites of copper on SiO <sub>2</sub> , top site (a), bridge site (b) and hollow site (c) .....	109
Figure 4- 14 Energies of Cu-SiO <sub>2</sub> (a) and Cu-Al-SiO <sub>2</sub> (b) with cutoff energy of 700 eV (top adsorption configurations).....	110
Figure 4- 15 Methanol conversion (a) and products selectivity (b) for CZZ catalyst ....	113
Figure 4- 16 Methanol conversion (a) and products selectivity (b, c, d) for bifunctional catalysts.....	115

Figure 4- 17 Thermodynamic simulation results for direct DME synthesis from CO <sub>2</sub> /H <sub>2</sub> .....	117
Figure 4- 18 Direct DME synthesis results of bifunctional catalysts .....	119
Figure 4-19 N <sub>2</sub> adsorption-desorption isotherms (a),and pore distribution (b) for bifunctional catalysts .....	122
Figure 4-20 XRD patterns of calcined (a) and reduced (b) (280 °C, 1 °C/min, 50 mL/min 10% H <sub>2</sub> /Ar bifunctional catalysts CZZ-Si/Al with different weight ratio between CZZ and Si-Al.....	123
Figure 4- 21 TPR patterns for bifunctional catalysts .....	124
Figure 4-22 Direct DME synthesis results of bifunctional catalysts CZZ-Si/Al-25 (7:3), CZZ-Si/Al-25 (5:3) and CZZ-Si/Al-25 (1:1).....	126
Figure 5- 1 Schematic diagram of bifunctional catalysts.....	138
Figure 5- 2 N <sub>2</sub> adsorption/desorption isotherms (a) and pore distribution (b) for the bifunctional catalysts <b>cs</b> , <b>pd</b> and <b>m</b> .....	139
Figure 5- 3 XRD patterns for CZZ and calcined bifunctional catalysts. ....	140
Figure 5- 4 XRD patterns for reduced bifunctional catalysts .....	143
Figure 5- 5 H <sub>2</sub> -TPR profiles.....	144
Figure 5- 6 CO <sub>2</sub> -TPD profiles for the catalysts <b>cs</b> , <b>pd</b> and <b>m</b> .....	145
Figure 5- 7 CO <sub>2</sub> (a) and H <sub>2</sub> conversion (b) .....	147
Figure 5- 8 Schematic diagram of the reduced catalyst <b>cs</b> .....	148
Figure 5- 9 Methanol (a), CO (b) and DME (c) selectivity .....	149
Figure 5- 10 Methanol (a) and DME (b) productivity .....	151
Figure 5- 11 Methanol conversion.....	154
Figure 5- 12 DME selectivity (a), methyl formate selectivity (b) and CO + CO <sub>2</sub> selectivity (c) over the bifunctional catalysts <b>pd</b> , <b>m</b> and <b>cs</b> .....	155
Figure 6- 1 Schematic diagram of a membrane reactor.....	166



## Tables list

Table 1- 1 Physical properties of DME .....	24
Table 1- 2 Effect of different feed on coke formation over Al-HMS-10 after 72h .....	34
Table 2- 1 Response factors .....	66
Table 2- 2 Temperature and pressure for columns and retention times and response factors for different compounds on each column .....	70
Table 3- 1 Textural properties of Al-TUD-1 .....	80
Table 3- 2 Acid properties of Al-TUD-1 from NH <sub>3</sub> -TPD .....	82
Table 4- 1 Catalysts list.....	93
Table 4- 2 Textural properties of catalysts .....	96
Table 4- 3 Copper crystallite sizes in the reduced bifunctional catalysts CZZ-Si/Al.....	98
Table 4- 4 Reducibility of the pure CZZ and the bifunctional catalysts.....	100
Table 4- 5 Copper surface area and dispersion.....	101
Table 4- 6 Surface acid sites properties of bifunctional catalysts.....	104
Table 4- 7 Adsorption energies for Cu-SiO <sub>2</sub> and Cu-Al-SiO <sub>2</sub> (Cu in top site).....	110
Table 4- 8 Catalytic results of direct DME synthesis from CO <sub>2</sub> /H <sub>2</sub> over pure CZZ catalyst (50 bars) and bifunctional catalyst CZZ-Si/Al-25 (50 bars and 20 bars) .....	120
Table 4-9 Physicochemical properties of catalysts .....	122
Table 4- 10 Metallic copper crystallite size in the reduced bifunctional catalysts .....	123
Table 4- 11 copper reducibility, copper surface area and copper dispersion of bifunctional catalysts.....	125
Table 5- 1 Textural properties of bifunctional catalysts .....	140
Table 5- 2 Ratio of intensities of characteristic peak of ZnO and CuO.....	141

Table 5- 3 CuO and ZnOcrystallite size of calcined bifunctional catalysts.....	142
Table 5- 4 Reducibility of the bifunctional catalysts prepared by different methods.....	145
Table 5- 5 The comparison of reported and the bench-marking of obtained catalytic results .....	153

## *R é s u m é*

### **1. Introduction**

Le haut niveau d'attention est concentré aujourd'hui sur l'amélioration de l'environnement par la réduction des émissions de gaz à effet de serre [1] et sur la recherche des carburants alternatifs [2, 3]. Depuis le début de 2000, le diméthylether (DME) est considéré comme un biocarburant prometteur et comme une alternative pour plusieurs applications énergétiques. Le DME trouve de nombreuses applications telles que un remplaçant du diesel dans les transports, une alternative au méthane dans les turbines à gaz, un complément au GPL (gaz de pétrole liquéfié) pour le gaz domestique et un vecteur pour le stockage de l'énergie [4, 5]. En outre, il est également un intermédiaire important pour la synthèse de produits chimiques couramment utilisés [6].

La synthèse classique de DME est un procédé en deux étapes [7], la 1<sup>ère</sup> étape est la synthèse du méthanol à partir de gaz de synthèse ( $\text{CO}/\text{CO}_2/\text{H}_2$ ) sur les catalyseurs à base de cuivre [5] et la 2<sup>ème</sup> étape est la déshydratation du méthanol en DME sur des catalyseurs acides solides [3]. Dans ce travail, la synthèse directe de DME à partir de l'hydrogénation du dioxyde de carbone est thermodynamiquement favorable et économique par rapport à la voie traditionnelle [4, 8]. Cette réaction directe nécessite la présence d'un catalyseur bifonctionnel combinant un catalyseur à base de cuivre et un catalyseur acide solide.

**Cu-ZnO-ZrO<sub>2</sub>** (CZZ) a été choisi comme le **catalyseur de synthèse du méthanol** en raison de la bonne performance dans la synthèse de méthanol à partir du dioxyde de carbone, qui est basé sur les travaux antérieurs du groupe [9, 10]. Le cuivre métallique fournit les sites actifs pour la dissociation de  $\text{H}_2$  et les oxydes ZnO et ZrO<sub>2</sub> sont importants pour l'adsorption et l'activation du  $\text{CO}_2$ , en plus ZnO joue le rôle d'une entretoise physique et a un effet favorable sur le comportement de frittage de cuivre [11].  $\gamma\text{-Al}_2\text{O}_3$  et HZSM-5 sont les matériaux les plus fréquemment étudiés pour la réaction de déshydratation du méthanol à l'échelle du laboratoire, ainsi que dans l'industrie, alors que ces deux composés montrent quelques inconvénients [12]. Dans notre travail, **Al-TUD-1**, un matériau mésoporeux amorphe à base de silice avec l'incorporation d'aluminium,

possédant grande surface et des pores modifiables tout comme son acidité a été choisi en tant que **catalyseur de déshydratation du méthanol**.

Le but de ce travail de thèse est la préparation de **systèmes catalytiques bifonctionnels** par différentes méthodes et une étude plus approfondie de leur comportement catalytique dans la synthèse directe du DME. Les catalyseurs bifonctionnels sont constitués de Cu-ZnO-ZrO<sub>2</sub> et Al-TUD-1, la teneur en cuivre métallique dans le Cu-ZnO-ZrO<sub>2</sub> est de 30% en poids, le rapport Si/Al dans Al-TUD-1 ainsi que le rapport entre les deux fonctions catalytiques seront modifiés.

## **2. Résultats et discussions**

Dans un premier temps, Al-TUD-1 avec différents rapports Si/Al a été préparé pour étudier l'influence de l'acidité dans la performance de déshydratation du méthanol. Puis, dans un second temps, les matériaux bifonctionnels Cu-ZnO-ZrO<sub>2</sub> @ Al-TUD-1 ont été préparés par un procédé de dépôt de co-précipitation, où Al-TUD-1 eu des rapports Si/Al différents. Leur comportement catalytique dans la déshydratation du méthanol et la synthèse directe du DME a été étudié. Dans le dernier temps, les matériaux bifonctionnels Cu-ZnO-ZrO<sub>2</sub> @ Al-TUD-1 ont été préparés par d'autres méthodes telles que le mélange physique et la méthode 'core-shell', et leur performance catalytique dans la synthèse directe de DME a été comparée à la méthode de co-précipitation.

### 2.1. Al-TUD-1 pour la déshydratation du méthanol en DME

Une série d'Al-TUD-1 avec différents rapports Si/Al = 25, 50, 75 et 100, ont été synthétisés par le procédé sol-gel [13]. Différentes méthodes de caractérisation ont été utilisées pour l'analyse des matériaux, telles que DRX (diffraction des rayons X), méthode d'adsorption/désorption de N<sub>2</sub>, TPD-NH<sub>3</sub> (désorption programmée température d'NH<sub>3</sub>) et MET (microscopie électronique à transmission). L'influence du rapport Si/Al sur l'activité dans la réaction de déshydratation du méthanol a été étudiée.

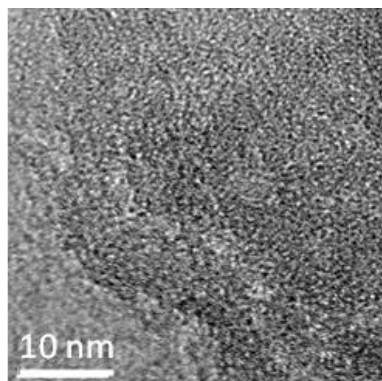
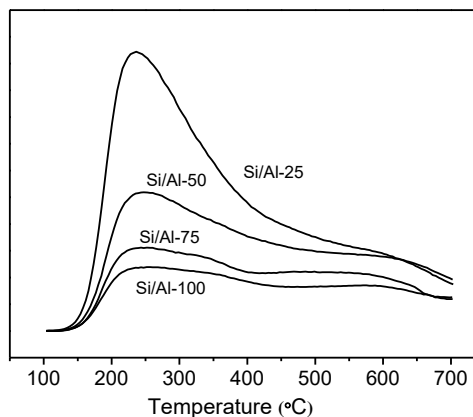


Fig.1 Image MET de Si/Al-25

Fig.2 Profils NH<sub>3</sub>-TPD d'Al-TUD-1

Ces matériaux sont amorphes et possèdent une structure d'une éponge. Ils montrent un seul pic à  $22^\circ$  dans le profil de DRX qui correspond à  $\text{SiO}_2$  amorphe [14, 15]. La morphologie amorphe avec de vastes pores vermiformes observés par MET (Fig.1) était conforme aux résultats de la DRX. Les matériaux Al-TUD-1 possèdent une répartition des pores de 3 à 7 nm avec les grandes surfaces spécifiques de  $610\text{-}804\text{ m}^2\text{g}^{-1}$ .

La propriété acide est le principal facteur de la réaction de déshydratation du méthanol pour former le DME. Les résultats de TPD-NH<sub>3</sub> (Fig.2) montrent que les quantités de sites acides augmentent avec la diminution du rapport Si/Al, qui est compatible avec le travail de Hanefeld [13]. Le NH<sub>3</sub> a été dans la plupart du temps désorbé en dessous de  $400^\circ\text{C}$ , ce qui signifie que la plus grande partie des sites acides sont de forces faibles et moyennes. Selon les travaux [8], les sites acides forts peuvent non seulement convertir le méthanol en DME, mais aussi produire davantage d'alcanes et d'oléfines. Cela montre que l'Al-TUD-1 avec le rapport de Si/Al = 25 ayant pour la plupart des sites acides avec faibles et moyens forces devrait être le plus actif dans la déshydratation du méthanol pour la synthèse de DME dans cette famille des matériaux.

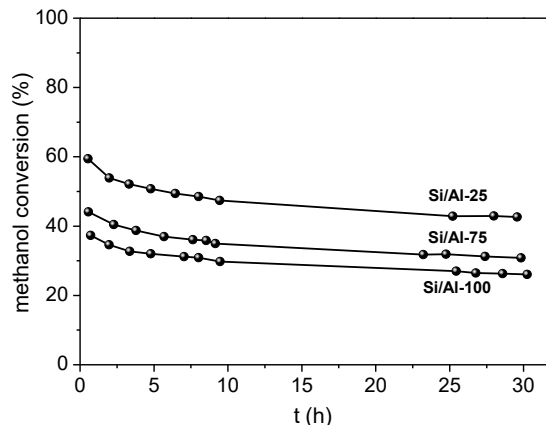


Fig.3 Conversion du méthanol sur Al-TUD-1

La déshydratation du méthanol pour la formation de DME a été réalisée dans un réacteur en quartz à lit fixe à la pression atmosphérique à 280 °C, et à VVH (vitesse volumétrique horaire) de 10000 h<sup>-1</sup>. On peut constater que la conversion du méthanol diminue avec le rapport Si/Al (Fig.3), ce qui correspond à la tendance de l'acidité mesurée par TPD-NH<sub>3</sub>. Le DME est le seul produit carboné formé lors de la déshydratation du méthanol, ce qui signifie que les sites acides faibles et moyens sont dominants. La conversion du méthanol diminue au début et devient presque constante après un temps de réaction de 24h. La désactivation des catalyseurs peut être provoquée par l'adsorption de l'eau qui est formé au cours du procédé sur les sites acides. Pour prouver cette supposition, des tests avec des quantités d'eau supplémentaires ont été effectués dans les mêmes conditions de réaction.

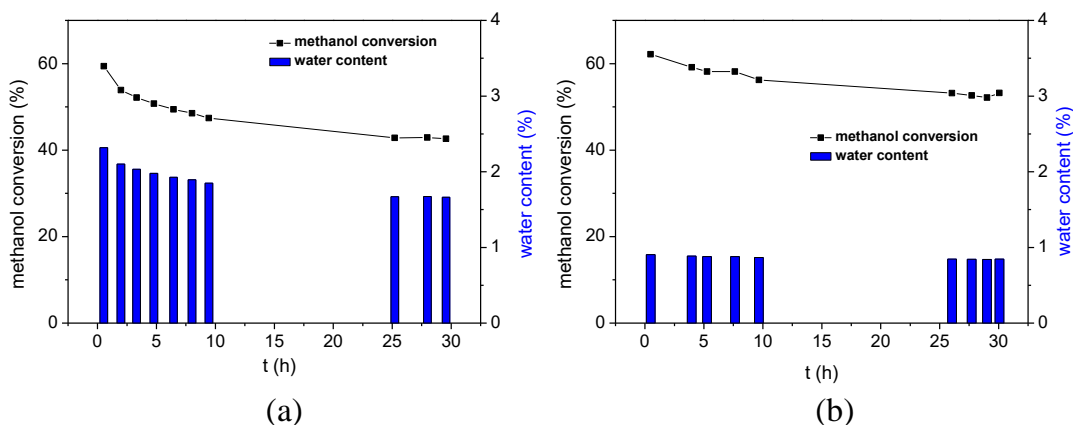


Fig.4 Résultats catalytiques pour Si/Al-25

La réaction de déshydratation du méthanol a été réalisée sur Si/Al-25 avec du méthanol (Fig.4a) et le mélange ( $n_{\text{methanol}}:n_{\text{water}}=1:5$ ) (Fig.4b). La conversion du méthanol et la teneur en eau dans la phase gazeuse ont été présentés dans le Fig.4. La conversion du méthanol devient constante après 24 h, la sélectivité en DME est de 100% dans les deux cas. On peut voir sur la Fig.4 que plus la teneur en eau est faible plus conversion du méthanol est stable et grande.

A partir des résultats catalytiques, on peut conclure que la conversion du méthanol diminue avec le rapport Si/Al et la présence de l'eau dégrade les performances catalytiques dans la réaction de déshydratation du méthanol.

## 2.2 Catalyseurs bifonctionnels préparés par la méthode de dépôt-co-précipitation

Dans cette partie, les catalyseurs bifonctionnels CZZ-Si/Al (Cu-ZnO-ZrO<sub>2</sub>@Al-TUD-1) ont été préparés par la méthode de dépôt de co-précipitation. Le catalyseur contenant du cuivre a été déposé sur le Al-TUD-1. Quatre catalyseurs bifonctionnels ont été préparés avec différents rapports Si/Al et avec le même rapport en poids entre le catalyseur de synthèse de méthanol et le catalyseur de déshydratation du méthanol (Cu-ZnO-ZrO<sub>2</sub>:Al-TUD-1 =7:3). En outre, deux autres catalyseurs bifonctionnels avec les rapports en poids différents ont été synthétisés, 5: 3 et 1: 1, respectivement. Ces catalyseurs ont été caractérisés par méthode d'adsorption/ désorption de N<sub>2</sub>, DRX, TPR (réduction programmée température), TPD-NH<sub>3</sub>, TPD-N<sub>2</sub>O (désorption programmée température d' N<sub>2</sub>O) et MET.

Table 1. Propriétés texturales et surface métallique de Cu des catalyseurs

Échantillon	S <sub>BET</sub> (m <sup>2</sup> g <sup>-1</sup> )	V <sub>pore</sub> (cm <sup>3</sup> g <sup>-1</sup> )	D <sub>p</sub> (nm)	surface Cu <sup>0</sup> (m <sup>2</sup> g <sub>cat</sub> <sup>-1</sup> )	taille de particules de Cu <sup>0</sup> (nm)
1 CZZ	76	0.36	31.5	13.9	-
2 CZZ-Si/Al-25	161	0.71	5.6, 50.9	10.3	5.6
3 CZZ-Si/Al-50	162	0.51	6.5, 47.2	5.8	4.7
4 CZZ-Si/Al-75	203	0.72	4.9, 49.1	<4	5.1
5 CZZ-Si/Al-100	161	0.70	6.5, 52.6	<4	4.9
6 CZZ-Si/Al-25 (5:3)	225	0.92	6.5, 32.9	6.1	5.4
7 CZZ-Si/Al-25 (1:1)	315	1.04	6.5, 32.9	<4	4.8

Les r éultats BET montrent que les catalyseurs bifonctionnels ont deux types de pores, environ 6 nm et 50 nm, ce qui est dû au support et au d épôt de catalyseurs au cuivre, respectivement. La surface sp écifique varie de 161 à 203 m<sup>2</sup>g<sup>-1</sup> (Table1).

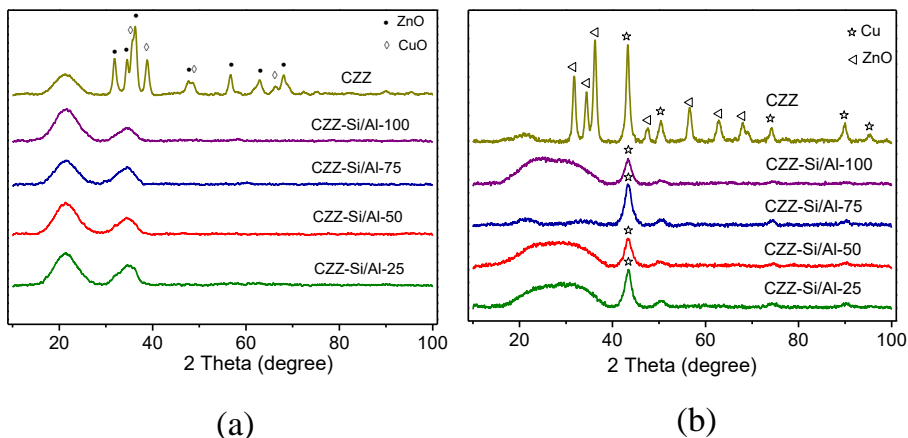


Fig.5 Profils DRX de catalyseurs bifonctionnels avant (a) et apr ès r éduction (b)

Catalyseurs bifonctionnels possèdent une structure amorphe vue sur le DRX (Fig.5a). Elle peut également être reconnue que le chevauchement des pics élargies de CuO et de ZnO conduit à la formation du pic amorphe dans la plage de 30° à 40° 2θ, ce qui signifie probablement une bonne dispersion et la taille des particules de CZZ sur Al-TUD-1 très petite. La surface de cuivre métallique n'est pas améliorée en supportant le composant CZZ sur Al-TUD-1. Elle augmente alors que le rapport Si/Al diminue, la meilleure surface de cuivre a été obtenue pour un matériau bifonctionnel CZZ-Si/Al-25 et est égale à 10.3 m<sup>2</sup>g<sub>cata</sub><sup>-1</sup> (Table 1). Les particules métalliques de Cu pour les catalyseurs réduits sont environ de 5 nm - résultats de DRX (Fig.5b), ce qui est conforme aux résultats de MET d'échantillons réduits (Fig.6)

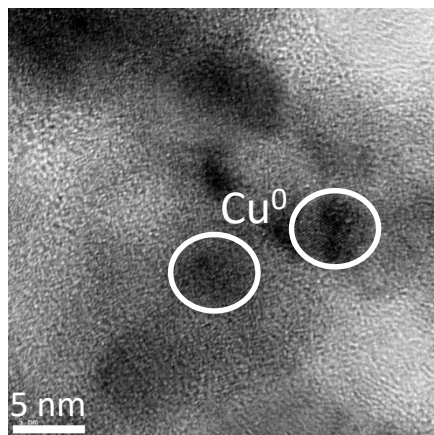


Fig.6 MET de CZZ-Si/Al-25 (réduction 280°C 1h)

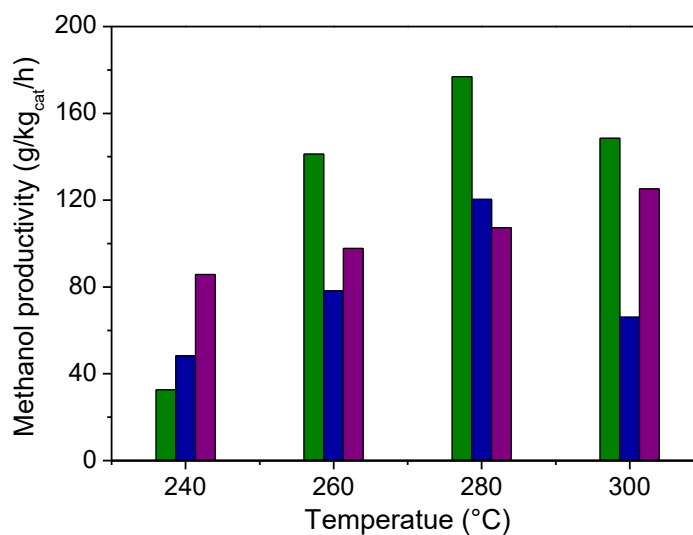


Fig.7 Productivité en méthanol sur les catalyseurs CZZ-Si/Al-25 (7:3) (olive), CZZ-Si/Al-75 (7:3) (bleu) et CZZ-Si/Al-100 (7:3) (voilet)

La synthèse directe de DME à partir de  $\text{CO}_2$  et  $\text{H}_2$  a été réalisée dans un réacteur à lit fixe sous pression (20 bar), la température varie de 240 à 300 °C et le VVH (vitesse volumétrique horaire) est de  $10000 \text{ h}^{-1}$ . Les résultats des tests catalytiques (Fig. 7) montrent que la conversion du  $\text{CO}_2$  augmente avec la température et la sélectivité du DME diminue avec la température qui montre la même tendance avec les résultats de la simulation thermodynamique. En comparant la productivité en méthanol de catalyseurs CZZ-Si/Al-25 (7:3), CZZ-Si/Al-75 (7:3) et CZZ-Si/Al-100 (7:3) (Fig.7), on voit

clairement que CZZ-Si/Al-25 (7:3) montre des valeurs plus élevée à 260-280-300 °C, probablement du à la plus grande surface métallique du cuivre. La sélectivité du DME est inférieure à 1% pour les trois catalyseurs probablement dû au blocage ou non-accessibilité des sites acides.

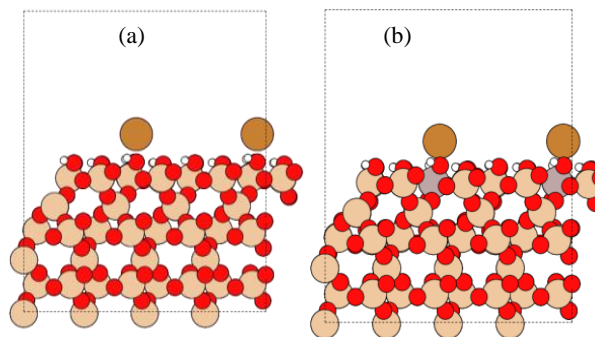


Fig.8 Top adsorption configuration of copper on pure SiO<sub>2</sub> (a) and Al-doped SiO<sub>2</sub> (b)

Compte tenu de l'influence du rapport Si/Al de cuivre sur la surface métallique de Cu, la théorie fonctionnelle de densité (DFT) a été utilisée pour étudier l'interaction entre le Cu et le support au niveau moléculaire. Le cuivre a été simplifié comme un atome de cuivre. La silice pure a été modélisée sous une forme amorphe  $\alpha$ -SiO<sub>2</sub>, qui a été saturé avec une groupe hydroxyle sur la surface (1 0 0) selon le modèle Zhuravlev [16], avec une hauteur de vide de 10 Å pour éviter l'interaction entre les différentes couches périodiques [17]. Al-TUD-1 a été modélisée comme la silice dopée par Al, à savoir que les cations tétravalents de silice ont été remplacés par des cations Al trivalents [18]. Les propriétés d'adsorption du cuivre sur de la silice pure et de la silice dopée avec Al (Fig.8) ont été calculées. Trois sites d'adsorption différents ont été pris en compte dans nos calculs, en position 'top' (sur le dessus d'un atome d'oxygène), le site du pont (sur le dessus d'un pont O-O) et le site creux (au centre entre trois atomes d'oxygène), respectivement. Les résultats montrent que la position 'top' est le site d'adsorption de cuivre la plus stable pour les deux supports. L'énergie d'adsorption pour sur SiO<sub>2</sub> dopée avec Al est -2.6012 eV, ce qui est beaucoup plus élevée que l'énergie d'adsorption du cuivre pour SiO<sub>2</sub> pure -0.2617 eV. Ca nous indique que lors de synthèse du dépôt de co-précipitation l'ancrage de Cu sur les sites d'Al est observé. En outre, on peut supposer que ça explique aussi que la surface métallique de cuivre augmente avec la diminution du rapport Si/Al.

Pour améliorer la sélectivité du DME, le rapport en poids du catalyseur de déshydratation du méthanol Al-TUD-1 a été augmenté (Table 1, échantillons 6 et 7). Les résultats BET montrent que la surface spécifique augmente à 225-315 m<sup>2</sup>g<sup>-1</sup> et ils montrent aussi deux types de pores (Table 1). La taille de particules métalliques de cuivre varie de 4.8 nm à 5.6 nm. La surface spécifique du cuivre diminue quand la teneur en cuivre diminue (une plus petite quantité de cuivre est présent dans le matériau). Les résultats catalytiques pour la réaction de synthèse directe de DME sont présentés dans Fig. 9. On constate que la conversion d'CO<sub>2</sub> diminue avec la diminution du rapport entre les deux fonctions de catalyseur bifonctionnel, qui peut être reliée à la diminution des sites actifs de cuivre dans le système catalytique global bifonctionnel. La productivité en méthanol a la même tendance. Même après l'augmentation du rapport en poids de catalyseur acide, la sélectivité du DME est toujours inférieure à 1.5%, tandis que la conversion du méthanol pour Si/Al-25 pur est de 40% après 30h dans la réaction de déshydratation du méthanol en DME (résultats de 2.1), ce qui signifie que en dehors de l'influence négative de l'eau, une autre raison de la faible sélectivité DME se produit. D'après les calculs DFT on suppose que la couverture des sites acides d'Al-TUD-1 par le cuivre métallique est en cause.

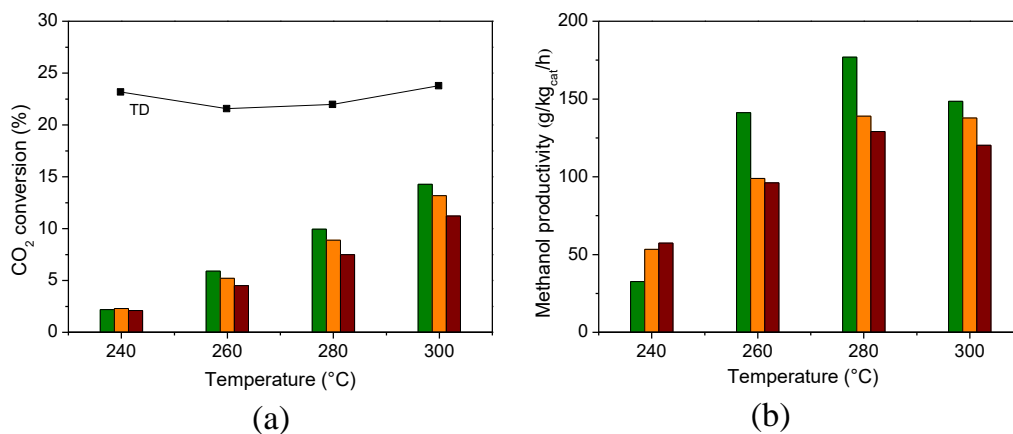


Fig.9 Conversion d'CO<sub>2</sub> (a) et productivité en méthanol (b) pour le synthèse directe de DME pour des catalyseurs CZZ-Si/Al-25 (7:3) (olive), CZZ-Si/Al-25 (5:3) (orange) and CZZ-Si/Al-25 (3:3) (vin rouge)

Pour les catalyseurs bifonctionnels préparés par un procédé de dépôt de co-précipitation, le cuivre a été bien dispersé avec la taille des particules de cuivre métallique autour de 5 nm et surface métallique de cuivre importante pour les petits

rappports Si/Al. L'énergie d'adsorption du cuivre trouv ée par DFT sur SiO<sub>2</sub> dop é avec Al éait plus élev ée que sur SiO<sub>2</sub> pur. Ca implique que l'incorporation d'Al peut induire l'ancrage du cuivre près d'Al et le blocage de ce site acide. L'activité catalytique augmente avec l'augmentation de la teneur en Al.

### 2.3 Catalyseurs bifonctionnels préparés par différentes méthodes

Afin d'améliorer le catalyseur bifonctionnel pour la synthèse directe de DME, deux autres méthodes de préparation, core-shell et mélange physique, ont été explorées dans cette partie. Tous les catalyseurs ont été préparés avec le même rapport en poids de deux fonctions (1:1). Méthode d'adsorption/désorption de N<sub>2</sub>, DRX, TPR, TPD- NH<sub>3</sub>, TPD-N<sub>2</sub>O et MET ont été employées pour la caractérisation des catalyseurs. Les schémas des trois catalyseurs préparés par des méthodes différentes sont présentés dans Fig.10.

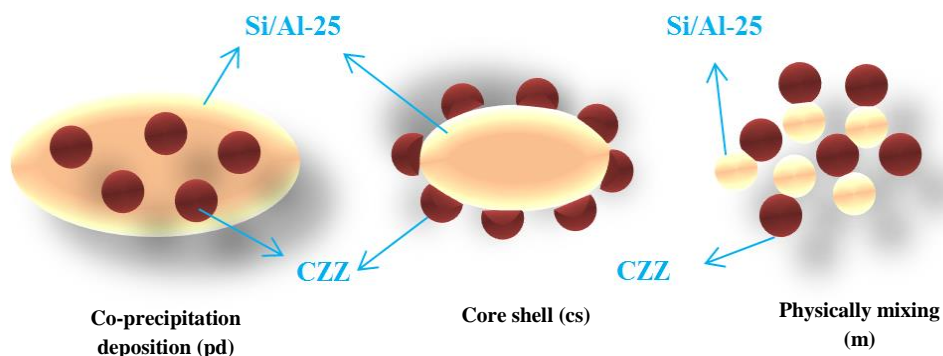


Fig.10 Catalyseurs bifonctionnels

Table 2 Taille des particules (résultats DRX)

Échantillon	Taille (nm)	
	CuO	ZnO
<b>cs</b>	15.0	8.9
<b>pd</b>	4.8 [Cu <sup>0</sup> ]	-
<b>m</b>	9.0	10.0

Parmi les 3 catalyseurs, le catalyseur préparé par le procédé de dépôt de co-précipitation a été décrit en 2.2. Les autres catalyseurs présentent les raies de CuO et ZnO sur DRX. La taille des particules de CuO avec le procédé de mélange physique (9.0 nm) est plus petite que la méthode core-shell (15.0 nm) (Table 2).

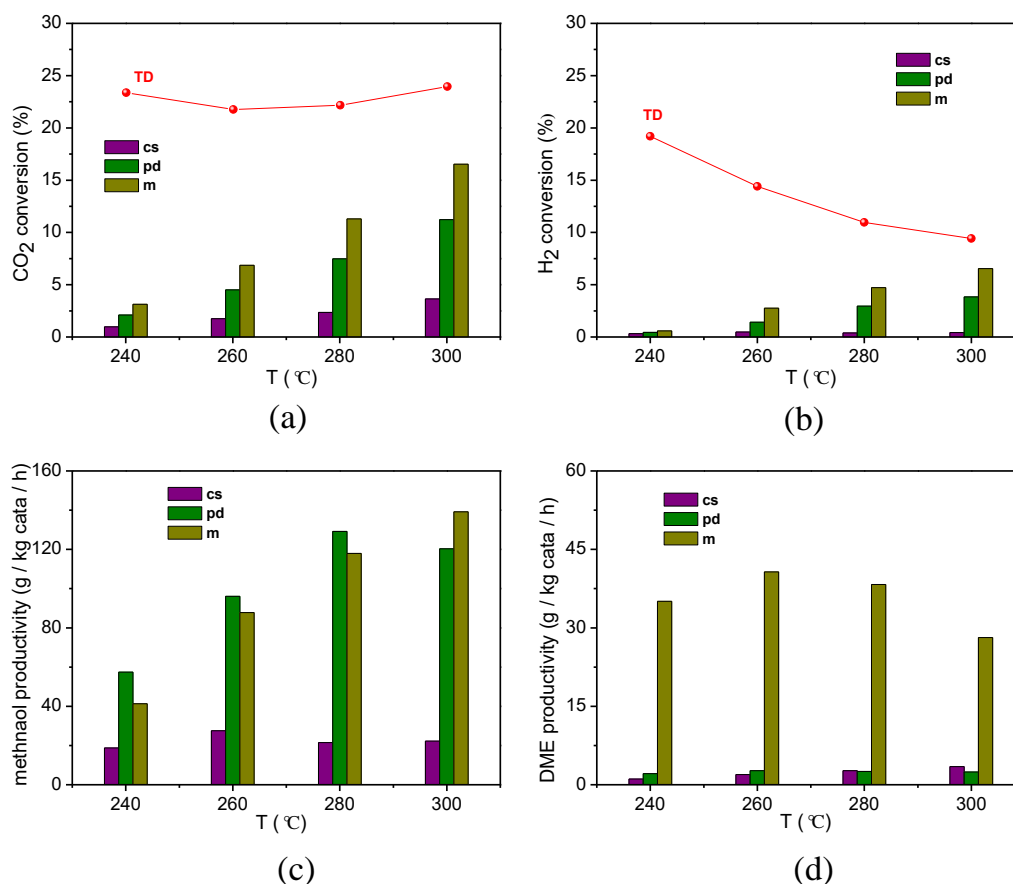


Fig.11 Conversion de CO<sub>2</sub> (a) et H<sub>2</sub> (b), productivité en méthanol (c) et en DME (d)

Les résultats catalytiques de synthèse directe de DME à partir de CO<sub>2</sub> et H<sub>2</sub> sur des catalyseurs bifonctionnels sont présentés dans Fig.11. Le catalyseur bifonctionnel préparé par un procédé de mélange physique présente une conversion la plus élevée de CO<sub>2</sub>, tandis que le catalyseur bifonctionnel préparé par la méthode ‘core-shell’ montre la conversion du CO<sub>2</sub> la plus basse, ce qui peut être dû au fait que les réactifs ne parviennent pas facilement au catalyseur à base de cuivre situé dans le cœur de ‘core-shell’. Le catalyseur bifonctionnel préparé par mélange physique présente une productivité en DME supérieure à celle des deux autres catalyseurs, avec la plus grande productivité de 33 g de DME par kg de catalyseur et par heure à 260 °C, et confirme les idées que la faible productivité en DME du catalyseur préparé par le procédé de dépôt de co-précipitation est due au blocage des sites acides par une partie de catalyseur au cuivre CZZ.

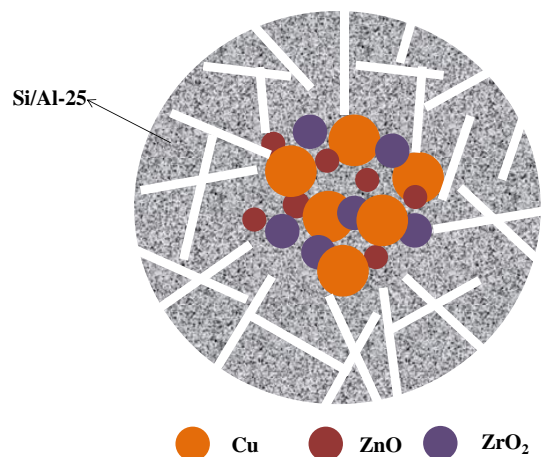


Fig.12 Diagramme sch ématique pour catalyseur **cs**

Afin d'expliquer la faible conversion de  $\text{CO}_2$  du catalyseur **cs**, le diagramme sch ématique du **cs** dans la r éaction de synth èse DME directe est pr ésent ée à la Fig.12. Le diam ètre des pores de Si/Al-25 est d'environ 4 nm, alors que la taille des cristallites de CuO et ZnO sont respectivement de 15,0 nm et 8,9 nm. Le gaz  $\text{CO}_2$  et  $\text{H}_2$  ne peuvent atteindre que quelques particules de Cu à travers les pores. Beaucoup de particules de Cu ne sont pas accessibles. Il a également é é souligné que l'interface Cu/Zn est le site actif pour la synth èse du m éthanol, car le cuivre m étallique fournit les sites de dissociation  $\text{H}_2$  et ZnO fournit des sites d'adsorption de  $\text{CO}_2$ . Du fait du faible diam ètre des pores du Si /Al de la coque, l'interface est difficilement accessible. Cela explique la faible conversion de  $\text{CO}_2$  du catalyseur **cs**.

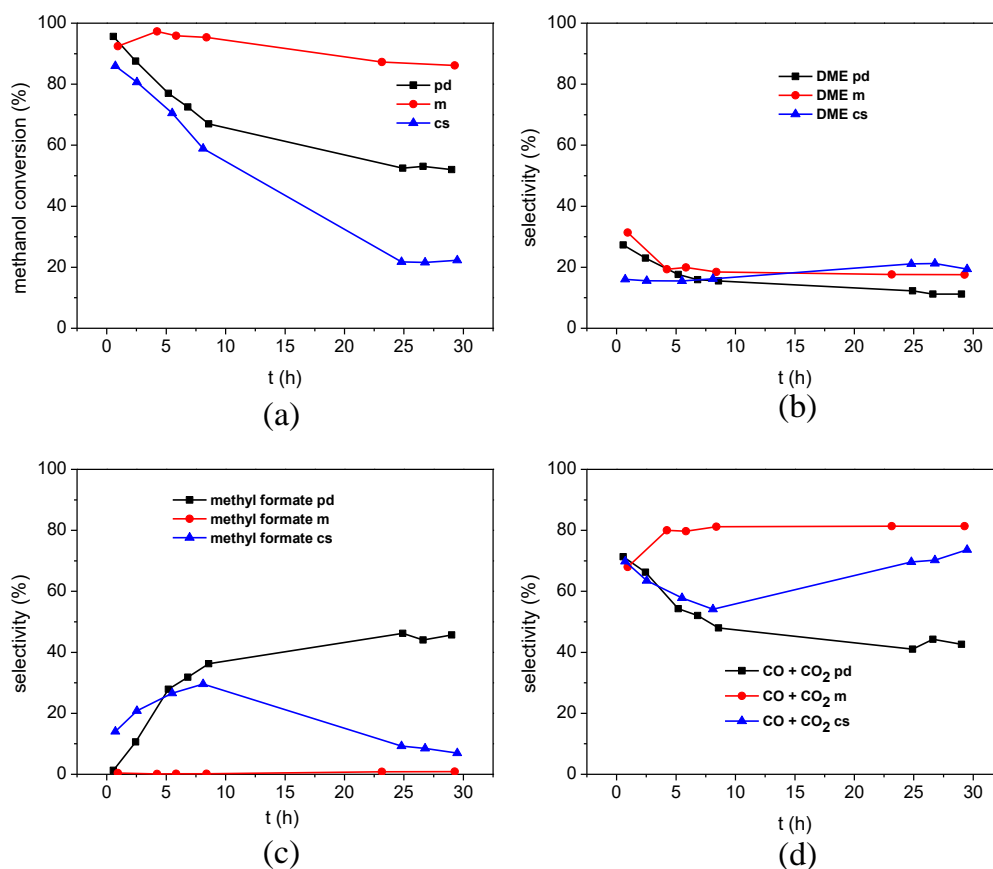


Fig.13 R éultats catalytiques pour la r éaction m éthanol vers DME

Afin de comprendre l'influence de la composante CZZ sur le comportement des sites acides dans la d éshydratation du m éthanol en DME, trois catalyseurs ont é té test é s dans la r éaction d é crite au 2.1, les r é sultats sont pr é sents dans Fig.13. Le catalyseur pr é par é par le proc é d é de m é l ange physique repr é sente la conversion la plus é lev é e du m é thanol et le catalyseur pr é par é par le proc é d é 'core-shell' montre la conversion la plus basse du m é thanol, ce qui a la m ê me tendance dans la r é action de synth è se directe de DME. En dehors de la r é action de d é shydratation du m é thanol en DME sur les sites acides, le cuivre m é tallique est é galeme nt impliqu é dans la r é action. Il a é t é rapport é que le formiate de m é thyle est d é shydrog é n é facilement en CO sur des sites basiques [19]. La s é lectivit é du formiate de m é thyle sur le catalyseur pr é par é par m é l ange physique est proche de 0, ce qui signifie que les sites basiques ne sont pas bloqu é s et le formiate de m é thyle est rapidement converti. Tandis que la s é lectivit é du formiate de m é thyle pour le catalyseur pr é par é par co-pr é cipitation proc é d é de d é p ô t augmente avec le temps, ç a

signifie que les sites basiques ont été bloqués lentement par les produits pendant la réaction. L'étude de la basicité des matériaux bifonctionnels ayant le caractère acido-basique est en cours.

Les catalyseurs bifonctionnels préparés par un procédé de mélange physique présentent une meilleure productivité en DME que les catalyseurs bifonctionnels préparés par deux autres méthodes. Cela confirme que, en dehors de l'influence négative de l'eau, la couverture des sites acides par le cuivre métallique est la principale raison de la faible sélectivité en DME des catalyseurs bifonctionnels.

### **3. Conclusion générale**

Al-TUD-1 avec des rapports différents Si/Al a été synthétisé. C'est un matériau mésoporeux spongieux avec une grande surface spécifique et une acidité modifiable. La quantité de sites acides augmente avec la diminution du rapport Si/Al. La conversion du méthanol augmente avec la diminution du rapport Si/Al et l'existence de l'eau montre l'effet négatif sur la déshydratation du méthanol pour la formation du DME.

Les catalyseurs bifonctionnels Cu-ZnO-ZrO<sub>2</sub>@Al-TUD-1 préparés par la méthode de dépôt de co-précipitation montrent une bonne dispersion de cuivre, avec des particules de cuivre métallique autour de 5 nm. La surface spécifique du cuivre augmente avec la diminution du rapport Si/Al. L'énergie d'adsorption du cuivre sur le support dopé par Al est plus grande que pour le support à base de silice pure (calculs DFT). Cela implique que l'incorporation d'Al peut induire l'ancrage du cuivre et le blocage de sites acides. Conversion du CO<sub>2</sub> et la productivité en méthanol augmentent avec la diminution du rapport Si/Al. La couverture des sites acides avec le cuivre et l'influence de l'eau sont les principales raisons de la faible sélectivité en DME observée pour la synthèse directe de DME.

Afin d'améliorer les catalyseurs bifonctionnels et de comprendre l'interaction entre les deux parties catalyseurs, trois méthodes de préparation différentes, co-précipitation-dépôt, core-shell et mélange physique ont été comparées. Les catalyseurs bifonctionnels préparés par un procédé de mélange physique présentent une meilleure productivité en DME que les catalyseurs bifonctionnels préparés par les deux autres

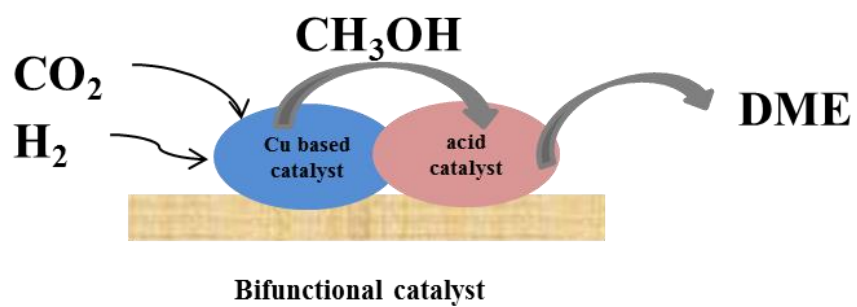
méthodes. Cela confirme que la couverture des sites acides avec cuivre est la principale raison de la faible sélectivité DME des catalyseurs bifonctionnels.

#### 4. Références

- [1] T. Witoon, T. Permsirivanich, N. Kanjanasootorn, C. Akkaraphataworn, A. Seubsai, K. Faungnawakij, C. Warakulwit, M. Chareonpanich, J. Limtrakul, Direct synthesis of dimethyl ether from CO<sub>2</sub> hydrogenation over Cu-ZnO-ZrO<sub>2</sub>/SO<sub>4</sub><sup>2-</sup>-ZrO<sub>2</sub> hybrid catalysts: effects of sulfur-to-zirconia ratios, *Catal Sci Technol*, 5 (2015) 2347-2357.
- [2] R.W. Liu, Z.Z. Qin, H.B. Ji, T.M. Su, Synthesis of Dimethyl Ether from CO<sub>2</sub> and H<sub>2</sub> Using a Cu-Fe-Zr/HZSM-5 Catalyst System, *Ind Eng Chem Res*, 52 (2013) 16648-16655.
- [3] F. Frusteri, G. Bonura, C. Cannilla, G.D. Ferrante, A. Aloise, E. Catizzone, M. Migliori, G. Giordano, Stepwise tuning of metal-oxide and acid sites of CuZnZr-MFI hybrid catalysts for the direct DME synthesis by CO<sub>2</sub> hydrogenation, *Appl Catal B-Environ*, 176 (2015) 522-531.
- [4] G.H. Yang, N. Tsubaki, J. Shamoto, Y. Yoneyama, Y. Zhang, Confinement Effect and Synergistic Function of H-ZSM-5/Cu-ZnO-Al<sub>2</sub>O<sub>3</sub> Capsule Catalyst for One-Step Controlled Synthesis, *Journal of the American Chemical Society*, 132 (2010) 8129-8136.
- [5] P.S.S. Prasad, J.W. Bae, S.H. Kang, Y.J. Lee, K.W. Jun, Single-step synthesis of DME from syngas on Cu-ZnO-Al<sub>2</sub>O<sub>3</sub>/zeolite bifunctional catalysts: The superiority of ferrierite over the other zeolites, *Fuel Process Technol*, 89 (2008) 1281-1286.
- [6] S.H. Kang, J.W. Bae, K.W. Jun, H.S. Potdar, Dimethyl ether synthesis from syngas over the composite catalysts of Cu-ZnO-Al<sub>2</sub>O<sub>3</sub>/Zr-modified zeolites, *Catal Commun*, 9 (2008) 2035-2039.
- [7] W.H. Chen, B.J. Lin, H.M. Lee, M.H. Huang, One-step synthesis of dimethyl ether from the gas mixture containing CO<sub>2</sub> with high space velocity, *Appl Energ*, 98 (2012) 92-101.
- [8] D.S. Mao, W.M. Yang, J.C. Xia, B. Zhang, Q.Y. Song, Q.L. Chen, Highly effective hybrid catalyst for the direct synthesis of dimethyl ether from syngas with magnesium oxide-modified HZSM-5 as a dehydration component, *J Catal*, 230 (2005) 140-149.
- [9] L. Angelo, K. Kobl, L.M.M. Tejada, Y. Zimmermann, K. Parkhomenko, A.C. Roger, Study of CuZnMO<sub>x</sub> oxides (M = Al, Zr, Ce, CeZr) for the catalytic hydrogenation of CO<sub>2</sub> into methanol, *Cr Chim*, 18 (2015) 250-260.

- [10] K. Kobl, L. Angelo, Y. Zimmermann, S. Sall, K. Parkhomenko, A.C. Roger, In situ infrared study of formate reactivity on water-gas shift and methanol synthesis catalysts, *Cr Chim*, 18 (2015) 302-314.
- [11] F. Arena, G. Italiano, K. Barbera, S. Bordiga, G. Bonura, L. Spadaro, F. Frusteri, Solid-state interactions, adsorption sites and functionality of Cu-ZnO/ZrO<sub>2</sub> catalysts in the CO<sub>2</sub> hydrogenation to CH<sub>3</sub>OH, *Appl Catal A-Gen*, 350 (2008) 16-23.
- [12] B. Sabour, M.H. Peyrovi, T. Hamoule, M. Rashidzadeh, Catalytic dehydration of methanol to dimethyl ether (DME) over Al-HMS catalysts, *J Ind Eng Chem*, 20 (2014) 222-227.
- [13] R. Anand, R. Maheswari, U. Hanefeld, Catalytic properties of the novel mesoporous aluminosilicate AlTUD-1, *J Catal*, 242 (2006) 82-91.
- [14] M.S. Hamdy, R. Amrollahi, I. Sinev, B. Mei, G. Mul, Strategies to Design Efficient Silica-Supported Photocatalysts for Reduction of CO<sub>2</sub>, *Journal of the American Chemical Society*, 136 (2014) 594-597.
- [15] F. Adam, T.S. Chew, J. Andas, A simple template-free sol-gel synthesis of spherical nanosilica from agricultural biomass, *J Sol-Gel Sci Techn*, 59 (2011) 580-583.
- [16] L.T. Zhuravlev, The surface chemistry of amorphous silica. Zhuravlev model, *Colloid Surface A*, 173 (2000) 1-38.
- [17] X. Huang, W. Chu, W.J. Sun, C.F. Jiang, Y.Y. Feng, Y. Xue, Investigation of oxygen-containing group promotion effect on CO<sub>2</sub>-coal interaction by density functional theory, *Appl Surf Sci*, 299 (2014) 162-169.
- [18] M. Gerosa, C. Di Valentin, C.E. Bottani, G. Onida, G. Pacchioni, Communication: Hole localization in Al-doped quartz SiO<sub>2</sub> within ab initio hybrid-functional DFT, *J Chem Phys*, 143 (2015).
- [19] Z.P. Lu, D.Z. Gao, H.B. Yin, A.L. Wang, S.X. Liu, Methanol dehydrogenation to methyl formate catalyzed by SiO<sub>2</sub>-, hydroxyapatite-, and MgO-supported copper catalysts and reaction kinetics, *J Ind Eng Chem*, 31 (2015) 301-308.



*Chapter 1: Introduction*



## 1.1 CO<sub>2</sub> utilization

The global climate changed drastically in last decades, which has been evidenced by the sea level rise with 17 cm in the last century [1], global temperature rise, warming of the oceans, shrinking ice sheets, declining Arctic sea ice, glacial retreat, extreme events, oceans' acidification, decreased snow cover. These are obviously accompanied by the industrialization development, which is induced by the human beings. The combustion of fossil fuels released a lot of CO<sub>2</sub>, nitrogen- and sulfur-containing compounds into the Earth atmosphere. The two latter compounds are the main factors for the forming of acid rain. CO<sub>2</sub> is the main greenhouse gas, which already drew all over the world's attention in recent years. The greenhouse gas in the atmosphere is relatively transparent to the sunlight with short-wavelength radiation, while it adsorbs the infrared radiation emitted by the Earth surface with the long-wavelength. Hence it traps heat near the Earth surface and the temperature at the Earth surface rise [2] (Figure 1- 1). It has been indicated that when the CO<sub>2</sub> concentration in the atmosphere rises the temperature at the Earth surface rises as well [2, 3].

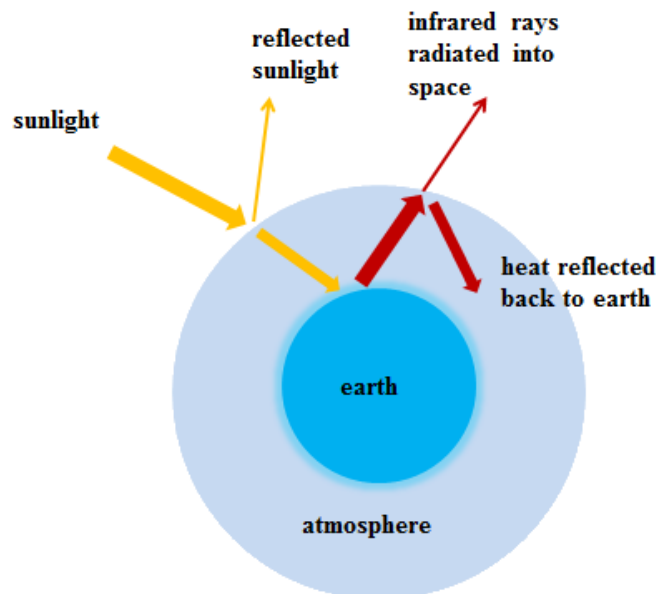


Figure 1- 1 Schematic diagram for the greenhouse gas effect

The CO<sub>2</sub> emissions percentages for different countries and areas in 2008 are presented in Figure 1-2. The top six countries or areas are China of 23 %, USA of 18 %, European Union 14 %, India of 6 %, Russia of 6 % and Japan of 4 %. The CO<sub>2</sub> emissions percentage for other countries is less than 1.5 %, which is not shown in details here. The CO<sub>2</sub> emissions in 2008, 2009 and 2010 were at the level of 29,888,121 kt, 31,629,955 kt and 33,508,901 kt, respectively, according to the CDIAC data [4]. It can be noticed that the emissions still present the rising trend even though a lot of countries have already taken reactions aiming at decreasing the CO<sub>2</sub> emission.

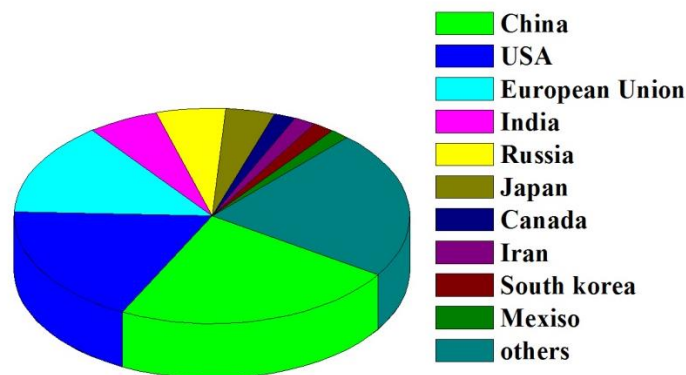


Figure 1-2 The CO<sub>2</sub> emissions percentages all over the world

Now carbon capture and storage (CCS) technologies has been put forward as the potential method for the decline of CO<sub>2</sub> in the atmosphere. Many research programs concerning these technologies have been conducted in the world wide. It has been divided into CO<sub>2</sub> geological storage, CO<sub>2</sub> ocean storage and CO<sub>2</sub> mineralization into inorganic carbonates. When CO<sub>2</sub> was injected into oil and gas field or the coalbed, it not only declines the CO<sub>2</sub> concentration in atmosphere but also promote the recovery of oil or coalbed methane, which are known as CO<sub>2</sub>-EOR and CO<sub>2</sub>-ECBM technologies [5]. It has already been conducted in Norway, USA, Canada, China, Japan.

Figure 1- 3 CO<sub>2</sub> applications

Compared with the CCS technologies, the carbon capture and utilization (CCU) method is a more efficient way for the abatement of the CO<sub>2</sub> emissions in the future. Different chemical products that derive from CO<sub>2</sub> are shown Figure 1- 3. CCU supposes the use of CO<sub>2</sub> as a carbon source to produce chemical products aiming at declining the CO<sub>2</sub> content as well as gaining the economic benefits. For example, using CO<sub>2</sub> as the carbon source to produce urea, salicylate, polycarbonate, and carbonates has been industrialized already. Now more and more researchers have been working on using CO<sub>2</sub> as the carbon source to produce fuels. The synthesis of light olefins and high alcohols from CO<sub>2</sub> is just at the beginning of investigation. Methane has been produced by CO<sub>2</sub> methanation reaction. Methane is a gaseous fuel and is very difficult to be liquified resulting in special requirements in transportation. Methanol can be obtained by CO<sub>2</sub> hydrogenation as well. While the methanol synthesis is an excellent way for CO<sub>2</sub> utilization its synthesis has some thermodynamic limits: high pressures are needed for a good conversion of CO<sub>2</sub> and low temperatures are needed for a good selectivity of methanol formation. Thus the research of good catalysts for the CO<sub>2</sub> hydrogenation to methanol is still a challenge. DME can be considered as a promising fuel, because it is easily liquefied and has a good energy density. Apart from this the DME direct synthesis from CO<sub>2</sub> is thermodynamically more favorable compared with the methanol synthesis, it proceeds at lower pressures [3, 6-14].

## 1.2 DME synthesis from CO<sub>2</sub>/H<sub>2</sub>

DME is a volatile substance which existed in the liquid form when the pressure is above 0.5 MPa, so it is usually stored as liquid. The physical properties of DME are presented in Table 1- 1. DME is non-toxic and environmentally benign, which has many applications nowadays, so it has attracted a lot of attention from the academy as well as from the industry. It can be used as a clean fuel, because it is the simplest ether which has only C-H bond and C-O bond without C-C bond and possesses a high oxygen content so low formation of solid particulates and CO can be achieved when using DME as fuel [15]. After burning, there is no nitrogen-containing or sulfur-containing compounds released which is detrimental for the environment. DME owns high cetane number of 55, which is higher than diesel fuel with the value 40-50, so it can be an excellent alternative fuel [16, 17]. It has the similar physicochemical properties as the LPG (liquefied petroleum gas), it can also be used as the substitute [17]. It is also a substitute for chlorofluorocarbons acting as an aerosol propellant because it is benign to the ozone layer [18, 19]. It can be employed as a chemical intermediate for the production of chemical products, such as alkyl aromatics, dimethyl sulfate, methyl acetate, olefins and so on [20]. Apart from these, it is also an efficient H<sub>2</sub> carrier for fuel cell application [3].

Table 1- 1 Physical properties of DME

---

Properties	
Molecular formula	C <sub>2</sub> H <sub>6</sub> O
Molar mass	46.07 g mol <sup>-1</sup>
appearance	Colorless gas
Odor	Typical
Density	0.735 g/mL (liquid, -25 °C)
Melting point	-141 °C
Boiling point	-24 °C
Solubility in water	71 g dm <sup>-3</sup> (at 20 °C)
logP	0.022
Vapor pressure	1.5 bar

---

The traditional DME synthesis method is a two steps process, firstly the methanol is synthesized from CO/H<sub>2</sub> in the first reactor under pressure (50-100 bar) and medium temperature (220-280 °C) over a copper based catalyst [21, 22], and secondly the methanol is dehydrated to DME in the second reactor under the ambient pressure over an acid catalyst. The schematic diagrams of the traditional two steps DME synthesis are shown in Figure 1-4.

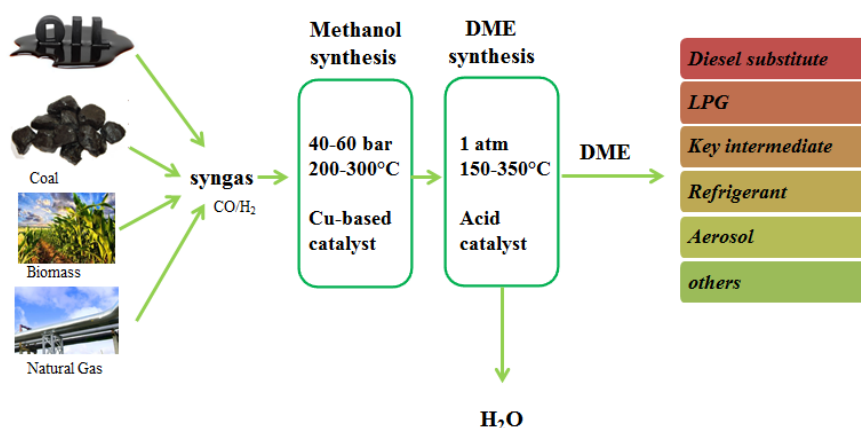


Figure 1-4 Schematic diagram for traditional DME synthesis

The direct DME synthesis method was put forward during the past several years, because it is thermodynamically favorable compared with the conventional method. The consumption of methanol in the methanol dehydration to DME reaction will break the equilibrium and the reaction will shift to the right [3]. The direct DME synthesis is also economically saving compared with the conventional method. It has been reported that the operating cost of the direct DME synthesis will be only 2/3 of DME production from methanol dehydration [23, 24].

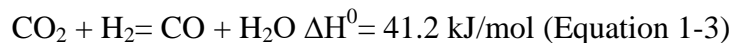
Some other carbon sources have been proposed for the direct DME synthesis reaction rather than the syngas obtained from oil, natural gas and coal, such as waste, biomass, CO<sub>2</sub> from capture and so on [20].

In our work, CO<sub>2</sub> will be employed as the carbon source for the direct DME synthesis because it is environmental friendly and resource saving. The direct DME

synthesis will be conducted in one reactor, which is economically saving and thermodynamically favorable.

### 1.3 Catalysts

Due to the instinct of two steps reaction of DME synthesis, methanol synthesis on copper based catalysts (Equation 1-1) and methanol dehydration to DME on acid catalysts (Equation 1-2), the direct DME synthesis needs the presence of a bifunctional catalyst consisting of these both functions.



The schematic diagram of the direct DME synthesis on a bifunctional catalyst is shown in Fig. 1-5.

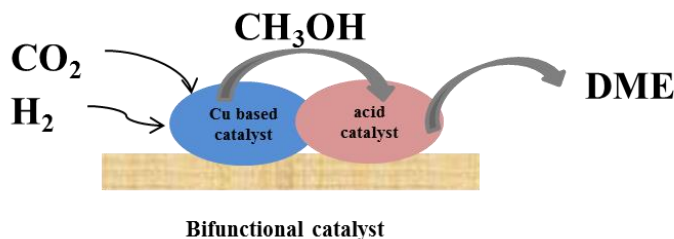


Figure 1- 5 Schematic diagram of the direct DME synthesis on a bifunctional catalyst

This bifunctional catalyst needs the intimate contact between the copper based part and the acid part, because the DME is obtained by the consecutive dehydration of methanol on the acid sites which is formed on the copper based part.

For this work it is needed to choose a good copper based catalyst and an acid catalyst as well as the preparation method of these bifunctional materials.

### 1.3.1 Copper based catalyst

Different catalysts have been employed in the methanol synthesis reaction. After the methanol synthesis way from CO and H<sub>2</sub> proposed by Sabatier in 1905, BASF conducted the methanol synthesis reaction from CO/H<sub>2</sub> using zinc/chromium oxide catalyst under high temperature and pressure (300-400 °C, 250-350 bars) [25]. In 1966, ICI (Imperial Chemical Industries) used Cu/ZnO as methanol synthesis catalyst at lower temperature and pressure (300 °C, 100 bars) with pure syngas as reactant gas. Afterwards, Lurgi improved the process at even lower temperature and pressure (230-250 °C, 40-50 bars) [25]. Then Cu/ZnO catalyst becomes the dominating catalyst for the methanol synthesis from CO/H<sub>2</sub> in industry as well as in academy. The Cu/ZnO catalyst has also been demonstrated as the efficient methanol synthesis catalyst from CO<sub>2</sub>/H<sub>2</sub> [26-28]. The optimized catalyst for the methanol synthesis from CO<sub>2</sub>/H<sub>2</sub> might require an increase of Zn promoted copper active sites [26]. From another hand owing to the acid character of CO<sub>2</sub>, the basic sites are needed.

For the copper based catalyst, the metallic copper surface area and the interface of Cu/Zn that have been mentioned are the influencing factors for methanol synthesis from CO<sub>2</sub>/H<sub>2</sub> performance [29]. The high temperature carbonates observed in the catalyst are reported to be beneficial. They have been discovered in the precursor of Cu/ZnO catalyst prepared by the co-precipitation method [30]. Behrens et al suggested that the high temperature carbonates are trapped at the Cu<sup>0</sup>-ZnO interfaces [31]. It may be considered as a growth inhibitor for the copper particles [30]. Schur et al put forward that the copper dispersion can be connected with the high temperature carbonates [32]. There are different decomposition temperatures for the high temperature carbonates reported for the copper based catalysts prepared by different methods [31, 33]. The decomposition temperature is an indicator for the strong interaction across Cu/Zn interfaces and grain boundaries [33].

According to Malte Behrens, the good methanol synthesis catalyst should have a high metallic copper surface area, defective copper nanoparticles and strong metal-support (Cu-Zn) interaction (SMSI). In order to obtain the methanol synthesis catalyst which satisfying these requirements, the content of the promoter should be noticed during

the preparation. For example, if the promoter content is much less than 0.5, the CuO can't be dispersed well and will aggregate to form big CuO particle size. When the promoter content is around 0.5, the CuO particles disperse well with small nanoparticles, thus with more copper surface exposed. The promoter can act as a physical spacer between Cu particles (Figure 1- 6).

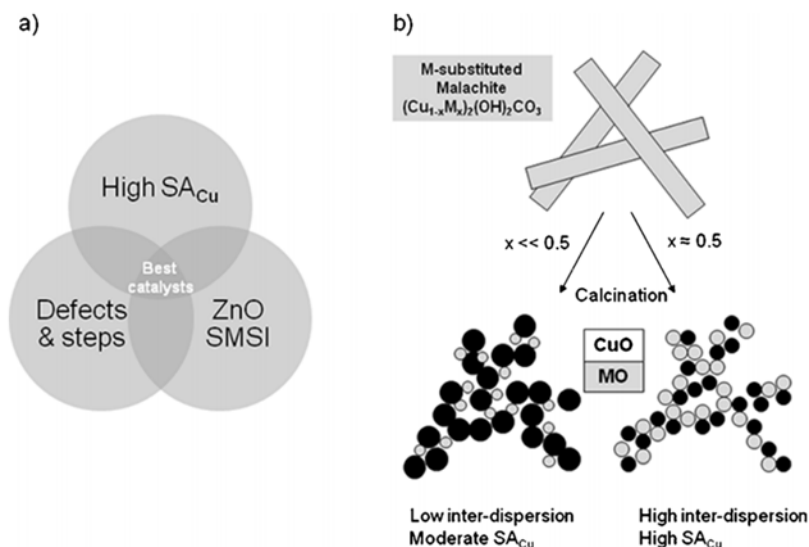


Figure 1- 6 (a) Schematic representations of the necessary ingredients for a high-performance methanol synthesis catalyst (b) The role of precursor composition for the Cu dispersion in the final catalyst

The role of Zn is to improve the dispersion of copper thus increasing the amount of active sites on the surface of the catalyst. Thus, ZnO has two functions: 1) it works as a physical spacer between the Cu<sup>0</sup> particles, stabilizes the structure and prevents the sintering of the copper particles; 2) it works as the thin layer on the surface of copper, which will form the interface of Cu/Zn. The presence of such interfaces will affect the adsorption properties of CO<sub>2</sub> [34].

Based on the Cu/ZnO model methanol synthesis catalyst, different promoters have been investigated to improve the methanol synthesis CO<sub>2</sub>/H<sub>2</sub> performance, such as Al, Ga, Zr as well as some additives such as SBA-15, SiO<sub>2</sub>, TiO<sub>2</sub>.

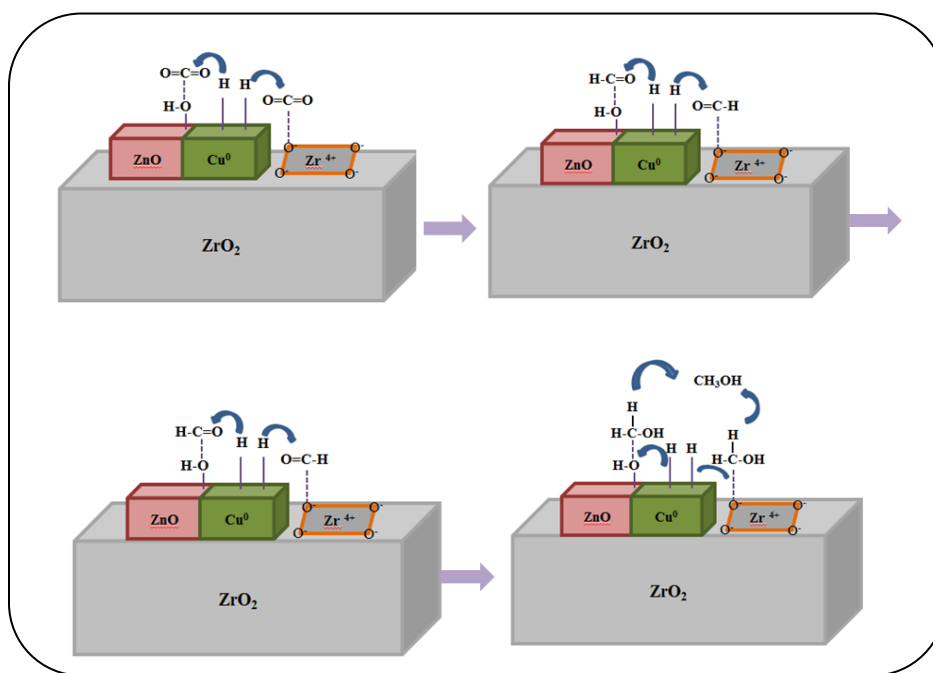
**Cu-ZnO-Al<sub>2</sub>O<sub>3</sub>** is the most widely investigated catalyst of the methanol synthesis from CO<sub>2</sub>/H<sub>2</sub>, it was chosen as the industrial catalyst for methanol synthesis from

CO/CO<sub>2</sub>/H<sub>2</sub> with the varying composition for different companies [25, 35-38]. The addition of Al increases the BET surface area and the copper dispersion, and inhibits the sintering of copper [39]. The effect of the promoters **SiO<sub>2</sub>**, **TiO<sub>2</sub>** and **SiO<sub>2</sub>-TiO<sub>2</sub>** on the performance of Cu/ZnO/Al<sub>2</sub>O<sub>3</sub> catalyst for methanol synthesis from CO<sub>2</sub> were investigated by Zhang et al [40]. The results show that all the promoters can enhance the dispersion of CuO. The CO<sub>2</sub> conversion and methanol selectivity were improved to 40.7 % and 41.2 % on SiO<sub>2</sub>-TiO<sub>2</sub> promoted CZA compared with the 15.8 % and 23.3 % on pure CZA. When the Cu-ZnO-Al<sub>2</sub>O<sub>3</sub> catalyst is employed in the methanol synthesis from CO<sub>2</sub>/H<sub>2</sub>, the big disadvantage of this catalyst is the insufficient hydrophobic ability and the insufficient basic sites number.

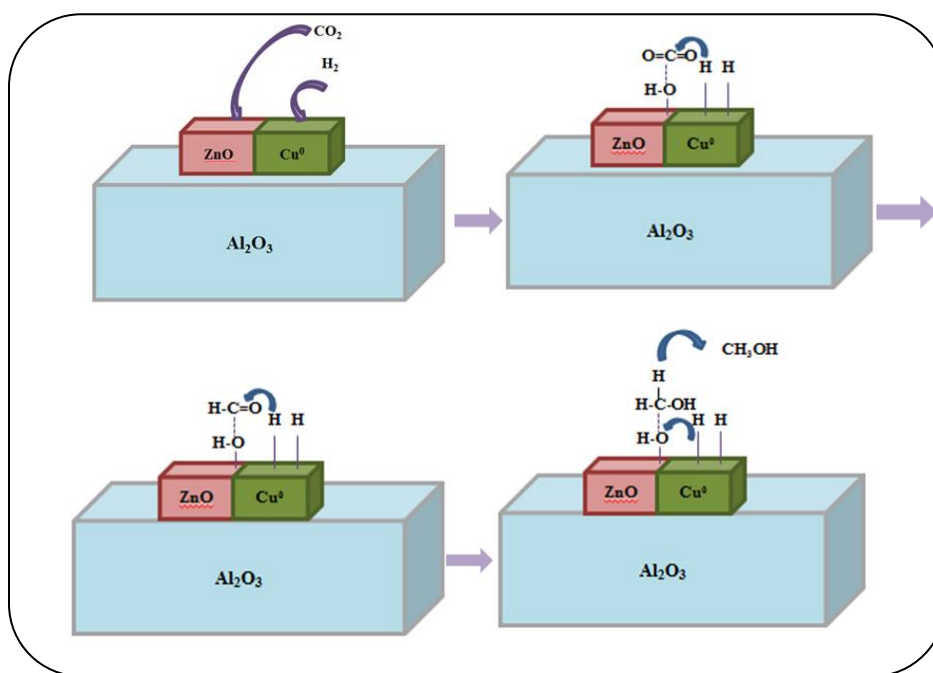
In order to get the well-confined copper particles, Cu/ZnO was incorporated into the pores of **SBA-15** by ammonia deposition-precipitation (ADP) method. The final catalyst with small copper particle size was obtained ( $d_{\text{Cu}} < 7$  nm). It shows the similar methanol synthesis performance as the industrial methanol synthesis catalyst CZA [41].

**Cu/Zn/Ga<sub>2</sub>O<sub>3</sub>** has been investigated in CO<sub>2</sub> hydrogenation to methanol reaction. The relation between Ga<sub>2</sub>O<sub>3</sub> promoting effect and the Ga<sub>2</sub>O<sub>3</sub> particle size was found. Small Ga<sub>2</sub>O<sub>3</sub> particle favored the formation of Cu<sup>+</sup>, which was thought related with the catalytic performance [42-44]. Despite its good performance the Ga<sub>2</sub>O<sub>3</sub> catalyzes the side reactions and some hydrocarbons have been detected in the products, such as methane, ethane and ethylene [44].

**Cu-ZnO-ZrO<sub>2</sub>** was also investigated intensively and was regarded as more active catalyst for this reaction because of the better water tolerance of zirconia compared with alumina [24, 45-49]. Apart from this Zr has been described as a good textural promoter [50, 51]. Especially for the CO<sub>2</sub> hydrogenation, there is more water formed than CO as the reactant. It also has been reported that the addition of Zr could enhance the basicity thus increasing the CO<sub>2</sub> conversion [52, 53]. The simplified sketch of reaction paths on Cu/ZnO/ZrO<sub>2</sub> and Cu-ZnO/Al<sub>2</sub>O<sub>3</sub> is shown in Figure 1-7 [48].



(a)



(b)

Figure 1-7 CO<sub>2</sub> hydrogenation mechanisms on Cu-ZnO/ZrO<sub>2</sub> and Cu-ZnO/Al<sub>2</sub>O<sub>3</sub> catalysts

The metallic copper is the active site for H<sub>2</sub> dissociation. The metal oxides, ZnO and ZrO<sub>2</sub> are the sites for the CO<sub>2</sub> adsorption. It has been reported the formation of reactive intermediate on the ZnO and ZrO<sub>2</sub> in the neighboring of copper is the rate

limiting step. So the extent of oxide/metal interface is an important factor to assess the methanol synthesis catalysts [48]. For the catalyst Cu-ZnO/ZrO<sub>2</sub> both ZnO and ZrO<sub>2</sub> provide the sites for CO<sub>2</sub> adsorption and activation. For the catalyst Cu-ZnO/Al<sub>2</sub>O<sub>3</sub>, only ZnO provides the sites for the CO<sub>2</sub> adsorption and activation, while the Al<sub>2</sub>O<sub>3</sub> plays a role of the support and the metallic copper particles spacer. It means that Cu-ZnO/ZrO<sub>2</sub> shows superiority in the methanol synthesis from CO<sub>2</sub>/H<sub>2</sub>.

Other copper based catalysts with additional promoters have been investigated. **Cu-Fe-Zr** was studied as the copper based catalyst in the direct DME synthesis reaction from CO<sub>2</sub> hydrogenation. It has been reported that iron can be a good promoter in preventing the sintering of active centers and dispersing the active centers crystallites [54-56]. The strong interaction between Cu and Fe also facilitates the adsorption of CO<sub>2</sub> and H<sub>2</sub>. The disadvantage of Cu-Fe in the methanol synthesis from CO<sub>2</sub> is that the CO<sub>2</sub> is easily reduced to CO and CH<sub>4</sub> on Fe [57, 58]. **La and Ce** also have been incorporated into Cu-Fe to promote the CuO dispersion and to improve the stability of the catalyst in hydrogenation of CO<sub>2</sub> to DME [59]. The disadvantage of Ce addition could be the formation of stable carbonates that cover the catalyst surface and thus lead to the decrease of the catalytic activity, this fact was enlightened in [60].

In general, Cu-ZnO-ZrO<sub>2</sub> seems to be the most promising methanol synthesis from CO<sub>2</sub> catalyst due to the synergy effect of Cu-ZnO, a good water tolerance, good basic properties and good textural properties of ZrO<sub>2</sub>.

Methanol synthesis catalysts have been synthesized by different preparation methods, such as co-precipitation method, sol gel method, microemulsion method and many others. The CuO was not well dispersed for the catalyst Cu-ZnO-ZrO<sub>2</sub> prepared by sol gel method [61]. For the catalyst prepared by microemulsion method, there is no intimate contact between metal oxides resulting in the small Cu<sup>0</sup>-ZnO interface. The copper based catalyst prepared by co-precipitation method was reported to own good CuO and ZnO dispersion [61] and has the existence of beneficial high temperature carbonates [31].

Therefore, Cu-ZnO-ZrO<sub>2</sub> will be investigated as the copper based catalyst of the methanol synthesis from CO<sub>2</sub>/H<sub>2</sub> without promoters to simplify the work. The weight ratios between Cu, ZnO and ZrO<sub>2</sub> will be fixed at 30wt%: 41wt%: 21.5% respectively based on [12].

### 1.3.2 Methanol dehydration to DME catalyst

The active sites for methanol dehydration to DME are the acid sites. Different solid acid catalysts have been investigated for methanol dehydration reaction, including  $\gamma$ -Al<sub>2</sub>O<sub>3</sub>, the modification of alumina with SiO<sub>2</sub>, TiO<sub>2</sub>-ZrO<sub>2</sub>, clays, ion exchange resins, and zeolites HZSM-5, HY, mordenites, SAPO, MCM and so on [20, 62]. The most widely investigated and most interesting solid acid catalysts are HZSM-5,  $\gamma$ -Al<sub>2</sub>O<sub>3</sub>, Al-HMS and S-ZrO<sub>2</sub>.

$\gamma$ -Al<sub>2</sub>O<sub>3</sub> was chosen as the methanol dehydration to DME catalyst by a lot of researchers because it is cost effective, has a high specific surface area, good thermal and mechanical stabilities and a high selectivity of DME formation [20, 63, 64]. Different modifications have been conducted on  $\gamma$ -Al<sub>2</sub>O<sub>3</sub>. It has been demonstrated that the sulfate treatment can increase the acidity of  $\gamma$ -Al<sub>2</sub>O<sub>3</sub> [65]. 1 wt. % titania modified  $\gamma$ -Al<sub>2</sub>O<sub>3</sub> was proved to show higher methanol dehydration activity than phosphoric acid modified  $\gamma$ -Al<sub>2</sub>O<sub>3</sub> [66]. Some researchers also found that silica modified  $\gamma$ -Al<sub>2</sub>O<sub>3</sub> shows better methanol dehydration to DME performance than the untreated one [67, 68].

Even though it has been already used as methanol dehydration to DME catalyst in academy as well as in industry, it is still of some disadvantages for this reaction. The acid sites of  $\gamma$ -Al<sub>2</sub>O<sub>3</sub> are mostly Lewis acid type [69]. The water formed during reaction strongly adsorbed on Lewis acid sites of  $\gamma$ -Al<sub>2</sub>O<sub>3</sub>, which will cause the decrease of methanol dehydration performance and inhibit the DME formation [70]. Another reason is that the optimal temperature for methanol dehydration to DME is not exactly the same as needed for the CO<sub>2</sub> hydrogenation to methanol reaction.

It is generally admitted that **HZSM-5** shows much higher activity than  $\gamma$ -Al<sub>2</sub>O<sub>3</sub> at moderate temperature range (240-280 °C). Considering the methanol synthesis condition on copper based catalyst, HZSM-5 is more thermodynamically favorable than  $\gamma$ -Al<sub>2</sub>O<sub>3</sub> [71,

72]. In the methanol dehydration to DME reaction, there is water formed. HZSM-5 is more hydrophobic compared with  $\gamma\text{-Al}_2\text{O}_3$ . While there are strong Brønsted acid sites existed in HZSM-5 which can further convert DME into hydrocarbons, some modifications have been done for HZSM-5 to have better DME selectivity. HZSM-5 was modified by addition of MgO to remove the strong Brønsted acid sites in order to decrease the undesired products like hydrocarbons. When MgO content is higher than 5wt%, the DME selectivity decreases markedly because of the insufficient acid sites content [18]. Apart from the strong acidity of HZSM-5 it also has been reported that the micropores in HZSM-5 also have been considered to restrain the quick diffusion [20].

The aluminated hexagonal mesoporous materials (**Al-HMS**) with different Si/Al ratios, 5, 10, 20 and 35, were tested in methanol dehydration to DME reaction [73]. It is concluded that the amount and the strength of acid sites increase with the decrease of Si/Al ratio from the  $\text{NH}_3$ -TPD results. Among all the materials investigated, Al-HMS-10 shows the optimal methanol conversion of 89% and the DME selectivity of 100% after the stability test of 72 h. Pure methanol and crude methanol (20 mol% water) were used as reactant respectively to investigate the influence of water (Figure 1-8). The methanol conversion is higher with pure methanol as reactant than crude methanol, which demonstrated that the water has negative effect on methanol dehydration to DME performance. The more obvious decrease of methanol conversion over the catalyst Al-HMS-5 is due to that there are more Lewis acid sites content and the water is adsorbed preferentially on Lewis acid sites than on Brønsted acid sites.

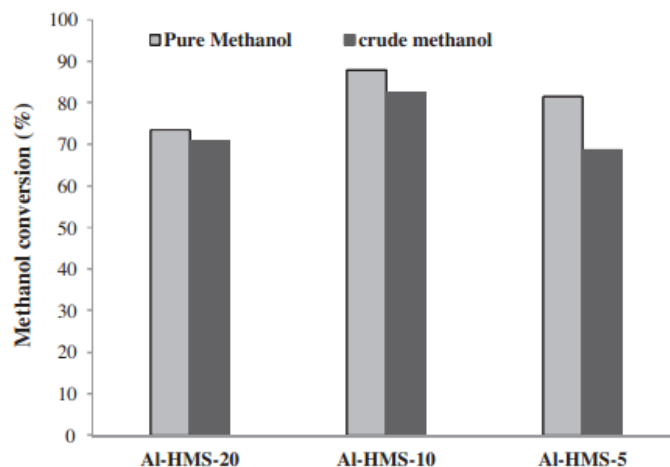


Figure 1-8 Methanol conversion variations for pure methanol and crude methanol (reaction conditions were 300 °C, 0.5 g catalyst, reaction time=72h, and WHSV= 1h<sup>-1</sup>)

The used catalyst Al-HMS-10 was measured by TG/DTA technique after the tests and the results are shown in Table 1- 2. It can be found that there is more coke formed for the catalyst Al-HMS-10 with pure methanol as reactant. So it can be conclude that water inhibits coke formation and can remove the coke in mesoporous molecular sieve [73].

Table 1- 2 Effect of different feed on coke formation over Al-HMS-10 after 72h

Sample	Temperature range (°C)	Coke content (wt. %)
Al-HMS-10 (used for pure methanol)	400-600	3.14
Al-HMS-10 (used for crude methanol)	445-520	0.9

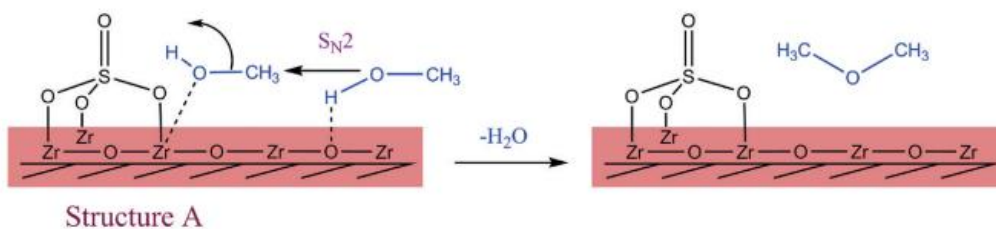
Though a good methanol conversion and a good DME selectivity were obtained over solid acid catalyst Al-HMS-10, the conditions for this reaction are quite mild. Nevertheless there is the coke formation on the catalysts Al-HMS-10, which can cause a severe deactivation.

**S-ZrO<sub>2</sub>** with different sulfur content: 5S-ZrO<sub>2</sub>, 10S-ZrO<sub>2</sub>, 15S-ZrO<sub>2</sub>, 20S-ZrO<sub>2</sub>, 30S-ZrO<sub>2</sub>, were tested in the methanol dehydration to DME. The sulfur content shows big influence on physicochemical properties, activity and stability of the sulfated zirconia catalysts. At the low sulfur contents (5S-ZrO<sub>2</sub>, 10S-ZrO<sub>2</sub>), the tridentate sulfate interacts with zirconia at the surface and induce the Lewis acid sites. At high sulfur content (15S-

ZrO<sub>2</sub>, 20S-ZrO<sub>2</sub>, 30S-ZrO<sub>2</sub>), -ZrOH is present in these catalysts, which acts as the Brønsted acid sites. The mechanisms for the methanol dehydration to DME on the sulfated zirconia catalysts are shown in Figure 1-9. The catalyst with high S content shows better stability than with low S content, because the Brønsted acid sites are more hydrophobic than Lewis acid sites. 20S-ZrO<sub>2</sub> shows similar methanol dehydration performance as HZSM-5 with Si/Al ratio of 24 [3].

While it is maybe a good methanol dehydration to DME catalyst coupled with the copper based catalyst [3], the deactivation of the metallic Cu<sup>0</sup> by sulfur is not enlightened.

### Pathway I



### Pathway II

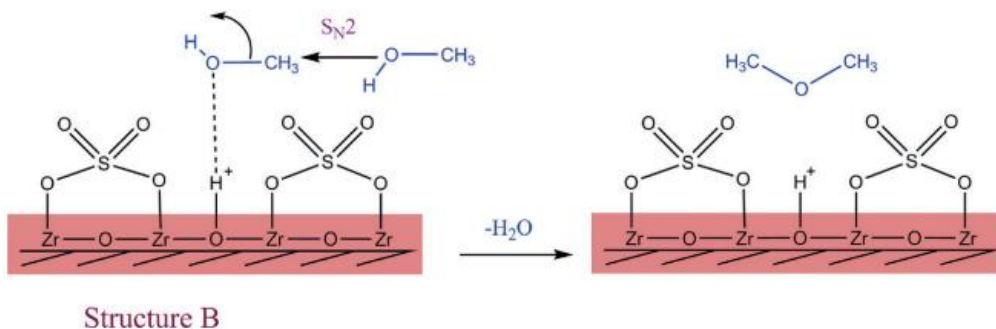


Figure 1-9 Proposed mechanisms for the formation of DME from methanol dehydration over the sulfated zirconia catalysts at low (pathway I) and high (pathway II) sulfur contents.

We didn't see the ideal methanol dehydration to DME catalyst which could be used in a couple with the copper based catalyst. The good methanol dehydration to DME catalyst should have weak and moderate acidity, good hydrophobic property, big surface

area and high hydrothermal stability. So regarding all these demands the **Al-TUD-1** materials were chosen as the methanol dehydration to DME catalysts.

TUD-1 (abbreviation for Technische Universiteit Delft), sponge-like amorphous mesoporous silica, was first published by Z. Shan et al [74, 75]. It shows three dimensional pore structure, which is demonstrated by the 3-D TEM in Figure 1-10 [76, 77]. This kind material owns big surface area, big pore volume and high hydrothermal stability. The pore size can be adjusted by changing the hydrothermal treatment time. It is also surfactant free during the synthesis [78], which attracts a lot of researches' attentions.

Modification of TUD-1 is very easy in the one pot synthesis. The incorporation of different heteroatoms is applied to modify the properties in order to adapt to different reactions [79]. For example, Ce-Ti-TUD-1 was employed to styrene oxidation [80], Fe-TUD-1 was applied to selective N<sub>2</sub>O induced propane oxidation [81], B-TUD-1 was demonstrated with high reactivity for the Prins cyclisation of citronellal in toluene [79]. Apart from these, the doping effect of Al [78], Co [82-84], Ga [85, 86], Ni [87], Mn [88], Zr [89, 90] and Cu [82, 91, 92] also have been investigated.

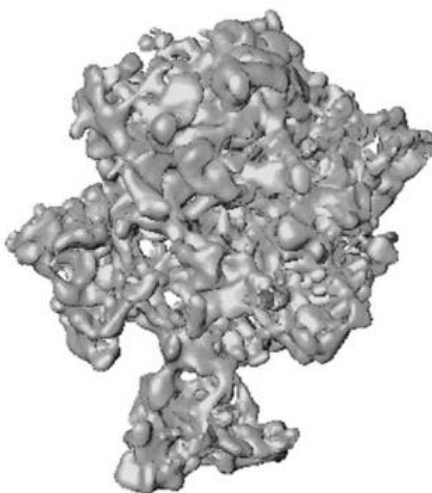


Figure 1-10 3-D TEM reconstruction of TUD-1[76]

The incorporation of Al into TUD-1 framework (Al-TUD-1) gives rise to tetra-, penta-, and hexa-coordinated aluminum sites, among which the tetrahedrally coordinated aluminum introduce Brønsted acid sites [74, 93, 94]. The replacement of Si atom by Al

atom introduces both Brønsted and Lewis acidic site (Figure 1-11) due to the different outer electron structure [93]. Owing to the acid properties, Al-TUD-1 has been investigated as the catalyst for the alkylation of phenol with TBA in gas phase and for the alkylation of phenol with MTBE in liquid phase [74].

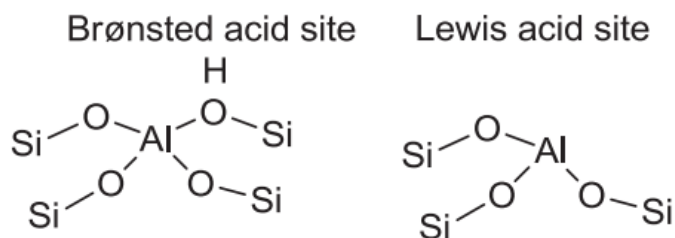


Figure 1-11 Models for Brønsted and Lewis acid sites

The acid properties of Al-TUD-1 were determined by  $\text{NH}_3$ -TPD by Hanefeld [74]. It shows that the amount of acid sites increase with the decrease of Si/Al ratio. The weak and medium acid sites are the predominant for all the Al-TUD-1 materials. In addition, this kind of materials is of the specific surface area of 686- 984  $\text{m}^2/\text{g}$ , and with the narrow pore distribution around 3.7 nm. Apart from the big specific surface area, the three dimensional pore structure of Al-TUD-1 provides more transportation possibilities for the reactants and products compared with the ordered zeolites [93].

Al-TUD-1 was never tested in the methanol dehydration to DME reaction previously. It is a promising acid catalyst which can be combined with the copper based catalyst.

### 1.3.3 Bifunctional catalyst

#### 1.3.3.1 Preparation method

Copper based catalyst has to be combined with acid catalyst for the direct DME synthesis from  $\text{CO}_2/\text{H}_2$ . Different preparation methods for the bifunctional catalytic materials provide the similar composition while with the different intrinsic characteristics, which affects the catalytic performance [42]. The good bifunctional catalyst should

satisfy these requirements: an intimate contact between two functions, a good copper dispersion, a good stability of the particle size, water tolerance and no coke formation. The preparation method is important to meet all these criteria.

Several preparation methods for the bifunctional catalysts applied in the direct DME synthesis reaction have been investigated during the recent decades [95]. For instance, Witoon et al prepared the bifunctional catalyst Cu-ZnO-ZrO<sub>2</sub>/ SiO<sub>4</sub><sup>2-</sup>-ZrO<sub>2</sub> by **physically mixing** these two parts together [3]. For the bifunctional catalyst prepared by physically mixing method, the disadvantage is the big distance between the copper based part and the acid part [96]. It has been reported that the close contact between methanol synthesis catalyst and methanol dehydration catalyst is beneficial for the DME synthesis performance, because the DME is obtained by the consecutive dehydration of methanol produced from copper based part [97]. To obtain the intimate contact between the methanol synthesis catalyst and the methanol dehydration catalyst, a new **physical sputtering** method was proposed for the preparation of bifunctional catalyst, which was conducted by directly loading copper and zinc clusters onto the solid acid catalyst surface [96]. The **core shell** structure catalyst CuO-ZnO-Al<sub>2</sub>O<sub>3</sub>@SiO<sub>2</sub>-Al<sub>2</sub>O<sub>3</sub> was prepared by adding the prepared CuO-ZnO-Al<sub>2</sub>O<sub>3</sub> particles into the aluminum nitrate and tetraethyl orthosilicate solution and then conducting the hydrothermal treatment [98]. Jong Wook Bae prepared the bifunctional catalyst Cu-ZnO-Al<sub>2</sub>O<sub>3</sub>/ Zr-modified ferrierite by **co-precipitation** of copper based part **deposited** on ZrFER and investigated the Zr influence on catalytic properties [99]. **Impregnation** method was also adopted by preparing bifunctional catalyst CuO-ZnO-Al<sub>2</sub>O<sub>3</sub>/HZSM-5, that is adding the HZSM-5 particles into the metal solution, then followed by drying and calcination procedure [95]. Using of ultra sound was employed as an assisted technology for the preparation of bifunctional catalysts for the direct DME synthesis to improve the dispersion of nanocatalyst by Reza Khoshbin [95].

Among the extensive choice of classical and alternative preparation methods the co-precipitation deposition method was chosen because metal oxides can be well dispersed and two functions have an intimate contact on the catalyst's surface. And the interaction between these two functions could prevent the sintering of Cu particles. Core

shell method is also investigated and the CZZ part is in the shell of the catalyst, which can be restrained by the shell from Cu agglomeration. Physically mixing method is employed for the comparison because these two functions are relatively independent.

### **1.3.3.2 Influencing factors in direct DME synthesis**

There are several factors that can influence the catalytic performance of the direct DME synthesis, such as metal-support interaction, copper dispersion, the copper sintering, coke formation, water existence [21, 100-102].

Mou et al [102] reported that the incorporation of Al into the SiO<sub>2</sub> support can promote the generation of defects in the support. The structure defects play an important role in stabilizing alloy nanoparticles and preventing them from sintering at high temperature treatment, thus creating the strong **metal support interaction (SMSI)**. Dai et al [103] prepared catalysts Cu/Al-HMS with different Si/Al ratio in the support by traditional incipient method. They proposed that the structure defects work in improving the dispersion of copper species and enhancing the interaction between copper and the support. The catalytic activity in the hydrogenation of dimethyl oxalate (DMO) to ethylene glycohol increases with increasing the Al content in the support and the highest values were obtained with the Si/Al ratio of 25. The schematic model of the interaction between copper species and support are shown in Fig. 1-12.

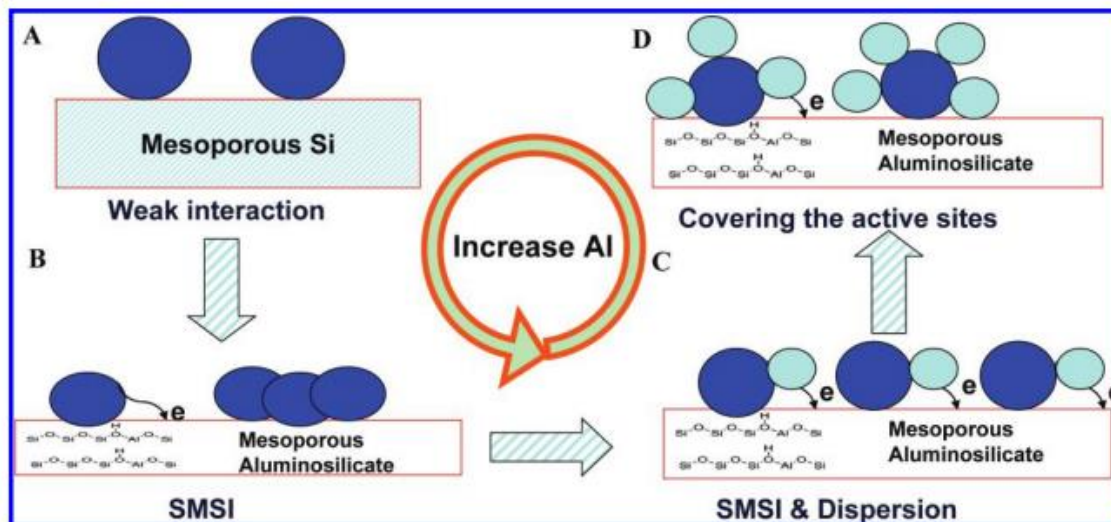


Figure 1- 12 Schematic model of the variation of Cu species with increasing Si/Al ratio

When no Al present in the framework of the support, the copper species can be dispersed well on the support. While the weak interaction between copper species and support can't stabilize for long time reaction. After the incorporation of Al, the defects generated not only can disperse the copper species but also enhance the interaction between copper species and support and improve the stability of the catalyst by the electron transfer. With increasing Al content in support, the excessive Al incorporated generate the aluminum oxide, which segregate on the surface of the copper species, leading to the decrease of copper surface area.

The **copper sintering** will lead to the decrease of copper surface area, thus reducing the active sites for methanol synthesis [104, 105]. It is of negative significance on the methanol synthesis reaction. A good copper dispersion and copper particles stabilization on the surface of the support would attenuate the sintering. It has been reported that 300 °C is the limit temperature for the avoiding of the metallic copper sintering [100]. So the reaction temperature shouldn't be performed above 300 °C.

The **coke** can be formed on both methanol synthesis catalyst and methanol dehydration catalyst [100, 106]. The TPO experiment was conducted on used CuO-ZnO- $\text{Al}_2\text{O}_3/\gamma\text{-Al}_2\text{O}_3$  by A.T. Aguayo [100] (Figure 1-13). It shows that there are two  $\text{CO}_2$  peaks. The first corresponds to the combustion of coke that is related to the metallic

function and the second corresponds to the combustion of coke deposited on acid sites. The coke formation on the metallic function will result in the decrease of metallic copper surface area thus leading to the decreased methanol synthesis performance. The coke formation on the acid sites can result in the decreased methanol dehydration performance.

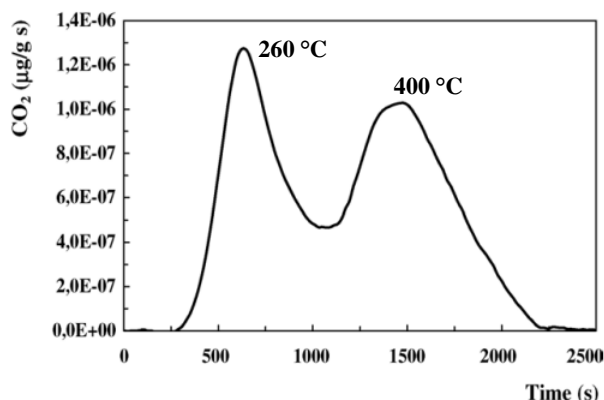


Figure 1-13 TPO profiles of the CuO-ZnO-Al<sub>2</sub>O<sub>3</sub>/γ-Al<sub>2</sub>O<sub>3</sub> catalyst after direct DME synthesis

**Water** shows both positive and negative influence on direct DME synthesis reaction [100, 107]. A.T. Aguayo et al [100] have conducted the direct DME synthesis reaction with and without water addition in feed syngas. It has been observed that the addition of water can prevent the decrease of DME selectivity with time on stream. Otherwise, the water also can compete with methanol in the adsorption on the acid sites. There are two situations in which the negative influence of water should be pay attentioned. When CO<sub>2</sub> is the reactant, there is more water formed than when CO is used as the reactant, so the water adsorption on acid sites should be noticed. When hydrophilic methanol dehydration catalyst is used, the coverage of water on acid sites will lead to the decrease of methanol dehydration performance.

In this work, it is planned to study in particular water influence as it is formed in all the reactions (Equation 1-1, 1-2, 1-3) and will be present in high quantity. The growth of the Cu<sup>0</sup> particles before and after tests will be monitored. Metal support interaction will be studied by numerous characterization techniques.

## 1.4 Objectives of the thesis

The objective of the thesis is the development of bifunctional catalytic materials for the direct DME synthesis from  $\text{CO}_2/\text{H}_2$ . The  $\text{Cu}/\text{ZnO}/\text{ZrO}_2$  is going to be used as the copper based catalyst for the first step of the methanol synthesis from  $\text{CO}_2/\text{H}_2$ . It will be combined with the mesoporous Al-TUD-1 materials as the acid catalyst of the second step – the methanol dehydration to DME. The bifunctional materials will be tested in the direct DME synthesis from  $\text{CO}_2/\text{H}_2$  under pressure. The influence of different factors on the direct DME synthesis will be investigated.

In the beginning the pure Al-TUD-1 materials with different Si/Al ratios will be prepared. Textural properties, crystalline phase, morphology and acid properties of Al-TUD-1 will be characterized. Their performance in the second step – the methanol dehydration to DME will be tested at atmospheric pressure (Chapter 3).

Then the bifunctional catalysts combining Al-TUD-1 materials with the copper based catalyst  $\text{Cu}/\text{ZnO}/\text{ZrO}_2$  will be prepared by co-precipitation deposition method. The materials will be fully characterized. The bifunctional catalysts with different Si/Al ratio in Al-TUD-1 support and the bifunctional catalysts with different weight ratio between the copper based catalyst and the Al-TUD-1 material will be tested in the direct DME synthesis from  $\text{CO}_2/\text{H}_2$  reaction under pressure as well as in the methanol dehydration to DME at atmospheric pressure. The Si/Al ratio influence and the weight ratio influence as well as the influencing factors on the activity of the catalytic system will be discussed (Chapter 4).

The bifunctional catalysts combining Al-TUD-1 materials with copper based catalyst  $\text{Cu}/\text{ZnO}/\text{ZrO}_2$  will be prepared by other preparation methods and tested in the direct DME synthesis from  $\text{CO}_2/\text{H}_2$ . The structural difference will be deeply analyzed and discussed. The ways of further improvement of the bifunctional catalysts for direct DME synthesis  $\text{CO}_2/\text{H}_2$  will be proposed (Chapter 5).

The outline of the thesis is shown in Figure 1-14.

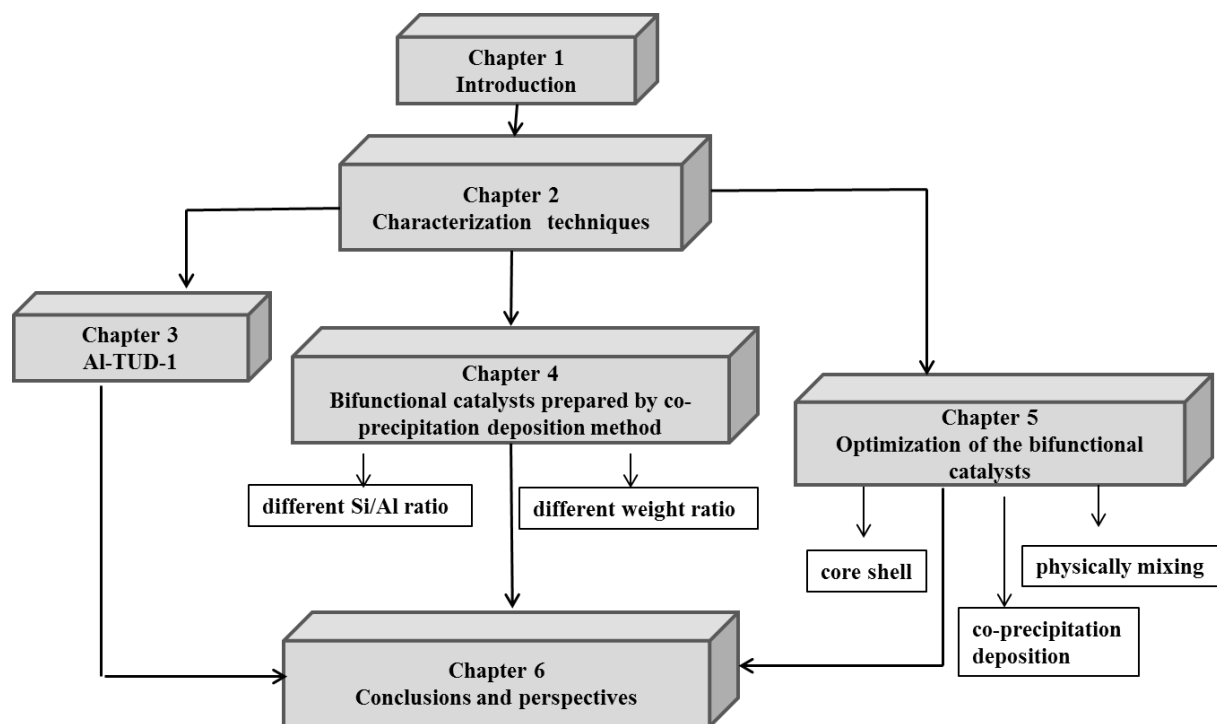


Figure 1-14 Thesis schematic flow-chart

## 1.5 References

- [1] O. Hoegh-Guldberg, P.J. Mumby, A.J. Hooten, R.S. Steneck, P. Greenfield, E. Gomez, C.D. Harvell, P.F. Sale, A.J. Edwards, K. Caldeira, N. Knowlton, C.M. Eakin, R. Iglesias-Prieto, N. Muthiga, R.H. Bradbury, A. Dubi, M.E. Hatziolos, Coral reefs under rapid climate change and ocean acidification, *Science*, 318 (2007) 1737-1742.
- [2] N.J. Rosenberg, W.E. Easterling III, P.R. Crosson, J. Darmstadter, *Greenhouse warming: Abatement and adaptation*, Routledge, 2016.
- [3] T. Witoon, T. Permsirivanich, N. Kanjanasootorn, C. Akkaraphataworn, A. Seubsai, K. Faungnawakij, C. Warakulwit, M. Chareonpanich, J. Limtrakul, Direct synthesis of dimethyl ether from CO<sub>2</sub> hydrogenation over Cu-ZnO-ZrO<sub>2</sub>/SO<sub>4</sub><sup>2-</sup>-ZrO<sub>2</sub> hybrid catalysts: effects of sulfur-to-zirconia ratios, *Catal Sci Technol*, 5 (2015) 2347-2357.
- [4] R.J. Andres, T.A. Boden, D.M. Higdon, Gridded uncertainty in fossil fuel carbon dioxide emission maps, a CDIAC example, *Atmos Chem Phys*, 16 (2016) 14979-14995.
- [5] Y. Tang, R.Z. Yang, X.Q. Bian, A Review of CO<sub>2</sub> Sequestration Projects and Application in China, *Sci World J*, (2014).
- [6] X. An, Y.Z. Zuo, Q. Zhang, D.Z. Wang, J.F. Wang, Dimethyl ether synthesis from CO<sub>2</sub> hydrogenation on a CuO-ZnO-Al<sub>2</sub>O<sub>3</sub>-ZrO<sub>2</sub>/HZSM-5 bifunctional catalyst, *Ind Eng Chem Res*, 47 (2008) 6547-6554.
- [7] S. Wang, D.S. Mao, X.M. Guo, G.S. Wu, G.Z. Lu, Dimethyl ether synthesis via CO<sub>2</sub> hydrogenation over CuO-TiO<sub>2</sub>-ZrO<sub>2</sub>/HZSM-5 bifunctional catalysts, *Catal Commun*, 10 (2009) 1367-1370.
- [8] S. Hu, M. Liu, F.S. Ding, C.S. Song, G.L. Zhang, X.W. Guo, Hydrothermally stable MOFs for CO<sub>2</sub> hydrogenation over iron-based catalyst to light olefins, *J CO<sub>2</sub> Util*, 15 (2016) 89-95.
- [9] J. Wei, J. Sun, Z.Y. Wen, C.Y. Fang, Q.J. Ge, H.Y. Xu, New insights into the effect of sodium on Fe<sub>3</sub>O<sub>4</sub>-based nanocatalysts for CO<sub>2</sub> hydrogenation to light olefins, *Catal Sci Technol*, 6 (2016) 4786-4793.
- [10] J.L. Zhang, S.P. Lu, X.J. Su, S.B. Fan, Q.X. Ma, T.S. Zhao, Selective formation of light olefins from CO<sub>2</sub> hydrogenation over Fe-Zn-K catalysts, *J CO<sub>2</sub> Util*, 12 (2015) 95-100.

- [11] K. Kobl, L. Angelo, Y. Zimmermann, S. Sall, K. Parkhomenko, A.C. Roger, In situ infrared study of formate reactivity on water-gas shift and methanol synthesis catalysts, *Cr Chim*, 18 (2015) 302-314.
- [12] L. Angelo, K. Kobl, L.M.M. Tejada, Y. Zimmermann, K. Parkhomenko, A.C. Roger, Study of CuZnMO<sub>x</sub> oxides (M = Al, Zr, Ce, CeZr) for the catalytic hydrogenation of CO<sub>2</sub> into methanol, *Cr Chim*, 18 (2015) 250-260.
- [13] Z.H. He, Q.L. Qian, J. Ma, Q.L. Meng, H.C. Zhou, J.L. Song, Z.M. Liu, B.X. Han, Water-Enhanced Synthesis of Higher Alcohols from CO<sub>2</sub> Hydrogenation over a Pt/Co<sub>3</sub>O<sub>4</sub> Catalyst under Milder Conditions, *Angew Chem Int Edit*, 55 (2016) 737-741.
- [14] M. Cui, Q.L. Qian, Z.H. He, Z.F. Zhang, J. Ma, T.B. Wu, G.Y. Yang, B.X. Han, Bromide promoted hydrogenation of CO<sub>2</sub> to higher alcohols using Ru-Co homogeneous catalyst, *Chem Sci*, 7 (2016) 5200-5205.
- [15] C. Arcoumanis, C. Bae, R. Crookes, E. Kinoshita, The potential of di-methyl ether (DME) as an alternative fuel for compression-ignition engines: A review, *Fuel*, 87 (2008) 1014-1030.
- [16] F. Frusteri, G. Bonura, C. Cannilla, G.D. Ferrante, A. Aloise, E. Catizzone, M. Migliori, G. Giordano, Stepwise tuning of metal-oxide and acid sites of CuZnZr-MFI hybrid catalysts for the direct DME synthesis by CO<sub>2</sub> hydrogenation, *Appl Catal B-Environ*, 176 (2015) 522-531.
- [17] J. Sun, G.H. Yang, Y. Yoneyama, N. Tsubaki, Catalysis Chemistry of Dimethyl Ether Synthesis, *Acs Catal*, 4 (2014) 3346-3356.
- [18] D.S. Mao, W.M. Yang, J.C. Xia, B. Zhang, Q.Y. Song, Q.L. Chen, Highly effective hybrid catalyst for the direct synthesis of dimethyl ether from syngas with magnesium oxide-modified HZSM-5 as a dehydration component, *J Catal*, 230 (2005) 140-149.
- [19] P.S.S. Prasad, J.W. Bae, S.H. Kang, Y.J. Lee, K.W. Jun, Single-step synthesis of DME from syngas on Cu-ZnO-Al<sub>2</sub>O<sub>3</sub>/zeolite bifunctional catalysts: The superiority of ferrierite over the other zeolites, *Fuel Process Technol*, 89 (2008) 1281-1286.
- [20] Z. Azizi, M. Rezaeimanesh, T. Tohidian, M.R. Rahimpour, Dimethyl ether: A review of technologies and production challenges, *Chem Eng Process*, 82 (2014) 150-172.

- [21] J. Abu-Dahrieh, D. Rooney, A. Goguet, Y. Saih, Activity and deactivation studies for direct dimethyl ether synthesis using CuO-ZnO-Al<sub>2</sub>O<sub>3</sub> with NH<sub>4</sub>ZSM-5, HZSM-5 or  $\gamma$ -Al<sub>2</sub>O<sub>3</sub>, *Chem Eng J*, 203 (2012) 201-211.
- [22] S. Lee, J.G. Speight, S.K. Loyalka, *Handbook of alternative fuel technologies*, crc Press, 2014.
- [23] Z. Li, J.Q. Li, M. Dai, Y.Q. Liu, D.Z. Han, J.H. Wu, The effect of preparation method of the Cu-La<sub>2</sub>O<sub>3</sub>-ZrO<sub>2</sub>/  $\gamma$ -Al<sub>2</sub>O<sub>3</sub> hybrid catalysts on one-step synthesis of dimethyl ether from syngas, *Fuel*, 121 (2014) 173-177.
- [24] F. Frusteri, M. Cordaro, C. Cannilla, G. Bonura, Multifunctionality of Cu-ZnO-ZrO<sub>2</sub>/ H-ZSM5 catalysts for the one-step CO<sub>2</sub>-to-DME hydrogenation reaction, *Appl Catal B-Environ*, 162 (2015) 57-65.
- [25] G. Bozzano, F. Manenti, Efficient methanol synthesis: Perspectives, technologies and optimization strategies, *Prog Energ Combust*, 56 (2016) 71-105.
- [26] E.L. Kunkes, F. Studt, F. Abild-Pedersen, R. Schlogl, M. Behrens, Hydrogenation of CO<sub>2</sub> to methanol and CO on Cu/ZnO/Al<sub>2</sub>O<sub>3</sub>: Is there a common intermediate or not?, *J Catal*, 328 (2015) 43-48.
- [27] F.Z. Meng, X.G. Li, M. Meng, Y. Ishizaka, N. Tsubaki, Effect of supercritical fluid of CO<sub>2</sub> drying during Cu/ZnO catalyst preparation on methanol synthesis from syngas at low temperature, *Res Chem Intermediat*, 37 (2011) 397-403.
- [28] H.Y. Yang, P. Gao, C. Zhang, L.S. Zhong, X.P. Li, S. Wang, H. Wang, W. Wei, Y.H. Sun, Core-shell structured Cu@m-SiO<sub>2</sub> and Cu/ZnO@m-SiO<sub>2</sub> catalysts for methanol synthesis from CO<sub>2</sub> hydrogenation, *Catal Commun*, 84 (2016) 56-60.
- [29] M. Behrens, A. Furche, I. Kasatkin, A. Trunschke, W. Busser, M. Muhler, B. Knief, R. Fischer, R. Schlogl, The Potential of Microstructural Optimization in Metal/ Oxide Catalysts: Higher Intrinsic Activity of Copper by Partial Embedding of Copper Nanoparticles, *Chemcatchem*, 2 (2010) 816-818.
- [30] B. Bems, M. Schur, A. Dassenoy, H. Junkes, D. Herein, R. Schlogl, Relations between synthesis and microstructural properties of copper/zinc hydroxycarbonates, *Chem-Eur J*, 9 (2003) 2039-2052.
- [31] M. Behrens, F. Girgsdies, A. Trunschke, R. Schlogl, Minerals as Model Compounds for Cu/ZnO Catalyst Precursors: Structural and Thermal Properties and IR Spectra of

Mineral and Synthetic (Zincian) Malachite, Rosasite and Aurichalcite and a Catalyst Precursor Mixture, *Eur J Inorg Chem*, (2009) 1347-1357.

[32] M. Schur, B. Bems, A. Dassenoy, I. Kassatkine, J. Urban, H. Wilmes, O. Hinrichsen, M. Muhler, R. Schlogl, Continuous coprecipitation of catalysts in a micromixer: Nanostructured Cu/ZnO composite for the synthesis of methanol, *Angew Chem Int Edit*, 42 (2003) 3815-3817.

[33] S. Kuhl, M. Friedrich, M. Armbruster, M. Behrens, Cu,Zn,Al layered double hydroxides as precursors for copper catalysts in methanol steam reforming - pH-controlled synthesis by microemulsion technique, *J Mater Chem*, 22 (2012) 9632-9638.

[34] S. Zander, E.L. Kunkes, M.E. Schuster, J. Schumann, G. Weinberg, D. Teschner, N. Jacobsen, R. Schlogl, M. Behrens, The Role of the Oxide Component in the Development of Copper Composite Catalysts for Methanol Synthesis, *Angew Chem Int Edit*, 52 (2013) 6536-6540.

[35] Z. Chu, H.B. Chen, Y. Yu, Q. Wang, D.Y. Fang, Surfactant-assisted preparation of Cu/ZnO/Al<sub>2</sub>O<sub>3</sub> catalyst for methanol synthesis from syngas, *J Mol Catal A-Chem*, 366 (2013) 48-53.

[36] F. Studt, M. Behrens, E.L. Kunkes, N. Thomas, S. Zander, A. Tarasov, J. Schumann, E. Frei, J.B. Varley, F. Abild-Pedersen, J.K. Norskov, R. Schlogl, The Mechanism of CO and CO<sub>2</sub> Hydrogenation to Methanol over Cu-Based Catalysts, *Chemcatchem*, 7 (2015) 1105-1111.

[37] H. Ren, C.H. Xu, H.Y. Zhao, Y.X. Wang, J. Liu, J.Y. Liu, Methanol synthesis from CO<sub>2</sub> hydrogenation over Cu/  $\gamma$ -Al<sub>2</sub>O<sub>3</sub> catalysts modified by ZnO, ZrO<sub>2</sub> and MgO, *J Ind Eng Chem*, 28 (2015) 261-267.

[38] Z.S. Hong, Y. Cao, J.F. Deng, K.N. Fan, CO<sub>2</sub> hydrogenation to methanol over Cu/ZnO/Al<sub>2</sub>O<sub>3</sub> catalysts prepared by a novel gel-network-coprecipitation method, *Catal Lett*, 82 (2002) 37-44.

[39] C. Baltes, S. Vukojevic, F. Schuth, Correlations between synthesis, precursor, and catalyst structure and activity of a large set of CuO/ZnO/Al<sub>2</sub>O<sub>3</sub> catalysts for methanol synthesis, *J Catal*, 258 (2008) 334-344.

- [40] L.X. Zhang, Y.C. Zhang, S.Y. Chen, Effect of promoter SiO<sub>2</sub>, TiO<sub>2</sub> or SiO<sub>2</sub>-TiO<sub>2</sub> on the performance of CuO-ZnO-Al<sub>2</sub>O<sub>3</sub> catalyst for methanol synthesis from CO<sub>2</sub> hydrogenation, *Appl Catal A-Gen*, 415 (2012) 118-123.
- [41] A. Garcia-Trenco, A. Martinez, A simple and efficient approach to confine Cu/ZnO methanol synthesis catalysts in the ordered mesoporous SBA-15 silica, *Catal Today*, 215 (2013) 152-161.
- [42] W.J. Cai, P.R. de la Piscina, J. Toyir, N. Homs, CO<sub>2</sub> hydrogenation to methanol over CuZnGa catalysts prepared using microwave-assisted methods, *Catal Today*, 242 (2015) 193-199.
- [43] J. Toyir, P.R. de la Piscina, J.L.G. Fierro, N. Homs, Catalytic performance for CO<sub>2</sub> conversion to methanol of gallium-promoted copper-based catalysts: influence of metallic precursors, *Appl Catal B-Environ*, 34 (2001) 255-266.
- [44] J. Toyir, P.R. de la Piscina, J.L.G. Fierro, N. Homs, Highly effective conversion of CO<sub>2</sub> to methanol over supported and promoted copper-based catalysts: influence of support and promoter, *Appl Catal B-Environ*, 29 (2001) 207-215.
- [45] G. Bonura, M. Cordaro, C. Cannilla, F. Arena, F. Frusteri, The changing nature of the active site of Cu-Zn-Zr catalysts for the CO<sub>2</sub> hydrogenation reaction to methanol, *Appl Catal B-Environ*, 152 (2014) 152-161.
- [46] G. Bonura, F. Arena, G. Mezzatesta, C. Cannilla, L. Spadaro, F. Frusteri, Role of the ceria promoter and carrier on the functionality of Cu-based catalysts in the CO<sub>2</sub>-to-methanol hydrogenation reaction, *Catal Today*, 171 (2011) 251-256.
- [47] F. Arena, G. Italiano, K. Barbera, G. Bonura, L. Spadaro, F. Frusteri, Basic evidences for methanol-synthesis catalyst design, *Catal Today*, 143 (2009) 80-85.
- [48] F. Arena, G. Italiano, K. Barbera, S. Bordiga, G. Bonura, L. Spadaro, F. Frusteri, Solid-state interactions, adsorption sites and functionality of Cu-ZnO/ZrO<sub>2</sub> catalysts in the CO<sub>2</sub> hydrogenation to CH<sub>3</sub>OH, *Appl Catal A-Gen*, 350 (2008) 16-23.
- [49] F. Arena, K. Barbera, G. Italiano, G. Bonura, L. Spadaro, F. Frusteri, Synthesis, characterization and activity pattern of Cu-ZnO/ZrO<sub>2</sub> catalysts in the hydrogenation of carbon dioxide to methanol, *J Catal*, 249 (2007) 185-194.

- [50] Y.Q. Zhao, J.X. Chen, J.Y. Zhang, Effects of  $\text{ZrO}_2$  on the performance of  $\text{CuO-ZnO-Al}_2\text{O}_3/\text{HZSM-5}$  catalyst for dimethyl ether synthesis from  $\text{CO}_2$  hydrogenation, *J Nat Gas Chem*, 16 (2007) 389-392.
- [51] J.B. Ko, C.M. Bae, Y.S. Jung, D.H. Kim,  $\text{Cu-ZrO}_2$  catalysts for water-gas-shift reaction at low temperatures, *Catal Lett*, 105 (2005) 157-161.
- [52] P. Gao, F. Li, N. Zhao, F.K. Xiao, W. Wei, L.S. Zhong, Y.H. Sun, Influence of modifier (Mn, La, Ce, Zr and Y) on the performance of  $\text{Cu/Zn/Al}$  catalysts via hydrotalcite-like precursors for  $\text{CO}_2$  hydrogenation to methanol, *Appl Catal A-Gen*, 468 (2013) 442-452.
- [53] P. Gao, F. Li, H.J. Zhan, N. Zhao, F.K. Xiao, W. Wei, L.S. Zhong, H. Wang, Y.H. Sun, Influence of Zr on the performance of  $\text{Cu/Zn/Al/Zr}$  catalysts via hydrotalcite-like precursors for  $\text{CO}_2$  hydrogenation to methanol, *J Catal*, 298 (2013) 51-60.
- [54] R.W. Liu, Z.Z. Qin, H.B. Ji, T.M. Su, Synthesis of Dimethyl Ether from  $\text{CO}_2$  and  $\text{H}_2$  Using a  $\text{Cu-Fe-Zr}/\text{HZSM-5}$  Catalyst System, *Ind Eng Chem Res*, 52 (2013) 16648-16655.
- [55] K. Sirichalprasert, A. Luengnaruemitchai, S. Pongstabodee, Selective oxidation of  $\text{CO}$  to  $\text{CO}_2$  over  $\text{Cu-Ce-Fe-O}$  composite-oxide catalyst in hydrogen feed stream, *Int J Hydrogen Energ*, 32 (2007) 915-926.
- [56] C.S. Chen, W.H. Cheng, S.S. Lin, Study of iron-promoted  $\text{Cu}/\text{SiO}_2$  catalyst on high temperature reverse water gas shift reaction, *Appl Catal A-Gen*, 257 (2004) 97-106.
- [57] S.G. Lee, A. Sardesai, Liquid phase methanol and dimethyl ether synthesis from syngas, *Top Catal*, 32 (2005) 197-207.
- [58] Y. Guo, Y.W. Wang, H.S. Li, J.H. Li, J.F. Wang, Cu-based catalyst LP201 for one-step synthesis of dimethyl ether from syngas in three-phase process, *Chinese J Catal*, 25 (2004) 429-430.
- [59] Z.Z. Qin, X.H. Zhou, T.M. Su, Y.X. Jiang, H.B. Ji, Hydrogenation of  $\text{CO}_2$  to dimethyl ether on La-, Ce-modified  $\text{Cu-Fe}/\text{HZSM-5}$  catalysts, *Catal Commun*, 75 (2016) 78-82.
- [60] K. Kilian, Aspects mécanistiques et cinétiques de la production catalytique de méthanol à partir de  $\text{CO}_2/\text{H}_2$ , Université de Strasbourg, 2015.

- [61] L. Angelo, Développement de catalyseurs pour la synthèse de méthanol produit par hydrogénation du dioxyde de carbone, Strasbourg, 2014.
- [62] M. Hirano, T. Yasutake, K. Kuroda, Dimethyl ether synthesis from carbon dioxide by catalytic hydrogenation, *Kansai Denryoku KK Soken Hokoku*, 60 (2002) 138-142.
- [63] M. Stiefel, R. Ahmad, U. Arnold, M. Doring, Direct synthesis of dimethyl ether from carbon-monoxide-rich synthesis gas: Influence of dehydration catalysts and operating conditions, *Fuel Process Technol*, 92 (2011) 1466-1474.
- [64] A.R. Keshavarz, M. Rezaei, F. Yaripour, Nanocrystalline  $\gamma$ -alumina: A highly active catalyst for dimethyl ether synthesis, *Powder Technol*, 199 (2010) 176-179.
- [65] D.S. Mao, W.M. Yang, J.C. Xia, B. Zhang, G.Z. Lu, The direct synthesis of dimethyl ether from syngas over hybrid catalysts with sulfate-modified  $\gamma$ -alumina as methanol dehydration components, *J Mol Catal A-Chem*, 250 (2006) 138-144.
- [66] L.D. Brake, Preparation of dimethyl ether by catalytic dehydration of methanol, Google Patents, 1986.
- [67] K.W. Jun, H.S. Lee, H.S. Roh, S.E. Park, Catalytic dehydration of methanol to dimethyl ether (DME) over solid-acid catalysts, *B Korean Chem Soc*, 23 (2002) 803-806.
- [68] F. Yaripour, F. Baghaei, I. Schmidt, J. Perregaard, Catalytic dehydration of methanol to dimethyl ether (DME) over solid-acid catalysts, *Catal Commun*, 6 (2005) 147-152.
- [69] Z. Hosseini, M. Taghizadeh, F. Yaripour, Synthesis of nanocrystalline  $\gamma$ - $\text{Al}_2\text{O}_3$  by sol-gel and precipitation methods for methanol dehydration to dimethyl ether, *J Nat Gas Chem*, 20 (2011) 128-134.
- [70] S. Hosseini, M. Taghizadeh, A. Eliassi, Optimization of hydrothermal synthesis of H-ZSM-5 zeolite for dehydration of methanol to dimethyl ether using full factorial design, *J Nat Gas Chem*, 21 (2012) 344-351.
- [71] A. Garcia-Trenco, A. Martinez, Direct synthesis of DME from syngas on hybrid CuZnAl/ ZSM-5 catalysts: New insights into the role of zeolite acidity, *Appl Catal A-Gen*, 411 (2012) 170-179.
- [72] T. Takeguchi, K. Yanagisawa, T. Inui, M. Inoue, Effect of the property of solid acid upon syngas-to-dimethyl ether conversion on the hybrid catalysts composed of Cu-Zn-Ga and solid acids, *Appl Catal A-Gen*, 192 (2000) 201-209.

- [73] B. Sabour, M.H. Peyrovi, T. Hamoule, M. Rashidzadeh, Catalytic dehydration of methanol to dimethyl ether (DME) over Al-HMS catalysts, *J Ind Eng Chem*, 20 (2014) 222-227.
- [74] R. Anand, R. Maheswari, U. Hanefeld, Catalytic properties of the novel mesoporous aluminosilicate AlTUD-1, *J Catal*, 242 (2006) 82-91.
- [75] Z. Shan, J.C. Jansen, L. Marchese, T. Maschmeyer, Synthesis, characterization and catalytic testing of a 3-D mesoporous titanosilica, Ti-TUD-1, *Micropor Mesopor Mat*, 48 (2001) 181-187.
- [76] K.P. de Jong, A.J. Koster, A.H. Janssen, U. Ziese, Electron tomography of molecular sieves, *Zeolites and Ordered Mesoporous Materials: Progress and Prospects*, 157 (2005) 225-242.
- [77] S. Telalovic, A. Ramanathan, G. Mul, U. Hanefeld, TUD-1: synthesis and application of a versatile catalyst, carrier, material ... *J Mater Chem*, 20 (2010) 642-658.
- [78] Z. Shan, J.C. Jansen, W. Zhou, T. Maschmeyer, Al-TUD-1, stable mesoporous aluminas with high surface areas, *Appl Catal A-Gen*, 254 (2003) 339-343.
- [79] A. Ranoux, K. Djanashvili, I.W.C.E. Arends, U. Hanefeld, B-TUD-1: a versatile mesoporous catalyst, *Rsc Adv*, 3 (2013) 21524-21534.
- [80] S. Mandal, S. Rahman, R. Kumar, K.K. Bando, B. Chowdhury, XAFS, XPS characterization of cerium promoted Ti-TUD-1 catalyst and its activity for styrene oxidation reaction, *Catal Commun*, 46 (2014) 123-127.
- [81] W. Wei, J.A. Moulijn, G. Mul, FAPO and Fe-TUD-1: Promising catalysts for N<sub>2</sub>O mediated selective oxidation of propane?, *J Catal*, 262 (2009) 1-8.
- [82] M.S. Hamdy, G. Mul, W. Wei, R. Anand, U. Hanefeld, J.C. Jansen, J.A. Moulijn, Fe, Co and Cu-incorporated TUD-1: Synthesis, characterization and catalytic performance in N<sub>2</sub>O decomposition and cyclohexane oxidation, *Catal Today*, 110 (2005) 264-271.
- [83] M.S. Hamdy, A. Ramanathan, T. Maschmeyer, U. Hanefeld, J.C. Jansen, Co-TUD-1: A ketone-selective catalyst for cyclohexane oxidation, *Chem-Eur J*, 12 (2006) 1782-1789.
- [84] A. Ramanathan, M.S. Hamdy, R. Parton, T. Maschmeyer, J.C. Jansen, U. Hanefeld, Co-TUD-1 catalysed aerobic oxidation of cyclohexane, *Appl Catal A-Gen*, 355 (2009) 78-82.

- [85] B. Karmakar, A. Sinhamahapatra, A.B. Panda, J. Banerji, B. Chowdhury, Ga-TUD-1: A new heterogeneous mesoporous catalyst for the solventless expeditious synthesis of alpha-aminonitriles, *Appl Catal A-Gen*, 392 (2011) 111-117.
- [86] S. Mandal, A. SinhaMahapatra, B. Rakesh, R. Kumar, A. Panda, B. Chowdhury, Synthesis, characterization of Ga-TUD-1 catalyst and its activity towards styrene epoxidation reaction, *Catal Commun*, 12 (2011) 734-738.
- [87] X.Y. Quek, D.P. Liu, W.N.E. Cheo, H. Wang, Y. Chen, Y.H. Yang, Nickel-grafted TUD-1 mesoporous catalysts for carbon dioxide reforming of methane, *Appl Catal B-Environ*, 95 (2010) 374-382.
- [88] G. Imran, M.P. Pachamuthu, R. Maheswari, A. Ramanathan, S.J.S. Basha, Catalytic activity of MnTUD-1 for liquid phase oxidation of ethylbenzene with tert-butyl hydroperoxide, *J Porous Mat*, 19 (2012) 677-682.
- [89] A. Ramanathan, M.C.C. Villalobos, C. Kwakernaak, S. Telalovic, U. Hanefeld, Zr-TUD-1: A lewis acidic, three-dimensional, mesoporous, zirconium-containing catalyst, *Chem-Eur J*, 14 (2008) 961-972.
- [90] M.P. Pachamuthu, V.V. Srinivasan, R. Maheswari, K. Shanthi, A. Ramanathan, Lewis acidic ZrTUD-1 as catalyst for tert-butylation of phenol, *Appl Catal A-Gen*, 462 (2013) 143-149.
- [91] R. Maheswari, M.P. Pachamuthu, R. Anand, Copper containing TUD-1: synthesis, characterization and catalytic behavior in liquid-phase oxidation of ethylbenzene, *J Porous Mat*, 19 (2012) 103-110.
- [92] M.P. Pachamuthu, A. Ramanathan, K. Santhi, R. Maheswari, Characterization and Catalytic activity of Cu-TUD-1 for Styrene Epoxidation, *Acs Sym Ser*, 1132 (2013) 195-211.
- [93] S. Telalovic, S.K. Karmee, A. Ramanathan, U. Hanefeld, Al-TUD-1: Introducing tetrahedral aluminium, *J Mol Catal A-Chem*, 368 (2013) 88-94.
- [94] C. Simons, U. Hanefeld, I.W.C.E. Arends, R.A. Sheldon, T. Maschmeyer, Noncovalent anchoring of asymmetric hydrogenation catalysts on a new mesoporous aluminosilicate: Application and solvent effects, *Chem-Eur J*, 10 (2004) 5829-5835.

- [95] R. Khoshbin, M. Haghghi, Direct syngas to DME as a clean fuel: The beneficial use of ultrasound for the preparation of CuO-ZnO-Al<sub>2</sub>O<sub>3</sub>/ HZSM-5 nanocatalyst, *Chem Eng Res Des*, 91 (2013) 1111-1122.
- [96] C.Y. Zeng, J. Sun, G.H. Yang, I. Ooki, K. Hayashi, Y. Yoneyama, A. Taguchi, T. Abe, N. Tsubaki, Highly selective and multifunctional Cu/ZnO/Zeolite catalyst for one-step dimethyl ether synthesis: Preparing catalyst by bimetallic physical sputtering, *Fuel*, 112 (2013) 140-144.
- [97] K.P. Sun, W.W. Lu, F.Y. Qiu, S.W. Liu, X.L. Xu, Direct synthesis of DME over bifunctional catalyst: surface properties and catalytic performance, *Appl Catal A-Gen*, 252 (2003) 243-249.
- [98] Y. Wang, W.L. Wang, Y.X. Chen, J.H. Ma, R.F. Li, Synthesis of dimethyl ether from syngas over core-shell structure catalyst CuO-ZnO-Al<sub>2</sub>O<sub>3</sub>@SiO<sub>2</sub>-Al<sub>2</sub>O<sub>3</sub>, *Chem Eng J*, 250 (2014) 248-256.
- [99] J.W. Bae, S.H. Kang, Y.J. Lee, K.W. Jun, Synthesis of DME from syngas on the bifunctional Cu-ZnO-Al<sub>2</sub>O<sub>3</sub>/ Zr-modified ferrierite: Effect of Zr content, *Appl Catal B-Environ*, 90 (2009) 426-435.
- [100] A.T. Aguayo, J. Erena, I. Sierra, M. Olazar, J. Bilbao, Deactivation and regeneration of hybrid catalysts in the single-step synthesis of dimethyl ether from syngas and CO<sub>2</sub>, *Catal Today*, 106 (2005) 265-270.
- [101] V.V. Ordonsky, M. Cai, V. Sushkevich, S. Moldovan, O. Ersen, C. Lancelot, V. Valtchev, A.Y. Khodakov, The role of external acid sites of ZSM-5 in deactivation of hybrid CuZnAl/ ZSM-5 catalyst for direct dimethyl ether synthesis from syngas, *Appl Catal A-Gen*, 486 (2014) 266-275.
- [102] A.Q. Wang, Y. Hsieh, Y.F. Chen, C.Y. Mou, Au-Ag alloy nanoparticle as catalyst for CO oxidation: Effect of Si/Al ratio of mesoporous support, *J Catal*, 237 (2006) 197-206.
- [103] A.Y. Yin, X.Y. Guo, W.L. Dai, K.N. Fan, Effect of Si/Al Ratio of Mesoporous Support on the Structure Evolution and Catalytic Performance of the Cu/ Al-HMS Catalyst, *J Phys Chem C*, 114 (2010) 8523-8532.

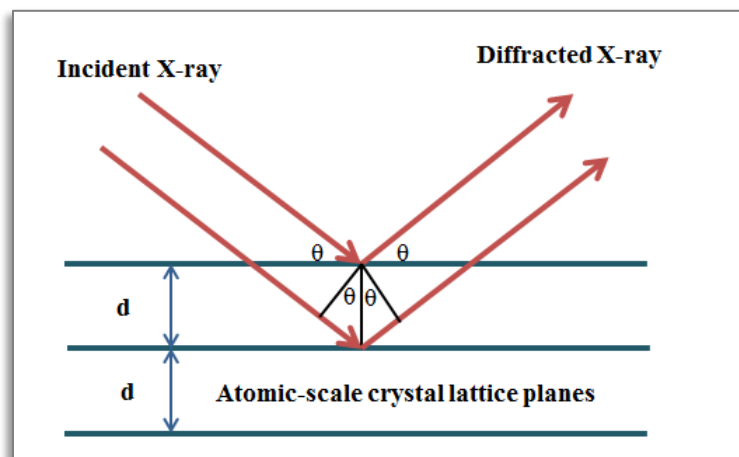
[104] F.S.R. Barbosa, V.S.O. Ruiz, J.L.F. Monteiro, R.R. de Avillez, L.E.P. Borges, L.G. Appel, The Deactivation Modes of Cu/ZnO/Al<sub>2</sub>O<sub>3</sub> and HZSM-5 Physical Mixture in the One-Step DME Synthesis, *Catal Lett*, 126 (2008) 173-178.

[105] G.R. Moradi, S. Nosrati, F. Yaripor, Effect of the hybrid catalysts preparation method upon direct synthesis of dimethyl ether from synthesis gas, *Catal Commun*, 8 (2007) 598-606.

[106] J. Erena, I. Sierra, M. Azar, A.G. Gayubo, A.T. Aguayo, Deactivation of a CuO-ZnO-Al<sub>2</sub>O<sub>3</sub>/  $\gamma$ -Al<sub>2</sub>O<sub>3</sub> catalyst in the synthesis of dimethyl ether, *Ind Eng Chem Res*, 47 (2008) 2238-2247.

[107] K.S. Yoo, J.H. Kim, M.J. Park, S.J. Kimb, O.S. Joo, K.D. Jung, Influence of solid acid catalyst on DME production directly from synthesis gas over the admixed catalyst of Cu/ZnO/Al<sub>2</sub>O<sub>3</sub> and various SAPO catalysts, *Appl Catal A-Gen*, 330 (2007) 57-62.

## *Chapter 2: Experimental techniques*





## 2.1 Catalysts characterization

### 2.1.1 N<sub>2</sub> adsorption/ desorption measurement

The textural properties of material can be measured by N<sub>2</sub> adsorption/desorption method. It can give the information of specific surface area, pore volume and pore distribution, which is of significance for materials. For example, the big surface area provides more possibility for the contact of reactant with catalyst. Molecular sieve is employed in gas separation process based on pore size and dynamic diameter of gas molecular. The pores in porous material can be classified by micropore (< 2nm), such as zeolite, activated carbon, metal organic framework, mesopore (2-50 nm), such as mesoporous silica, activated carbon and macropore (> 50 nm), such as sintered metals and ceramics according to the pore size [1].

In our case, the textural properties of catalysts were characterized by nitrogen adsorption/ desorption measurements at -77 °C on Micromeritics ASAP 2420 apparatus. Specific surface area was calculated by Brunauer– Emmet– Teller (BET) method. Pore volume was determined by Barrett- Joyner- Halenda (BJH) method. Pore distribution were determined using desorption branch by BJH method. Catalysts were degassed under vacuum at 250 °C over night to desorb the physisorbed moisture before analysis.

### 2.1.2 X-ray powder diffraction (XRD)

XRD is a rapid and widely used analytical technique, which can provide the information of composition from details of phases present in the sample, lattice parameter, crystal structure, hkl parameters, crystallinesize (estimated from Scherrer equation) and so on.

When a sample is irradiated by X-rays with certain wavelength and at certain incident angles, intense reflected X-rays are produced when the wavelengths of the scattered X-rays interfere constructively, which is well known as Bragg's Law (Figure 2-1). The diffraction peaks including positions and intensities provide informations of the sample.

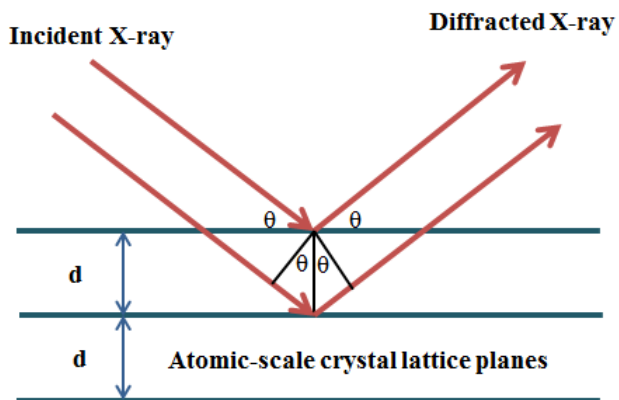


Figure 2- 1 Bragg's Law reflection

The Scherrer equation was always used to determine the crystalline size, which was described as following,

$$d = \frac{k\lambda}{\beta \cos(\theta)}$$

Where,

$d$  is the average crystalline size,

$\lambda$  is the X-ray wavelength.

$k$  is dimensionless shape factor with the value of 0.89,

$\beta$  is the full width at half maximum of the diffraction peak (FWHM),

$\theta$  is the Bragg angle.

XRD measurements were carried out on a Bruker D-8 Advance diffractometer with a Cu K $\alpha$  radiation in the 10-100° ( $2\theta$ ) range with a scan step of 0.020°. The characteristic incident X-ray by Cu radiation is 1.5418 Å.

### 2.1.3 Thermo-gravimetric analysis (TGA)

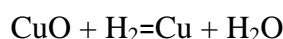
Thermo-gravimetric analysis (TGA) is used for the measurement of weight change with the increase of temperature for the material. It can provide the

information about phase transition. As for catalyst, it is an important tool for choosing the calcination temperature and measuring the carbon deposition after reaction.

Thermo-gravimetric analyses of our sample were carried out on a Setaram apparatus under air with the flow rate of 25 ml/min and with the ramp of 10 °C/min to 750 °C.

#### 2.1.4 Temperature programmed reduction (TPR)

Temperature programmed reduction (TPR) can be employed to understand reduction temperature of metal oxides in catalyst and get the further information such as reducibility from the H<sub>2</sub> consumption. TPR was carried out on Micromeritics Auto-Chem II 2920. 50mg catalyst was loaded in “U” shape quartz cell and flushed with 10% H<sub>2</sub>/Ar until baseline is stable. To reduce the samples, they were heated from room temperature to 500 °C with temperature rate of 10 °C/min under 10% H<sub>2</sub>/Ar (flow rate 50 mL/min) and kept at 500 °C until baseline is stable. The H<sub>2</sub> consumption signal was recorded by thermal conductivity detector (TCD). The H<sub>2</sub> consumption peak was integrated and the H<sub>2</sub> consumption was given automatically according to the pre calibration by 10% H<sub>2</sub>/Ar. The consumption of H<sub>2</sub> was assumed by the reduction of CuO, because the reduction of Zn species needs higher temperature [2]. The reduction stoichiometry of CuO by H<sub>2</sub> was described as following:



The temperature programmed reduction of catalysts with the temperature ramp of 1 °C/min were also performed to determine the reduction temperature of catalyst for reaction.

The reduction degree of copper was reflected by the reducibility ( $R_{\text{copper}}$ ), which is calculated by the H<sub>2</sub> consumption calculated from TPR divided by theoretical H<sub>2</sub> consumption needed for the reduction of all the reducible elements of the sample (theoretical copper content from synthesis).

$$R_{\text{copper}} = (\text{H}_2 \text{ consumption from TPR} / \text{theoretical H}_2 \text{ consumption}) * 100\%$$

### **2.1.5 Temperature programmed desorption of NH<sub>3</sub> (NH<sub>3</sub>-TPD)**

Acidic properties of catalysts were characterized by NH<sub>3</sub> temperature programmed desorption (NH<sub>3</sub>-TPD) on Micromeritics ASAP-2100 setup. The strength of the acid sites can be reflected by the NH<sub>3</sub> desorption temperature [3]. The stronger the acid sites, the higher the desorption temperature [4].

For the Al-TUD-1 samples

Samples were heated in He from room temperature to 400 °C to clean the surface. Afterwards they were saturated with 5% NH<sub>3</sub>/He with flow rate of 50ml/min for 8h (make sure the adsorption is saturated) at 100 °C and then were purged by 50ml/min He for 4h until equilibrium. The desorption process was performed from 100-750 °C with the heating rate of 5 °C/min. The signals were recorded by MS detector. The 5% NH<sub>3</sub>/Ar was calibrated before to know the relations between NH<sub>3</sub> area and the NH<sub>3</sub> amount, and then to calculate the amount of acid sites on these samples.

For bifunctional catalysts

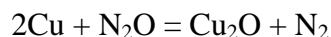
Samples were heated in H<sub>2</sub> from room temperature to 280 °C with the ramp of 1 °C/min and stayed at 280 °C for 1h in order to be reduced completely. The other procedures followed were the same as described above for Al-TUD-1 samples.

### **2.1.6 Temperature programmed desorption of CO<sub>2</sub> (CO<sub>2</sub>-TPD)**

The surface basic property was determined by CO<sub>2</sub> temperature programmed desorption (CO<sub>2</sub>-TPD) [5], which was carried out on the Micromeritics ASAP-2100 setup. It follows the sample principle as the NH<sub>3</sub>-TPD. CO<sub>2</sub> is the small acid gas molecule, so it can be employed to measure the basic property [6]. Firstly, samples were loaded in in “U” shape quartz cell and heated under 10% H<sub>2</sub>/Ar (50 ml/min) from room temperature to 280 °C with the ramp of 1 °C/min and stayed at 280 °C for 1h to reduce the catalyst. Afterwards, the temperature decreased to 100 °C. Catalysts were saturated with 5% CO<sub>2</sub>/He with the flow rate of 50ml/min for 8h and purged with 50ml/min He for 4h. Then the temperature was programmed increased to 700 °C with the ramp of 10 °C. The signals of outlet were recorded by MS detector.

### 2.1.7 Temperature programmed desorption of N<sub>2</sub>O (N<sub>2</sub>O-TPD)

Surface metallic copper was characterized by N<sub>2</sub>O temperature programmed desorption (N<sub>2</sub>O-TPD) which is carried out on Micromeritics Auto- Chem II 2920. Firstly, 400 mg catalyst was reduced under flow of 10% H<sub>2</sub>/Ar (flow rate 50 mL/min) at 280 °C overnight with heating rate of 1 °C/min. Then it was oxidized by 2% N<sub>2</sub>O/Ar (which was obtained by dilution of 10% N<sub>2</sub>O/Ar by Ar) for 15min at 50 °C. The N<sub>2</sub> signal was recorded by thermal conductivity detector (TCD). The equation was described as:



The N<sub>2</sub>O-TPD profile is shown in Figure 2- 2. It can be seen that the top of the curve is flat, which can be assumed that the injected N<sub>2</sub>O was completely converted to N<sub>2</sub> (100% N<sub>2</sub>).

After taking a specific value of  $\Delta t$ , the area of A1 (light blue area) can be calculated as,

$$A1 = Y1 * \Delta t$$

The amount of N<sub>2</sub> produced is equal to the amount of N<sub>2</sub>O injected, which can be calculated as,

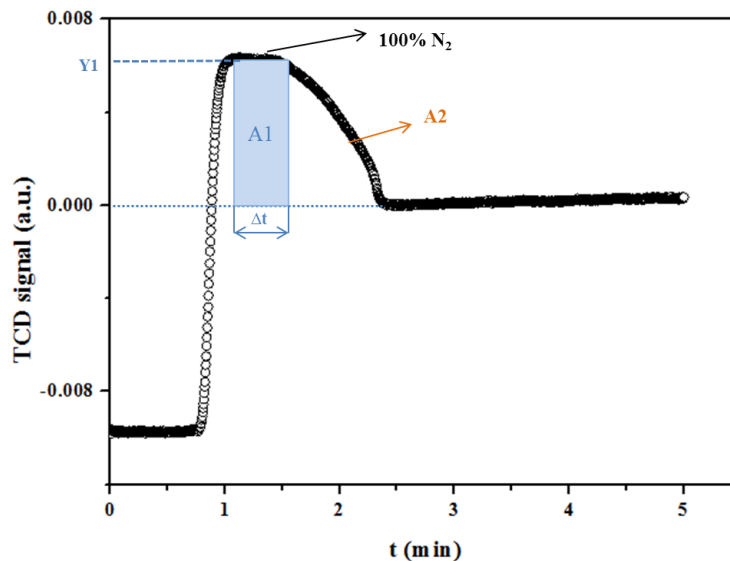
$$n1 = 50 \text{ ml/min} * 0.001 * 2\% * \Delta t / 22.4$$

The area of the curve between Y1 and Y=0 can be integrated automatically, which is A2. The total amount of N<sub>2</sub> produced can be calculated as,

$$n2 = n1 * (A2 / A1)$$

It is known that  $6.02 * 10^{23}$  atoms are existed in 1 mol substance. The surface area of Cu<sup>0</sup> was determined by assuming  $1.47 * 10^{19}$  Cu atoms/ m<sup>2</sup>. Considering all the conditions above, the metallic copper surface area per gram catalyst can be calculated as,

$$S_{\text{Cu}^0} = 2 * n2 * 6.02 * 10^{23} / (1.47 * 10^{19} * m_{\text{cata}})$$

Figure 2- 2 N<sub>2</sub>O-TPD profile

The copper dispersion ( $D_{\text{copper}}$ ) was calculated by the surface copper calculated from N<sub>2</sub>O-TPD divided by the H<sub>2</sub> consumption from H<sub>2</sub>-TPR before the chemisorption of N<sub>2</sub>O [7].

$$D_{\text{copper}} = (n_{\text{surface copper}} / n_{\text{H}_2 \text{ consumption}}) * 100\%$$

### 2.1.8 Transmission electron microscopy (TEM)<sup>1</sup>

In the transmission electron microscopy (TEM), a beam of electrons were accelerated and then were transmitted onto the very thin sample layer. The electrons interact with the atoms in sample thus influencing the direction of electrons and generating the solid angle scattering. Scattering angle is relevant with the density and thickness of the sample, so it can present the image with different intensity. The images can be magnified and focused on the image device.

The procedures for preparing samples for TEM is as: firstly, the sample was grinded into very fine powders. It was dispersed in ethanol under ultra sound for 3 min. Then one drop of liquid was deposited on copper grid. After evedorated under room temperature, it was transferred into the chamber of TEM. It was operated on Topcon EM002B microscope.

<sup>1</sup> Acknowledgements to Corinne BOUILLET from IPCMS for the TEM characterization

## 2.2 Catalytic tests

In this part, two different reactions are described, the methanol dehydration to DME reaction and the direct DME synthesis. In both cases, the schemes of the setup and the operating conditions are presented as well as the details of products' analyses and the calculations of conversions and selectivities.

### 2.2.1 Methanol dehydration to DME

The methanol dehydration to DME reaction is presented in the equation 2-1.



DME formation was monitored at 280 °C and 1 bar in diluted CH<sub>3</sub>OH/Ar mixture with total flow rate of 40 ml/min. CH<sub>3</sub>OH or CH<sub>3</sub>OH + water mixture was generated by the bubbling system at 0 °C (see Figure 2- 3).

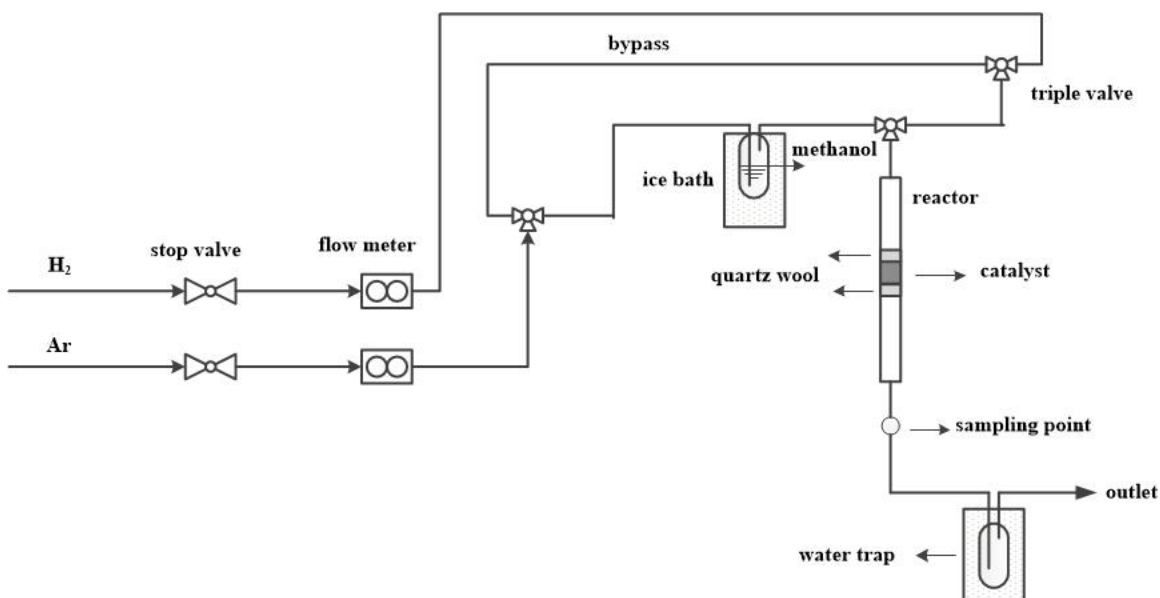


Figure 2- 3 Scheme of the methanol dehydration to DME reaction setup

Methanol was kept in the ice bath. The reactor was heated by the thermocoax heating line. The temperature was controlled by placing the thermocouple outside of the reactor with the end at the level of the catalyst bed. The reactor and the thermocouple were isolated to keep the temperature stable. The gas flows were measured by the flow

meters purchased from BROOKS Company. The hydrogen flow rate for the reduction of the catalytic materials was 9.47 mL/min. The Ar flow rate was 40 mL/min, which is used as a vector gas for methanol.

The analysis of reaction products was performed by gas chromatography on Agilent Technologies 6890N, equipped with SOLGELWAX column (length of 60 m, diameter of 0.25 mm and thickness of 0.25  $\mu\text{m}$ ) and FID detector. The gas sampling was performed with the aid of a syringe (0-2.5ml) through the septum (diameter of 11 mm) placed at the exit of the reactor.

For methanol dehydration reaction on both Al-TUD-1 materials and bifunctional materials, no online analysis is employed. The carbon balance is not considered and only comparison between samples in terms of methanol conversion, DME, MF and  $\text{CH}_4$  selectivity are calculated.

### **2.2.1.1 Methanol concentration**

#### Pure methanol as reactant

When pure methanol was used as the reactant, the methanol concentration in the gas phase with argon which goes to the reactor was calculated as following:

According to Antoine's equation [8]:

$$\text{Log}_{10} P \text{ mm Hg} = 7.87863 - 1473.11 / (230.0 + T)$$

When  $T = 0 \text{ }^\circ\text{C}$ ,  $\text{Log}_{10} P \text{ mm Hg} = 1.4738039$

$$P \text{ mm Hg} = 29.7717 \text{ mm Hg} = 3969.2 \text{ Pa}$$

According to  $PV = nRT$

$$C = n/V = P / RT = 3969.2 / (8.315 * 273.15) = 1.7476 \text{ mol/m}^3$$

When  $T = 0 \text{ }^\circ\text{C}$ ,  $P = 101.325 \text{ k Pa}$ ,  $V_m = 22.4 \text{ L/mol}$

Methanol concentration =  $1.7476 * 22.4 / 1000 = 3.9 \%$  (molar concentration)

So when pure methanol was used as the reactant its concentration in the gas phase was 3.91 %.

Water/methanol mixture as reactant

In order to investigate the water influence, methanol and water mixture was used. 14.8g water was mixed with 5.2g methanol and was placed in the bubbler at 0 °C. The methanol and water concentration in the gas phase was calculated as following:

The concentration of methanol in mixture (methanol and water) solution:

$$C_{\text{methanol}} = n_{\text{methanol}} / (n_{\text{methanol}} + n_{\text{water}}) = (5.2 / 32) / (5.2 / 32 + 14.8 / 18) = 16.5\%$$

The concentration of water in mixture solution:

$$C_{\text{water}} = n_{\text{water}} / (n_{\text{methanol}} + n_{\text{water}}) = (14.8 / 18) / (5.2 / 32 + 14.8 / 18) = 83.5\%$$

The saturated vapor pressure of methanol ( $P_w$ , methanol) and water ( $P_w$ , water) at 0 °C are 3.969 k Pa and 0.6113 k Pa, respectively.

The partial pressure of water:

$$P_{\text{water}} = P_{w, \text{water}} * C_{\text{water}} = 0.6113 * 83.5\% = 0.5104 \text{ k Pa}$$

The partial pressure of methanol:

$$P_{\text{methanol}} = P_{w, \text{methanol}} * C_{\text{methanol}} = 3.969 * 16.5\% = 0.6549 \text{ k Pa}$$

The concentration of saturated methanol vapor in gas phase:

$$C_{\text{methanol}}' = P_{\text{methanol}} / RT = 0.6549 * 1000 / (8.315 * 273.15) = 0.2883 \text{ mol / m}^3$$

The concentration of saturated water vapor in gas phase:

$$C_{\text{water}}' = P_{\text{water}} / RT = 0.5104 * 1000 / (8.315 * 273.15) = 0.2247 \text{ mol / m}^3$$

When  $T=0$  °C,  $P= 101.325$  k Pa,  $V_m=22.4$  L/mol

Methanol concentration =  $0.2883 * 22.4 / 1000 = 0.6\%$  (molar concentration)

Water concentration =  $0.2247 \times 22.4 / 1000 = 0.5\%$  (molar concentration)

So when the methanol and water mixture was used as the reactant, the methanol and water concentration in the gas phase are 0.6% and 0.5%, respectively. The using methanol/H<sub>2</sub>O mixture methanol quantity is 7 times smaller. Water produced during the reaction is also considered.

### 2.2.1.2 Methanol dehydration to DME on Al-TUD-1

The response factors [9] for methanol, methyl formate, DME and methane are shown in Table 2- 1.

Table 2- 1 Response factors

Compound	Response factor
methanol	0.23
methyl formate	0.22
DME	0.46
methane	0.97

Note: CO and CO<sub>2</sub> are not visible on FID detector

In this reaction with Al-TUD-1 as catalyst, the DME is the only product.

The methanol conversion was calculated as:

$$x_{\text{methanol}} = \frac{2 \cdot n_{\text{DME}}}{n_{\text{methanol}} + 2 \cdot n_{\text{DME}}} = \frac{2 \cdot A_{\text{DME}} / R_{\text{DME}}}{A_{\text{methanol}} / R_{\text{methanol}} + 2 \cdot A_{\text{DME}} / R_{\text{DME}}}$$

$x_{\text{methanol}}$ - methanol conversion,

$A_{\text{methanol}}, A_{\text{DME}}$ - integrated peak area of methanol and DME,

$R_{\text{methanol}}, R_{\text{DME}}$ - response factor of methanol and DME.

### 2.2.1.3 Methanol dehydration to DME on bifunctional catalysts

First of all, blank experiment was conducted at 280 °C without catalyst to determine the methanol area of the reactant. 0.5 ml gas was injected several times to the gas chromatography for analysis and the average area of methanol was recorded as  $A_{\text{blank}}$ .

Methanol, methyl formate, DME and methane were found in the gas analysis after reaction by gas chromatography. The relative response factor of methyl formate to methanol was calibrated.

The methanol conversion was calculated as following,

$$x_{\text{methanol}} = 100\% * (A_{\text{blank}} - A_{\text{methanol}}) / A_{\text{blank}}$$

The selectivity of DME, methyl formate and methane was calculated as following,

$$S_{\text{DME}} = 100\% * (2 * A_{\text{DME}} / R_{\text{DME}}) / [(A_{\text{blank}} - A_{\text{methanol}}) / R_{\text{methanol}}]$$

$$S_{\text{MF}} = 100\% * (2 * A_{\text{MF}} / R_{\text{MF}}) / [(A_{\text{blank}} - A_{\text{methanol}}) / R_{\text{methanol}}]$$

$$S_{\text{methane}} = 100\% * (2 * A_{\text{methane}} / R_{\text{methane}}) / [(A_{\text{blank}} - A_{\text{methanol}}) / R_{\text{methanol}}]$$

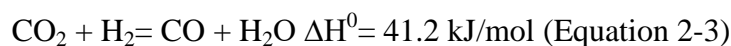
The selectivity of CO/CO<sub>2</sub> can't be calculated directly because they can't be separated by the column used, so the S<sub>CO+CO<sub>2</sub></sub> will be calculated as following,

$$S_{\text{CO+CO}_2} = 100\% - S_{\text{DME}} - S_{\text{MF}} - S_{\text{methane}}$$

### 2.2.2 Direct DME synthesis from CO<sub>2</sub>/H<sub>2</sub>

#### Thermodynamic simulation

Thermodynamic simulation of the direct DME synthesis from CO<sub>2</sub>/H<sub>2</sub> mixture at was performed by ProSimPlus. The Gibbs reactor was used with the system based on the minimization of Gibbs energy. The thermodynamic simulation was done using the same reactants' flow composition as for catalytic tests: total flow 40 mL/min, H<sub>2</sub>/CO<sub>2</sub>/N<sub>2</sub> ratio equal to 3/1/0.16. The different reactions can happen in this system: methanol synthesis by CO<sub>2</sub> hydrogenation (Equation 2-2), methanol dehydration into DME (Equation 2-1) and Reverse Water Gas Shift reaction (Equation 2-3) [10, 11].



The products that could be formed are: DME, methanol, CO and water. The reactants and products together constitute the thermodynamic system. The temperature of the Gibbs reactor was varied from 200 to 320 °C, the pressure was fixed at 20 bars.

### Catalytic tests

The scheme of setup for direct DME synthesis from CO<sub>2</sub>/H<sub>2</sub> is shown in Figure 2-4.

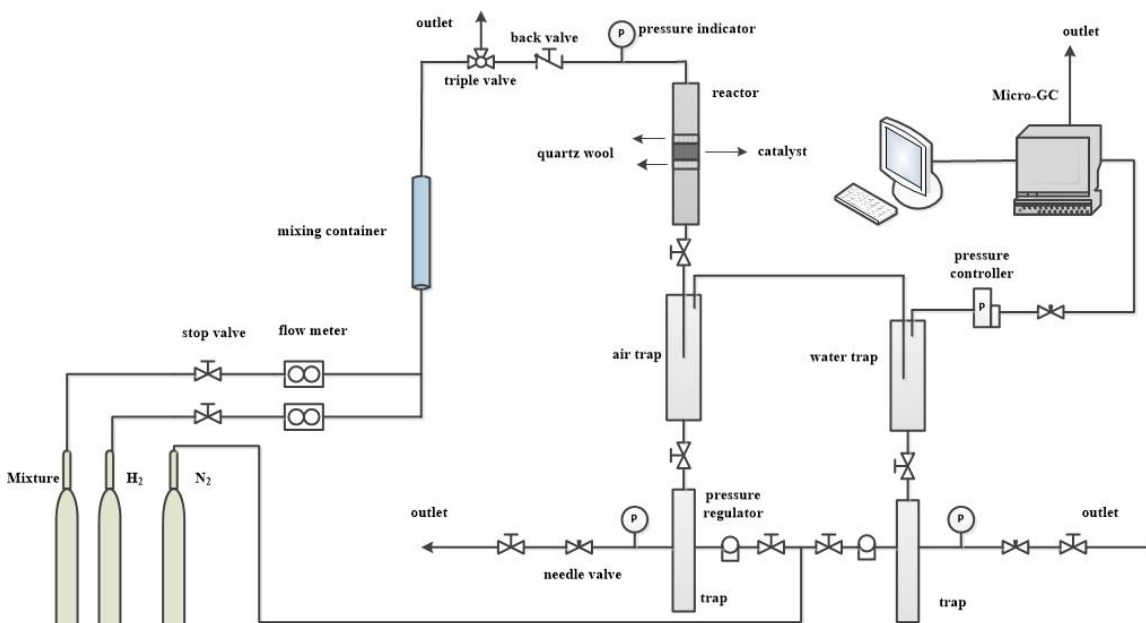


Figure 2- 4 Scheme of setup for direct DME synthesis from CO<sub>2</sub>/H<sub>2</sub>

Two high pressure gas bottles were connected to the setup, mixture bottle (63.5% H<sub>2</sub>/ 31.5% CO<sub>2</sub>/ 5% N<sub>2</sub>) and H<sub>2</sub> bottle, respectively. Firstly, load the catalyst (particle size 100-200 μm) in the middle of reactor with quartz wool under and above catalyst. Secondly, increase the pressure with pure H<sub>2</sub> to 20 bars. Then the catalyst was reduced with 9.47 ml/min H<sub>2</sub> at 20 bars, 280 °C with the ramp of 1 °C/min for 12h. Afterwards, blank experiment was conducted at 100 °C, 20 bars under 30.53 ml/min mixture/ 9.47 ml/min H<sub>2</sub>. The direct DME synthesis reaction was carried out at 240 °C, 260 °C, 280 °C and 300 °C with the GHSV of 10,000 h<sup>-1</sup>. The mass loading for catalyst is around 100mg depending on the specific density of each catalyst. And the size for catalyst is 100-200 μm.

The liquid after reaction are collected in two traps, air and water cooled, respectively. The gas phase is analyzed by online micro-GC. The collected liquid phase is analyzed by GC.

### Gas phase analysis

Micro-Gas Chromatograph R-3000 is from SRA Company equipped with three columns and three TCD (Thermal Conductivity Detector) detectors. These three columns were 5A micro-sieve column (column A), 8m plot (Porous Layer Open Tubular) U column (column B), 8m plot Q column (column C). Argon acted as carrier gas for column A and helium performed as carrier gas for column B and column C.

H<sub>2</sub>, N<sub>2</sub> (internal standard gas), CH<sub>4</sub> and CO were analyzed by column A, CO<sub>2</sub>, DME and CH<sub>3</sub>OH by column B and N<sub>2</sub>, CO, CH<sub>4</sub>, CO<sub>2</sub> by column C. Column A and column C were connected by individual peaks N<sub>2</sub>, CO on column A and overlapped peak N<sub>2</sub>-CO on column C. Column B and column C were connected by individual peak CO<sub>2</sub> on both columns.

The response factors (MRM, relative molar response factor, which use benzene as primary standard substance) for N<sub>2</sub>, CO, CO<sub>2</sub>, CH<sub>4</sub>, CH<sub>3</sub>OH are taken from literature [9]. The response factor for DME was calibrated using the standard gas bottle form air liquid with 99.5134436% Ar and 0.4865564% dimethyl ether (volume ratio).

The response factors for H<sub>2</sub>, N<sub>2</sub>, CO, CH<sub>4</sub> on column A are calibrated using the standard mixture bottle (20% H<sub>2</sub>/ 20% N<sub>2</sub>/ 20% CH<sub>4</sub>/ 20% CO / 20% CO<sub>2</sub>). By assuming the response factor of CH<sub>4</sub> as 1.0000, the relative response factors for H<sub>2</sub>, N<sub>2</sub>, CO and methane were obtained.

The temperatures and pressures for each column in the chromatography method, the retention times and response factors for different compounds are presented in Table 2- 2.

Table 2- 2 Temperature and pressure for columns and retention times and response factors for different compounds on each column

	Column A				Column B			Column C		
Temperature ( °C)	110				80			46		
Pressure (psi)	25				37			17		
Compound	H <sub>2</sub>	N <sub>2</sub>	CH <sub>4</sub>	CO	CO <sub>2</sub>	DME	CH <sub>3</sub> OH	N <sub>2</sub> -CO	CH <sub>4</sub>	CO <sub>2</sub>
Retention time (s)	44	64	77	105	15	110	209	29	31	35
Response factor	0.1984	2.2564	1.0000	2.3282	48	70.7	55	42	35.7	48

### Liquid phase analysis

The liquid phase was analyzed by gas chromatograph from Agilent Technologies with the type 6890N. Different components were separated with different retention time on the column SolGel-WAX (length of 60m, diameter of 0.25 mm and thickness of 0.25 μm).

About 10% (mass ratio) 1-propanol was added into the liquid phase as the external standard substance for the calculation. The retention time for methanol is around 4.68 min and for methanol 1-propanol is around 6.12 min. Only methanol was detected in liquid phase and the rest is water.

### Calculations

Carbon balance was calculated by the sum of all the CO<sub>2</sub> coming out, the c-containing products in gas phase and methanol in liquid phase.

$$n_{c\ enter} = n_{co2} + n_{co} + n_{CH3OH} + 2 * n_{DME}$$

Hydrogen atom balance were also calculated by the sum of all the H<sub>2</sub> coming out, the H-containing products in gas phase and methanol and water in liquid phase.

$$n_{H\ enter} = 2 * n_{H2} + 4 * n_{CH3OH} + 6 * n_{DME} + 2 * n_{H2O}$$

The CO<sub>2</sub> and H<sub>2</sub> conversion were calculated as following (the area in the formula has been corrected):

$$x_{CO_2} = \left( \frac{n_C \text{ in products}}{n_{CO_2 \text{ outlet}} + n_C \text{ in products}} \right) * 100\%$$

$$X_{H_2} = \left( \frac{n_H \text{ in products}}{n_{H_2 \text{ outlet}} + n_H \text{ in products}} \right) * 100\%$$

The selectivities of DME, methanol and CO were calculated as following:

$$S_{DME} = 2 * \frac{n_{DME}}{n_C \text{ in products}} * 100\%$$

$$S_{CH_3OH} = \frac{n_{CH_3OH (gas)} + n_{CH_3OH (liquid)}}{n_C \text{ in products}} * 100\%$$

$$S_{CO} = \frac{n_{CO}}{n_C \text{ in products}} * 100\%$$

## 2.3 References

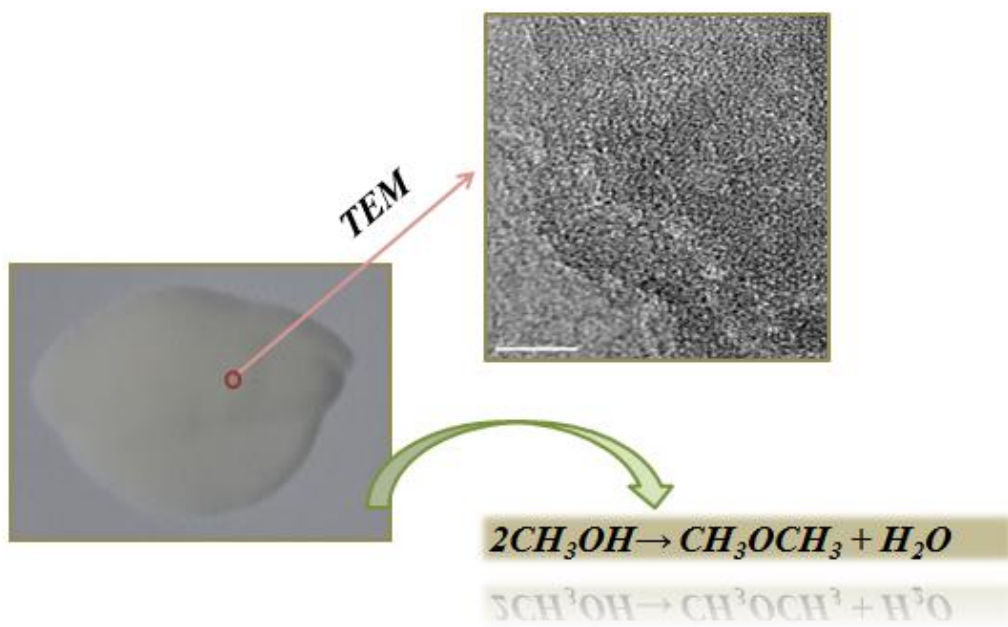
- [1] K.S.W. Sing, D.H. Everett, R.A.W. Haul, L. Moscou, R.A. Pierotti, J. Rouquerol, T. Siemieniewska, Reporting Physisorption Data for Gas Solid Systems with Special Reference to the Determination of Surface-Area and Porosity (Recommendations 1984), *Pure Appl Chem*, 57 (1985) 603-619.
- [2] G. Prieto, J.D. Meeldijk, K.P. de Jong, P.E. de Jongh, Interplay between pore size and nanoparticle spatial distribution: Consequences for the stability of CuZn/SiO<sub>2</sub> methanol synthesis catalysts, *J Catal*, 303 (2013) 31-40.
- [3] C. Fang, D.S. Zhang, S.X. Cai, L. Zhang, L. Huang, H.R. Li, P. Maitarad, L.Y. Shi, R.H. Gao, J.P. Zhang, Low-temperature selective catalytic reduction of NO with NH<sub>3</sub> over nanoflaky MnO<sub>x</sub> on carbon nanotubes in situ prepared via a chemical bath deposition route, *Nanoscale*, 5 (2013) 9199-9207.
- [4] I. Daldoul, S. Auger, P. Picard, B. Nohair, S. Kaliaguine, Effect of temperature Ramp on hydrocarbon desorption profiles from zeolite ZSM-12, *Can J Chem Eng*, 94 (2016) 931-937.
- [5] Y.M. Shen, J.W. Yi, Y.B. Yan, D.B. Liu, L.H. Fan, S.F. Li, Hydrogenation and Condensation of Acetone over Ni/MgO-Al<sub>2</sub>O<sub>3</sub> Prepared from Hydrotalcite Precursors, *J Chem Eng Jpn*, 49 (2016) 656-662.
- [6] H.P. Gao, J.M. Pan, D.L. Han, Y.L. Zhang, W.D. Shi, J. Zeng, Y.X. Peng, Y.S. Yan, Facile synthesis of microcellular foam catalysts with adjustable hierarchical porous structure, acid-base strength and wettability for biomass energy conversion, *J Mater Chem A*, 3 (2015) 13507-13518.
- [7] F. Dong, G.Q. Ding, H.Y. Zheng, X.M. Xiang, L.F. Chen, Y.L. Zhu, Y.W. Lia, Highly dispersed Cu nanoparticles as an efficient catalyst for the synthesis of the biofuel 2-methylfuran, *Catal Sci Technol*, 6 (2016) 767-779.
- [8] J. Speight, *Lange's handbook of chemistry*, McGraw Hill Professional, 2016.
- [9] S. Ahuja, S. Scypinski, *Handbook of modern pharmaceutical analysis*, Academic press, 2010.
- [10] H.G. Ahn, H.G. Lee, M.C. Chung, K.P. Park, K.J. Kim, B.M. Kang, W.J. Jeong, S.C. Jung, D.J. Lee, Catalytic Activity of Nanosized CuO-ZnO Supported on Titanium Chips

in Hydrogenation of Carbon Dioxide to Methyl Alcohol, *J Nanosci Nanotechno*, 16 (2016) 2024-2027.

[11] J.W. Bae, H.S. Potdar, S.H. Kang, K.W. Jun, Coproduction of methanol and dimethyl ether from biomass-derived syngas on a Cu-ZnO-Al<sub>2</sub>O<sub>3</sub>/γ-Al<sub>2</sub>O<sub>3</sub> hybrid catalyst, *Energ Fuel*, 22 (2008) 223-230.



*Chapter 3: Al-TUD-1 as the catalyst of methanol dehydration to  
DME*





### 3.1 Introduction

In this chapter, Al-TUD-1 with different Si/Al ratios were prepared by one-pot sol-gel method according to U. Hanefeld [1]. Different characterization methods were used for the analysis of these materials, such as X-ray diffraction (XRD), N<sub>2</sub> adsorption/desorption method, NH<sub>3</sub> temperature programmed desorption (NH<sub>3</sub>-TPD) and transmission electron microscopy (TEM). The catalytic tests of the methanol dehydration to DME reaction will be conducted at 280 °C and atmospheric pressure. The influence of the Si/Al ratio is studied. The water influence on the catalytic activity of these materials is investigated by using water/methanol mixture as the reactant.

### 3.2 Catalysts preparation

Mesoporous aluminosilicate materials were prepared using a surfactant free sol gel procedure according to U. Hanefeld [1]. Al-TUD-1 with different Si/Al ratios can be synthesized by adjusting the molar ratio of SiO<sub>2</sub>: xAl<sub>2</sub>O<sub>3</sub>: (0.5-1) TEA: (0.3-0.5) TEAOH: (10-20) H<sub>2</sub>O. Typically, Al-TUD-1 with Si/Al ratio of 25 was prepared by adding 10.5187 g tetraethyl orthosilicate (TEOS, 98%, ACROS) into 0.1142 g aluminum isopropoxide (98%, Aldrich) ethanol solution. After stirring for a few minutes, the well-mixed 7.6093 g triethanolamine (TEA, 97%, ACROS) and 5.7326 g water was added drop by drop, followed by the addition of 10.8304g tetraethyl ammonium hydroxide (TEAOH, 20% wt in water, ACROS) drop by drop. Afterwards, the mixture was under stirring overnight and then left to age at room temperature until clear gel formed. After that the gel was dried at 100 °C for 24h for the evaporation of H<sub>2</sub>O and ethanol, followed by hydrothermal treatment at 180 °C for 3h with ramp of 5 °C/min and calcination at 600 °C for 8h with ramp of 2 °C/min. The molar ratio of SiO<sub>2</sub>: Al<sub>2</sub>O<sub>3</sub>: TEA: TEAOH: H<sub>2</sub>O we obtained for Al-TUD-1 with the Si/Al ratio of 25 is 1.00: 0.04: 1.00: 0.30: 6.41.

The other three Al-TUD-1 materials with the Si/Al ratio of 50, 75 and 100 were also prepared with the procedures described above.

The catalysts after hydrothermal treatment and after calcination are shown in Figure 3- 1.

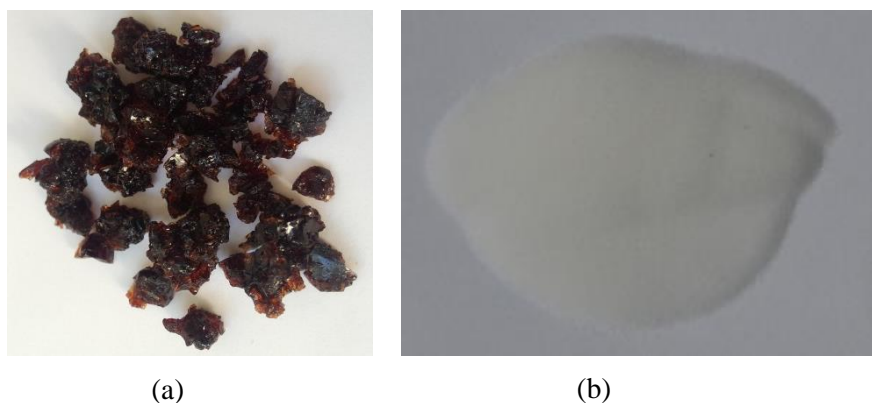


Figure 3- 1 Agglomerated catalysts after hydrothermal treatment (a) and sieved catalyst (100-200  $\mu\text{m}$ ) after calcination (b)

### 3.3 Characterization results

These materials are characterized by difference methods, such as XRD for crystalline phase and size,  $\text{N}_2$  adsorption/desorption for textural properties (specific surface area, pore volume, pore distribution),  $\text{NH}_3$ -TPD for acid property and TEM for surface morphology.

#### 3.3.1 Crystalline phase and morphology

Powder X-ray diffraction (XRD) was employed for the characterization of Al-TUD-1 materials and XRD patterns are shown in Figure 3- 2. Only one amorphous peak around  $22^\circ$  is observed for all the samples, which belongs to the amorphous  $\text{SiO}_2$  [2-5]. The absence of  $\text{Al}_2\text{O}_3$  crystalline peaks means that Al atoms are incorporated into the framework of  $\text{SiO}_2$  [6-10].

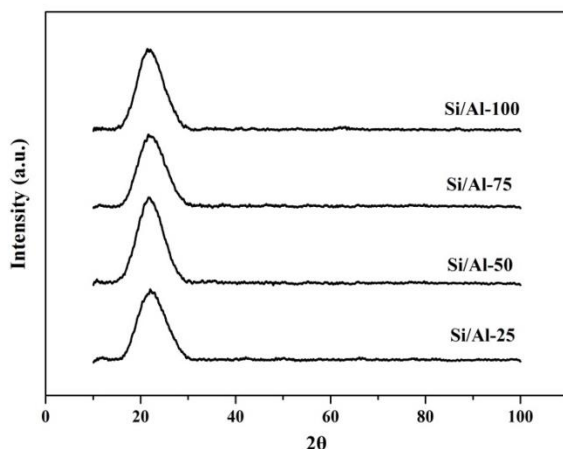


Figure 3- 2 XRD patterns of Al-TUD-1

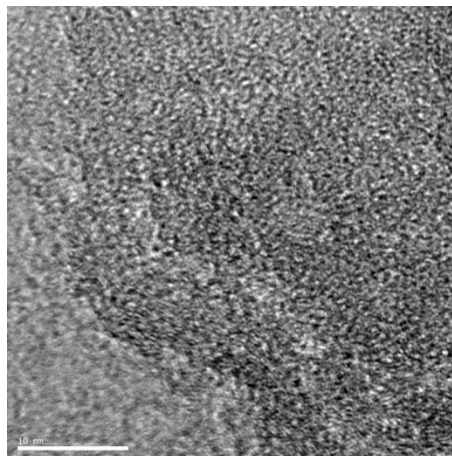


Figure 3- 3 TEM image for Si/Al-25

The materials were characterized by transmission electron microscopy. The representative TEM image of Si/Al-25 is shown in Figure 3- 3. TEM shows amorphous morphology with the presence of unordered worm-like pores and presents amorphous walls [1, 11, 12]. There is no crystal particles detected, which means Al was incorporated into the framework as expected [6]. It also confirms the XRD results, while the pore diameter can't be seen obviously from the TEM images because of the unordered pore structure.

### 3.3.2 Textural properties

The N<sub>2</sub> adsorption/desorption isotherm and pore distribution of Al-TUD-1 (before sieved) are shown in Figure 3- 4. The textural property results are shown in Table 3- 1. The specific surface area for the sieved samples (100-200 μm) ranges from 607-711 m<sup>2</sup>g<sup>-1</sup>, which is quite bigger than the frequently used methanol dehydration material γ-Al<sub>2</sub>O<sub>3</sub> (216 m<sup>2</sup>g<sup>-1</sup>) [13] and HZSM-5 (331.2 m<sup>2</sup>g<sup>-1</sup>, Si/Al=38) [14], and the pore volume varies from 1.06 to 1.24 cm<sup>3</sup>g<sup>-1</sup>. The pore distribution estimated from BJH desorption branch is quite narrow, with the maximum peak of 6.4 nm for Si/Al-25, 4.3 nm for Si/Al-75 and 6.4 nm for Si/Al-100. It shows two peaks in the pore distribution for Si/Al-50, which may

be caused by the insufficient stirring after the addition of template TEA or partial decomposition of initial aluminum isopropoxide during the synthesis. Considering the classification of pores [15], prepared Al-TUD-1 are mesoporous materials.

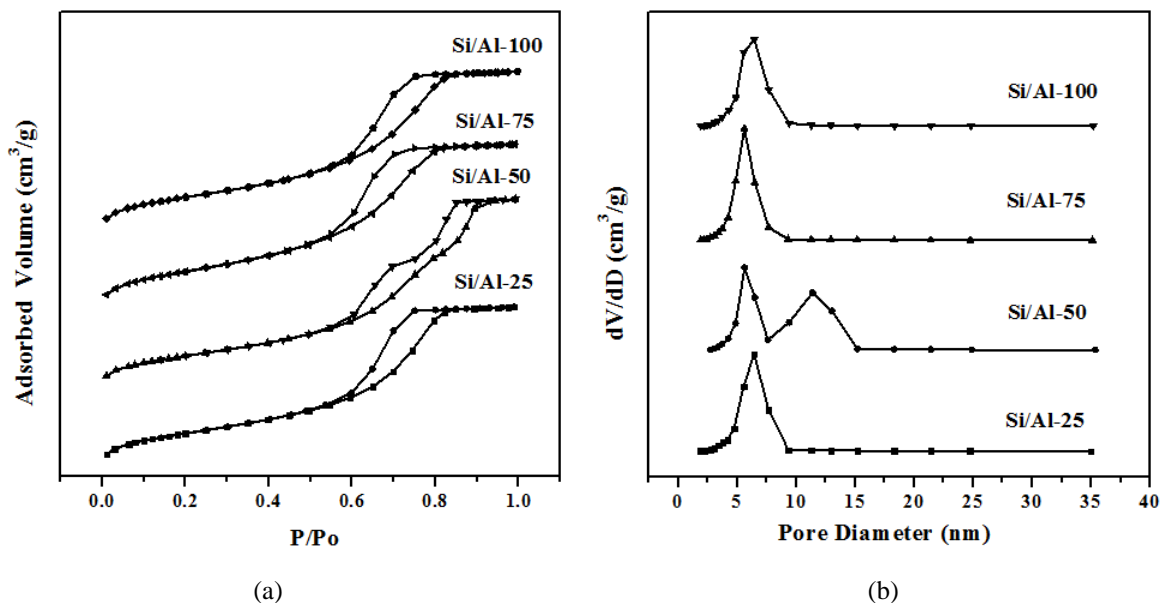


Figure 3- 4 N<sub>2</sub> adsorption/ desorption isotherm (a) and pore distribution (b) of Al-TUD-1

Al-TUD-1 displays typical type IV isotherm [1, 4, 7, 16, 17], which is related to capillary condensation in mesopores [15], and shows H1 type hysteresis loop [4, 11, 18], which is associated with porous material consisting of narrow pore distributions with “cylindrical” pore shape [15]. This is consistent with the pore distribution results shown in Table 3- 1, demonstrating that it is mesoporous material. The bimodal curve of pore distribution of Si/Al-50 probably dues to the incomplete mixing during the synthesis.

Table 3- 1 Textural properties of Al-TUD-1

sample	$S_{\text{BET}}$ (m <sup>2</sup> g <sup>-1</sup> )	$V_{\text{pore}}$ (cm <sup>3</sup> g <sup>-1</sup> )	$D_p$ (nm)
Si/Al-25	610	1.07	6.4
Si/Al-50	607	1.24	5.6, 11.4
Si/Al-75	711	1.12	5.6
Si/Al-100	662	1.06	6.4

In general, Al-TUD-1 is mesoporous material with big surface area and narrow pore distribution.

### 3.3.3 Acid properties

The acid sites concentration and their strength of these samples were measured by  $\text{NH}_3$  temperature programmed desorption ( $\text{NH}_3$ -TPD), which is shown in Figure 3- 5.

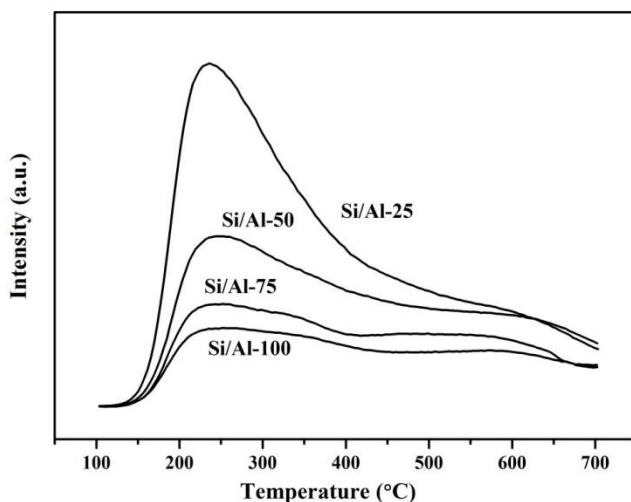


Figure 3- 5  $\text{NH}_3$  desorption profiles for Al-TUD-1

In general, the  $\text{NH}_3$  absorbed on weak acid sites, having weak interaction with the acid sites, will desorb at low temperature. To the contrary, the  $\text{NH}_3$  absorbed on strong acid sites will desorb at higher temperature. Broadly speaking, the stronger the acid sites, the higher the  $\text{NH}_3$  desorption temperature. All the samples show broad peaks for  $\text{NH}_3$  desorption, suggesting that these samples have acid sites with different acid strength.

From the  $\text{NH}_3$  desorption curves, we can see that most of  $\text{NH}_3$  desorb below 400 °C, which means most of the acid sites are weak and medium. According to the work has been published, strong acid sites not only can convert methanol into DME but also can convert further to alkanes and olefins [14], which illustrates that the strong acid sites are not expected for DME synthesis catalyst. The acid properties of these samples are

listed in Table 3- 2. The acid sites follow the order Si/Al-25 > Si/Al-50 > Si/Al-75 > Si/Al-100. Si/Al-25 is supposed to be the optimal catalyst for methanol dehydration to DME reaction among the four materials because it has the highest acidity with weak and medium force.

Table 3- 2 Acid properties of Al-TUD-1 from NH<sub>3</sub>-TPD

	Total acidity (mmol NH <sub>3</sub> /g)
Si/Al-25	0.966
Si/Al-50	0.593
Si/Al-75	0.414
Si/Al-100	0.349

### 3.4 Catalytic test: Methanol dehydration to DME

The methanol dehydration reaction was carried out in a fixed bed quartz reactor (inner diameter = 6.60 mm) at atmospheric pressure. The Si/Al catalyst was first treated at 280 °C for 12h with the H<sub>2</sub> flow rate of 9.47 ml/min (In order to keep the same reaction condition as bifunctional catalyst in the methanol dehydration to DME reaction). Afterwards, reactor was purged with pure Ar with the flow rate of 40 ml/min for 20min. Then Ar was passing through methanol in bubbler, which was kept at 0 °C in ice bath, and then went through catalyst at 280 °C with GHSV of 10,000 h<sup>-1</sup>. The particle size of the catalyst is 100-200 µm. The GHSV was kept constant and the mass loading was adjusted according to the apparent density.

0.5 mL gas probe was taken from the septum by the syringe (from SGE Analytical Science) and then analyzed by gas chromatography equipped with SOLGELWAX column possessing the length of 60m, diameter of 0.25 mm and thickness of 0.25 µm and FID detector.

In this part, two reaction conditions were studied in methanol dehydration to DME reaction, pure methanol (3.91 %) as reactant and mixture (0.65% methanol + 0.50 %

water) as reactant. In these two reaction conditions, the influence of Si/Al ratio and the influence of water existence were investigated.

### 3.4.1 Pure methanol as reactant

Methanol dehydration to DME reaction was carried out on Al-TUD-1 materials with different Si/Al ratio at 280 °C. The methanol conversion with time and with total acidity is shown in Figure 3- 6 (A) and Figure 3- 6 (B), respectively.

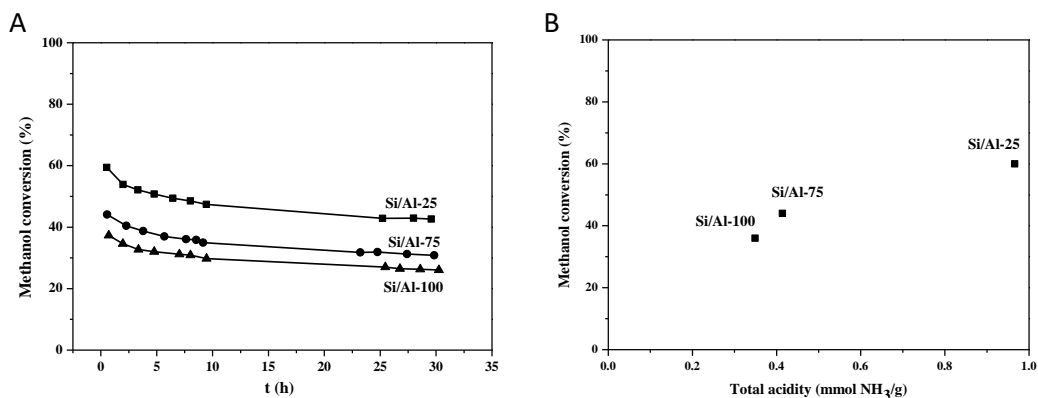


Figure 3- 6 Methanol conversion for Al-TUD-1 with time (A) and with total acidity (B)

It can be seen that the methanol conversion decreases with the Si/Al ratio, which shows the origin methanol conversion for Si/Al-25, Si/Al-75 and Si/AL-100 is 60%, 44% and 37%, respectively. In Figure 3-6 (B), the relation between methanol conversion and total acidity is presented. It can be clearly observed that the methanol conversion increases with the total acidity and it doesn't obey the strict linear relationship. DME is the only C-containing product for methanol dehydration, which demonstrates that the weak and medium acid sites are dominant, so the catalysts are selective. Methanol conversion decreases at the beginning and becomes almost constant after 24h. The deactivation of catalyst may be caused by the adsorption of water on active sites, which is formed during the methanol dehydration process. To prove that tests with additional amounts of water were performed in the same reaction conditions.

### 3.4.2 Water/methanol mixture as reactant

Methanol dehydration reaction to DME was conducted on Si/Al-25 with pure methanol and with mixture ( $n_{\text{methanol}}: n_{\text{water}}=1:5$ ), in which the methanol content is 3.9% and 0.6%, respectively. The methanol conversion is shown according to the water content in the media in Figure 3- 7.

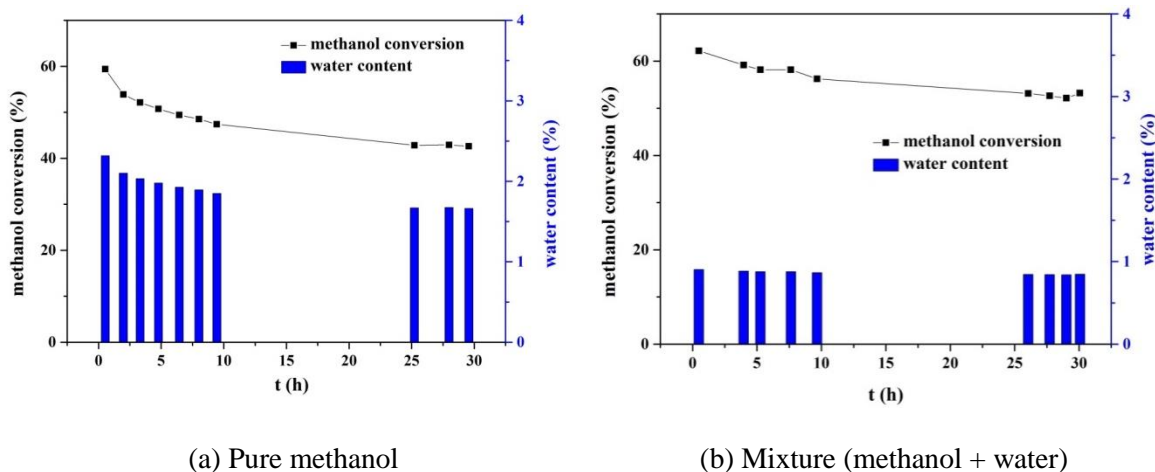


Figure 3- 7 Catalytic results for Si/Al-25

The water content is the total content of the water formed during reaction and introduced in the reactor as the reactant. The methanol conversion becomes constant after 24h and the selectivity of DME formation is 100% in both cases. It can be seen in Figure 3- 7 that the higher the water content smaller is the methanol conversion in the beginning of the reaction. The important difference between these two conditions is the stability of the methanol conversion – it drops more when more water is present in the reaction media.

From the catalytic results, it can be concluded that the methanol conversion decreases with the Si/Al ratio and the presence of water deteriorate the catalytic performance in the methanol dehydration to DME reaction.

### 3.5 Conclusions

Al-TUD-1 materials with different Si/Al ratios (25, 50, 75 and 100) were synthesized. They are sponge like mesoporous materials, with amorphous morphology, big surface area and narrow pore distribution. The amount of acid sites increases with the decrease of Si/Al ratio, following the trend  $\text{Si/Al-25} > \text{Si/Al-50} > \text{Si/Al-75} > \text{Si/Al-100}$ .

From the catalytic test (methanol dehydration to DME), it can be concluded that the methanol conversion increases with the decrease of Si/Al ratio and the water existence shows the negative effect on methanol dehydration to DME performance. The best results were observed for Si/Al-25 which possesses higher Al content and thus higher acidity necessary for the methanol to DME reaction.

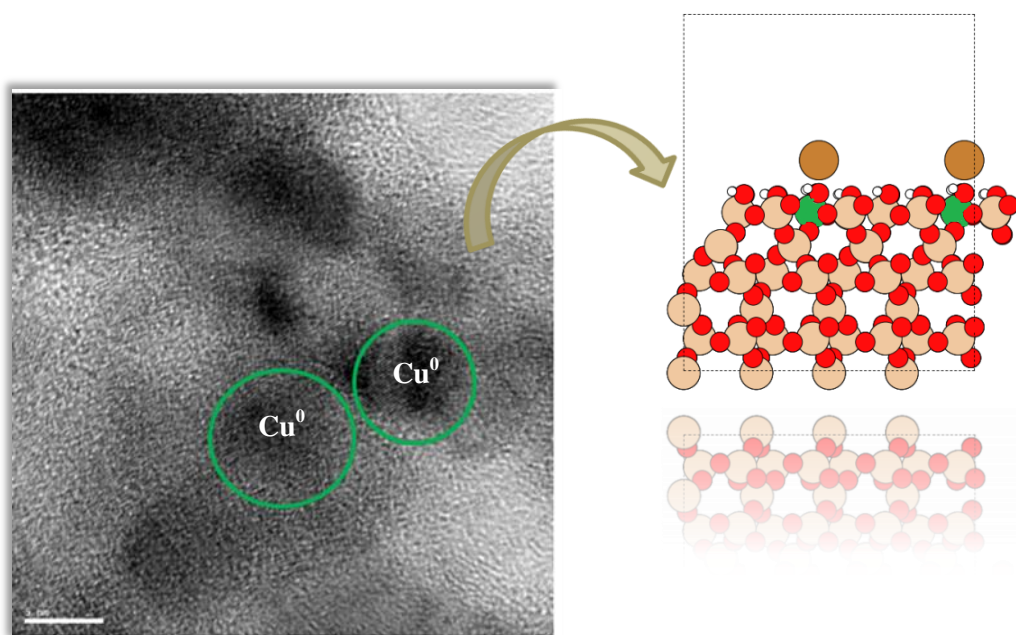
### 3.6 References

- [1] R. Anand, R. Maheswari, U. Hanefeld, Catalytic properties of the novel mesoporous aluminosilicate AlTUD-1, *J Catal*, 242 (2006) 82-91.
- [2] M.S. Hamdy, R. Amrollahi, I. Sinev, B. Mei, G. Mul, Strategies to Design Efficient Silica-Supported Photocatalysts for Reduction of CO<sub>2</sub>, *Journal of the American Chemical Society*, 136 (2014) 594-597.
- [3] F. Adam, T.S. Chew, J. Andas, A simple template-free sol-gel synthesis of spherical nanosilica from agricultural biomass, *J Sol-Gel Sci Techn*, 59 (2011) 580-583.
- [4] S. Telalovic, U. Hanefeld, Noncovalent immobilization of chiral cyclopropanation catalysts on mesoporous TUD-1: Comparison of liquid-phase and gas-phase ion-exchange, *Appl Catal A-Gen*, 372 (2010) 217-223.
- [5] S. Lima, M.M. Antunes, A. Fernandes, M. Pillinger, M.F. Ribeiro, A.A. Valente, Acid-Catalysed Conversion of Saccharides into Furanic Aldehydes in the Presence of Three-Dimensional Mesoporous Al-TUD-1, *Molecules*, 15 (2010) 3863-3877.
- [6] S. Telalovic, A. Ramanathan, J.F. Ng, R. Maheswari, C. Kwakernaak, F. Soulimani, H.C. Brouwer, G.K. Chuah, B.M. Weckhuysen, U. Hanefeld, On the Synergistic Catalytic Properties of Bimetallic Mesoporous Materials Containing Aluminum and Zirconium: The Prins Cyclisation of Citronellal, *Chem-Eur J*, 17 (2011) 2077-2088.
- [7] Z.G. Wang, J.Y. Fu, Y.C. Deng, A.J. Duan, Z. Zhao, G.Y. Jiang, J. Liu, Y.C. Wei, S.Q. Zhao, Synthesis of aluminum-modified 3D mesoporous TUD-1 materials and their hydrotreating performance of FCC diesel, *Rsc Adv*, 5 (2015) 5221-5230.
- [8] S. Telalovic, J.F. Ng, R. Maheswari, A. Ramanathan, G.K. Chuah, U. Hanefeld, Synergy between Bronsted acid sites and Lewis acid sites, *Chemical communications*, (2008) 4631-4633.
- [9] L. Li, T.I. Koranyi, B.F. Sels, P.P. Pescarmona, Highly-efficient conversion of glycerol to solketal over heterogeneous Lewis acid catalysts, *Green Chem*, 14 (2012) 1611-1619.
- [10] S. Telalovic, U. Hanefeld, Investigation of the cyanosilylation catalysed by metal-siliceous catalysts, *Catal Commun*, 12 (2011) 493-496.

- [11] Z. Shan, J.C. Jansen, W. Zhou, T. Maschmeyer, Al-TUD-1, stable mesoporous aluminas with high surface areas, *Appl Catal A-Gen*, 254 (2003) 339-343.
- [12] S. Telalovic, A. Ramanathan, G. Mul, U. Hanefeld, TUD-1: synthesis and application of a versatile catalyst, carrier, material ... *J Mater Chem*, 20 (2010) 642-658.
- [13] J.M. Chen, R.W. Gillham, L. Gui, Passivation of bimetallic catalysts used in water treatment: Prevention and reactivation, *J Environ Sci Heal A*, 48 (2013) 48-56.
- [14] D.S. Mao, W.M. Yang, J.C. Xia, B. Zhang, Q.Y. Song, Q.L. Chen, Highly effective hybrid catalyst for the direct synthesis of dimethyl ether from syngas with magnesium oxide-modified HZSM-5 as a dehydration component, *J Catal*, 230 (2005) 140-149.
- [15] K.S.W. Sing, D.H. Everett, R.A.W. Haul, L. Moscou, R.A. Pierotti, J. Rouquerol, T. Siemieniewska, Reporting Physisorption Data for Gas Solid Systems with Special Reference to the Determination of Surface-Area and Porosity (Recommendations 1984), *Pure Appl Chem*, 57 (1985) 603-619.
- [16] Z.X. Zhang, P. Bai, B.J. Xu, Z.F. Yan, Synthesis of mesoporous alumina TUD-1 with high thermostability, *J Porous Mat*, 13 (2006) 245-250.
- [17] M.S. Hamdy, G. Mul, TUD-1-Encapsulated HY Zeolite: A New Hierarchical Microporous/Mesoporous Composite with Extraordinary Performance in Benzylation Reactions, *Chemcatchem*, 5 (2013) 3156-3163.
- [18] S. Telalovic, S.K. Karmee, A. Ramanathan, U. Hanefeld, Al-TUD-1: Introducing tetrahedral aluminium, *J Mol Catal A-Chem*, 368 (2013) 88-94.



*Chapter 4: Bifunctional catalysts prepared by co-precipitation-deposition method*





## 4.1 Introduction

In this chapter, firstly the copper based catalyst CZZ was synthesized by co-precipitation method. Then the bifunctional catalysts with both the copper based part and the Al-TUD-1 (Si/Al) part were synthesized by co-precipitation deposition method. The copper content in the copper based part was fixed; the Si/Al ratio in the Al-TUD-1 part was varied as in the Chapter 3. These materials were characterized by different techniques such as BET, XRD, H<sub>2</sub>-TPR, NH<sub>3</sub>-TPD, N<sub>2</sub>O-TPD and TEM. They were tested in the methanol dehydration to DME and in the direct DME synthesis from CO<sub>2</sub>/H<sub>2</sub>. The influence of the weight ratio between two functions in the bifunctional material CZZ-Si/Al-25 was also investigated.

## 4.2 Catalysts preparation

### 4.2.1 Copper based catalyst CZZ

Co-precipitation method was employed to prepare the methanol synthesis catalyst CZZ with the mass ratio of CuO: ZnO: ZrO<sub>2</sub>=37.5: 41: 21.5. In a standard synthesis 4.6582 g copper nitrate hexahydrate (98%, Alfa Aesar), 5.9685 g zinc nitrate hexahydrate (99%, Aldrich) and 1.8662 g zirconium dinitrate oxide hydrate (99.9%, Alfa Aesar) were dissolved in distilled water to prepare the metal solution with the concentration of 1M. 8.5213 g sodium carbonate (99.8%, Acros Organic) was dissolved in distilled water to prepare solution with the carbonate concentration of 1.6M, which was then used as the precipitating agent[1]. The diagram of synthesis installation is shown in Figure 4- 1.

The co-precipitation was conducted at the temperature range of 60-65°C and pH between 6 and 6.5 under stirring. After the co-precipitation, the precipitate was aged for 3h under heating and stirring and then filtrated by 1.5 L distilled water, dried at 100 °C for 5 days until water completely evaporated, followed by calcination at 400 °C for 4h with ramp of 2°C/min.

The chosen composition of this copper based catalyst was kept constant for all

further syntheses. This catalytic material was named CZZ and it was used for comparison with bifunctional materials.

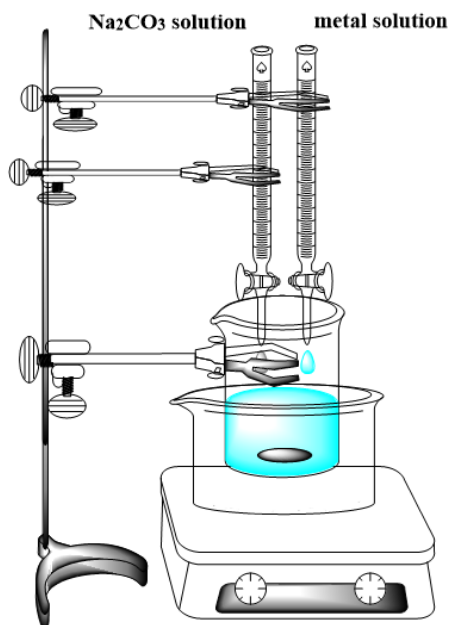


Figure 4- 1Diagrams for CZZ synthesis by co-precipitation method

#### 4.2.2 Bifunctional catalysts CZZ-Si/Al

Bifunctional catalysts CZZ-Si/Al ( $\text{CuO-ZnO-ZrO}_2@$ Al-TUD-1) were prepared by co-precipitation deposition method, with the copper based part deposited on the Al-TUD-1 particles.

In the beginning four Al-TUD-1 materials with different Si/Al ratio (25, 50, 75 and 100) were prepared as explained in 3.2, they were sieved in order to obtain the particles size of 100-200  $\mu\text{m}$  and then used as the supports for the deposition of copper based part of the bifunctional catalysts. The weight ratio between the copper based catalyst CZZ and the Al-TUD-1 (Si/Al) catalyst was kept constant  $m_{\text{Cu-ZnO-ZrO}_2} : m_{\text{Al-TUD-1}} = 7:3$ . In a standard synthesis 48.1 mL metal solution (1M) and 48.1mL  $\text{Na}_2\text{CO}_3$  solution (1.6M) were prepared in advance. In a beaker 1.8182 g of sieved Al-TUD-1 was added into 100 mL of distilled water under stirring and the pH was adjusted to the range 6-6.5 using  $\text{HNO}_3$  and  $\text{Na}_2\text{CO}_3$  solutions. Then the co-precipitation, aging, filtration, drying and calcination were performed as described in 4.2.1. The precursor after drying and the

catalyst after calcination are shown in Figure 4- 2 as well as the pure CZZ copper based catalyst.



Figure 4- 2 Precursors after drying (a) and catalyst after calcination at 400 °C (b)

Other two bifunctional catalysts with the different weight ratio between the copper based catalyst CZZ and the Al-TUD-1 (Si/Al) catalyst were prepared ( $m_{\text{Cu-ZnO-ZrO}_2} : m_{\text{Al-TUD-1}} = 5:3, 1:1$ ) with Si/Al-25 as the support. The synthesis process was the same as described above.

All the prepared catalysts, copper based catalyst CZZ and the bifunctional catalysts are shown in Table 4- 1.

Table 4- 1 Catalysts list

	Samples (mass ratio)
Copper based catalyst	CZZ
	CZZ-Si/Al-25 (7:3)
	CZZ-Si/Al-50 (7:3)
Bifunctional catalysts with <b>different Si/Al ratio</b>	CZZ-Si/Al-75 (7:3)
	CZZ-Si/Al-100 (7:3)
Bifunctional catalysts with <b>different weight ratio</b> between copper based part and Al-TUD-1 (Si/Al=25) part	CZZ-Si/Al-25 (5:3)
	CZZ-Si/Al-25 (1:1)

## **4.3 The influence of Si/Al ratio**

### **4.3.1 Characterization**

Different characterization methods were used to have a better understanding of these samples, such as BET, XRD, TPR, NH<sub>3</sub>-TPD, N<sub>2</sub>O-TPD and TEM.

#### **4.3.1.1 Textural properties**

The textural properties of catalysts were measured using **N<sub>2</sub> adsorption/desorption method**. The isotherms and pore distributions for methanol synthesis catalyst CZZ and the four bifunctional catalysts are shown in Figure 4- 3.

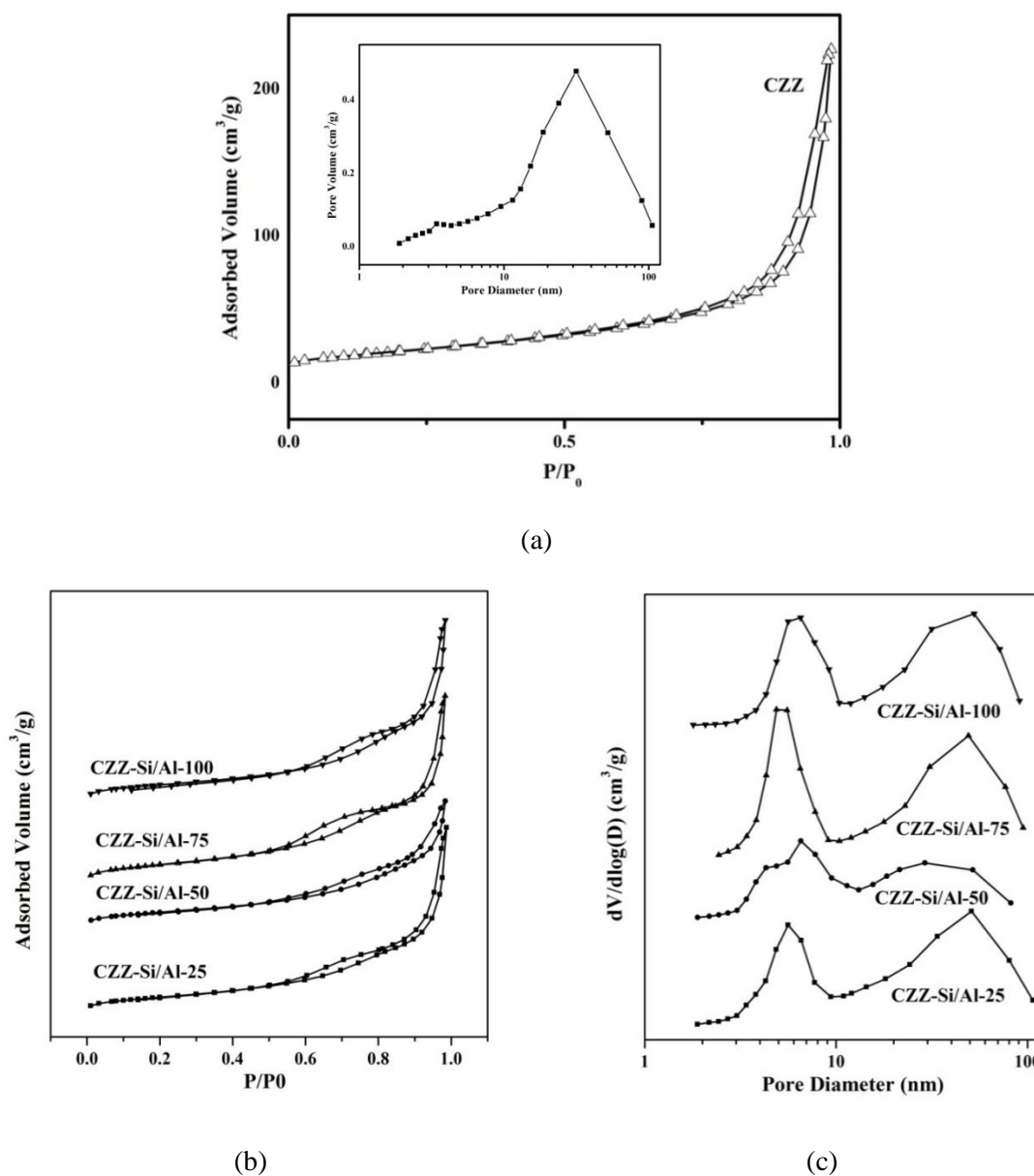


Figure 4- 3 N<sub>2</sub> adsorption/ desorption isotherms and pore distribution for CZZ (a), isotherms (b) and pore distributions (c) for bifunctional catalysts

The isotherm of the pure catalyst CZZ presents type IV isotherm with H3-type hysteresis loop (Figure 4- 3a). It has been reported that this kind of hysteresis loop is related to the aggregates of plate like particles generating “slit” shaped pores [2]. The pure CZZ catalyst shows a large peak for the pore distribution, mainly ranges from 10 nm to 100 nm, which may due to the existence of both the intragranular porosity and intergranular porosity. The textural properties are shown in Table 4- 2. The specific

surface area is  $76 \text{ m}^2 \text{ g}^{-1}$ . The pore volume is  $0.36 \text{ cm}^3 \text{ g}^{-1}$ , but it may be not exact due to the intergranular porosity.

The pure Al-TUD-1 materials are mesoporous materials with the specific surface area ranges from 610 to  $804 \text{ m}^2 \text{ g}^{-1}$  and the pore distribution ranges from 3 to 7 nm, which has been shown in the BET results in the chapter 3.3.2.

The  $\text{N}_2$  adsorption-desorption isotherms and the pore distribution graphs of the bifunctional catalysts CZZ-Si/Al are presented in Figure 4- 3b and Figure 4- 3c, respectively. Two kinds of pores are exhibited by bimodal pore distribution, around 6nm and 50 nm (Figure 4- 3c), and two hysteresis loops in the isotherms, H1 and H3-type hysteresis loops with “cylindrical” and “slit” shaped pore, respectively (Figure 4- 3b). The former is introduced by the Al-TUD-1 (Si/Al) itself and the latter arises from the structure of CZZ [3]. It explains that the pore structures of both methanol synthesis catalyst CZZ and Si/Al support are preserved and the copper based part is not incorporated into the siliceous framework or not hidden completely in the pores of the support, thus presenting two instinct hysteresis loops [4, 5].

Table 4- 2 Textural properties of catalysts

Sample	$S_{\text{BET}}$ ( $\text{m}^2 \text{ g}^{-1}$ )	$V_{\text{pore}}$ ( $\text{cm}^3 \text{ g}^{-1}$ )	$D_p$ (nm)
CZZ	76	(0.36)	(31.5)
CZZ-Si/Al-25	161	0.71	5.6, 50.9
CZZ-Si/Al-50	162	0.51	6.5, 47.2
CZZ-Si/Al-75	203	0.72	4.9, 49.1
CZZ-Si/Al-100	161	0.70	6.5, 52.6

The surface area of the bifunctional catalysts CZZ-Si/Al varies from 161-203  $\text{m}^2 \text{ g}^{-1}$ . Taking the weight ratio of copper based catalyst and the Si/Al support into consideration, the surface area is decreased comparing with initial value for the Si/Al support. It may be caused by the blockage of pores by particles or agglomerates of the copper based part formed during the precipitation and calcination procedure of the catalyst preparation. It shows the same trend as the copper based catalyst was deposited

on a porous support prepared by S. Behrens [6]. While comparing with the pure catalyst CZZ, the specific surface area and the total pores' volume of the bifunctional catalysts were largely improved more than twice (Table 4- 2).

#### 4.3.1.2 Crystalline structure

**Powder X-ray diffraction (XRD)** was employed for the characterization of the phase composition of the catalysts and the XRD patterns for the pure CZZ and the bifunctional catalysts are shown in Figure 4- 4.

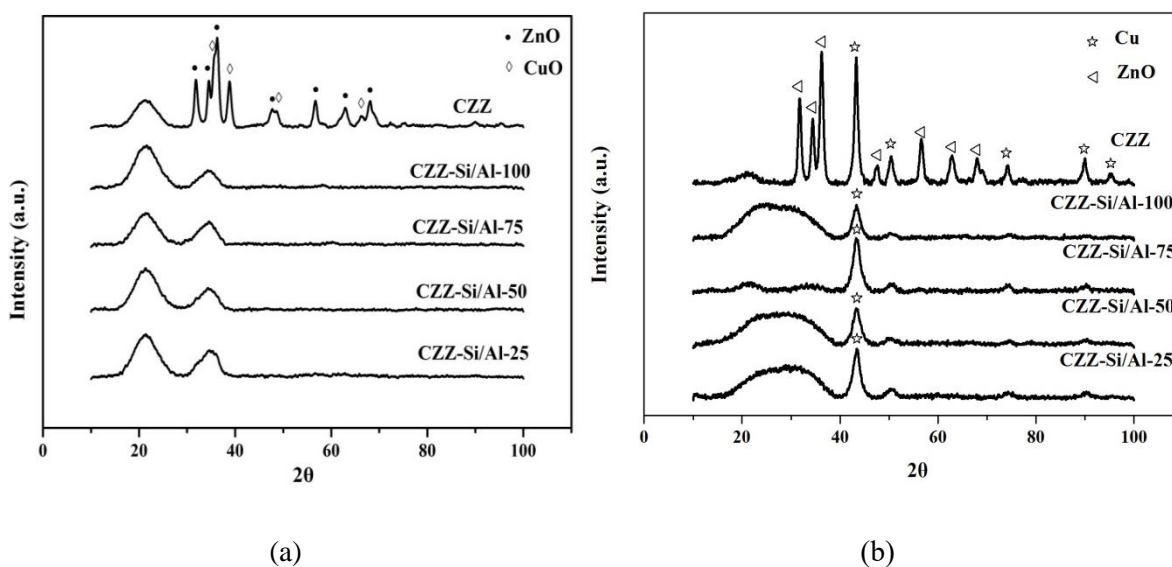


Figure 4- 4 XRD patterns of fresh (a) and reduced (b) CZZ and bifunctional catalysts CZZ-Si/Al

CuO and ZnO crystalline peaks were observed in the CZZ catalyst (Figure 4- 4a). The  $ZrO_2$  crystalline peaks are absent in the XRD patterns so  $ZrO_2$  is supposed to be present in the amorphous form [7, 8]. In the case of bifunctional catalysts, the crystalline peaks belonging to CuO and ZnO disappeared. Instead of the individual metal oxide crystalline characteristic peaks, one amorphous peak emerged in the range of  $30^\circ$ - $40^\circ$   $2\theta$  (Figure 4- 4a), which may due to the overlapping of broadened CuO and ZnO peaks [8]. It is obvious that the intensity of the amorphous peak is weakened compared with the CuO and ZnO peaks in the pure CZZ. Probably in the case of the bifunctional catalysts we obtain strong interaction between metal oxides and Al-TUD-1 (Si/Al) support which leads to the better dispersion of CuO and ZnO thus resulting in the weak and broadened

CuO and ZnO peaks [5, 9, 10]. The amorphous peak presents in the range of 10-30 ° may come from the sample holder during the XRD analysis.

XRD spectra of reduced CZZ-Si/Al (reduction at 280°C for 1h) are shown in Figure 4- 4b. The Cu<sup>0</sup> crystallite sizes are estimated by Debye- Scherrer equation and presented in Table 4- 3.

Table 4- 3Copper crystallite sizes in the reduced bifunctional catalysts CZZ-Si/Al

sample	Cu crystallite size (nm)
CZZ	10.9
CZZ-Si/Al-25	5.6
CZZ-Si/Al-50	4.7
CZZ-Si/Al-75	5.1
CZZ-Si/Al-100	4.9

A broad amorphous peak (in the range of 10-40°) and metallic copper peaks are detected on the XRD patterns of reduced bifunctional catalysts (Figure 4- 4b). For the broad peak, it can be considered as the overlapping of amorphous SiO<sub>2</sub> coming from the sample holder. The metallic copper crystallite sizes calculated from Scherrer equation are around 5nm. They are much smaller than the copper crystallite size for the reduced pure CZZ catalyst. The small crystallite size means that the Si/Al support surely plays a very important role in the anchoring and dispersing the copper.

#### **4.3.1.3 Redox properties**

**H<sub>2</sub> temperature programmed reduction (H<sub>2</sub>-TPR)** was employed to investigate the reduction behaviors of the pure CZZ catalyst and the bifunctional catalysts. The TPR profiles are shown in Figure 4- 5. Since ZnO and ZrO<sub>2</sub> can't be reduced in this temperature range, the H<sub>2</sub> consumption peaks are attributed to the reduction of CuO [11].

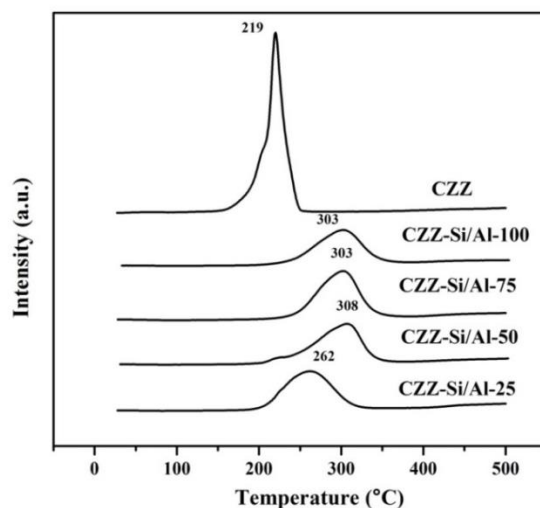


Figure 4- 5TPR profiles for the CZZ and the bifunctional catalysts

For the pure catalyst CZZ, a main sharp reduction peak around 219 °C was observed, with a shoulder peak around 200 °C. These two peaks may be attributed to the reduction of CuO with different particle sizes [11, 12]. They can be also attributed to different insertions of copper in the support or interactions between copper and the ZnO and ZrO<sub>2</sub> [13, 14].

The intensity and the area for H<sub>2</sub> signal of the bifunctional catalysts is much smaller than for CZZ, probably due to the less copper content in the bifunctional catalysts, 30 wt% of copper in CZZ and 21wt% of copper in the bifunctional catalysts.

It can be observed that the bifunctional catalysts own higher reduction temperature compared to CZZ. In principle, small CuO particles are easier to be reduced compared with big and bulk CuO [5, 8]. It has been reported that apart from the particle size, the extent of the interaction between CuO and promoter or support also plays an important role in reduction behavior [5]. In our case, not only the interaction between CuO and ZnO, CuO and ZrO<sub>2</sub>, but also the interaction between CuO and Si/Al support act in the retarding the reduction of CuO.

Among all the bifunctional catalysts, CZZ-Si/Al-25 shows the lowest reduction temperature, which is caused by more copper anchoring sites provided by aluminum

species [15]. Other three bifunctional catalysts show similar reduction temperatures, 308 °C for CZZ-Si/Al-50, 303 °C for CZZ-Si/Al-75 and 303 °C for CZZ-Si/Al-100.

The reducibility of copper is shown in Table 4- 4. The reduction degree of copper was reflected by the reducibility calculated from the H<sub>2</sub> consumption during the H<sub>2</sub>- TPR analysis. The reducibility of the bifunctional catalysts varies from 70% to 87%. The uncomplete reduction of copper is probably due to the embedded copper oxide in the pores of the support or the formation of other copper containing species that are difficult to be reduced.

Table 4- 4 Reducibility of the pure CZZ and the bifunctional catalysts

sample	Reducibility (%)
CZZ	107
CZZ-Si/Al-25	83
CZZ-Si/Al-50	82
CZZ-Si/Al-75	87
CZZ-Si/Al-100	70

The CZZ shows bigger reducibility, lower reduction temperature and bigger crystallite size than the bifunctional catalysts. It means that there is a good copper distribution and SMSI interaction in the bifunctional catalysts.

#### **4.3.1.4 Copper surface area**

The metallic copper surface area and metallic copper dispersion was determined by N<sub>2</sub>O-TPD, the results are shown in Table 4- 5. The determination of copper surface area is very important, because the metallic copper is regarded as the main active component of copper based catalyst for the CO<sub>2</sub> hydrogenation to methanol reaction [16]. The copper surface area of CZZ is 11.6 m<sup>2</sup>/g<sub>cata</sub>. The metallic copper surface area of the bifunctional catalysts CZZ-Si/Al-25 and CZZ-Si/Al-50 are 10.3 m<sup>2</sup>/g<sub>cata</sub> and 5.8 m<sup>2</sup>/g<sub>cata</sub>, respectively. The metallic copper surface area of CZZ-Si/Al-75 and CZZ-Si/Al-100 are not shown here, because it is less than 4 m<sup>2</sup>/g<sub>cata</sub>, which is the limit for N<sub>2</sub>O-TPD continuous method for measuring the metallic copper surface area.

Table 4- 5 Copper surface area and dispersion

Sample	Cu surface area ( $\text{m}^2\text{g}_{\text{cata}}^{-1}$ )	Cu surface area ( $\text{m}^2\text{g}_{\text{copper}}^{-1}$ )	Cu dispersion (%)	Cu/Al (mol/mol)
CZZ	11.6	38.7	5.3	-
CZZ-Si/Al-25	10.3	49.0	6.6	17
CZZ-Si/Al-50	5.8	27.6	4.6	34
CZZ-Si/Al-75	<4	-	-	50
CZZ-Si/Al-100	<4	-	-	67

The metallic copper surface area of CZZ-Si/Al-25 is less than for the pure catalyst CZZ, which is probably due to the smaller content of copper in CZZ-Si/Al-25 (21 wt%) than in CZZ (30 wt%). The specific copper surface area calculated based on the copper weight is  $38.7 \text{ m}^2/\text{g}_{\text{copper}}$  for CZZ and  $49.0 \text{ m}^2/\text{g}_{\text{copper}}$  for CZZ-Si/Al-25, respectively. This means that the copper is better dispersed in CZZ-Si/Al-25 than in CZZ. The molar ratio of Cu/Al for CZZ-Si/Al-25, CZZ-Si/Al-50, CZZ-Si/Al-75 and CZZ-Si/Al-100 is 17, 34, 50 and 67, respectively. Comparing the metallic copper surface areas for the bifunctional catalysts, it can be found that the copper surface decreases with the increase of the Si/Al ratio in the support.

All the reduced bifunctional catalysts share almost the same Cu crystallite size around 5 nm (XRD results from 4.3.1.2). While the Al content is changing, the different metallic copper surface area is observed keeping the same trend: the more aluminum is present in the sample the bigger is the metallic copper surface area. This indicates that CZZ-Si/Al-25 has more surface anchoring sites for copper than other bifunctional catalysts.

The metallic copper dispersion is shown in Table 4- 5. It is equal to 6.6% for CZZ-Si/Al-25 and it is bigger than for the pure CZZ catalyst despite the smaller metallic surface area. This is due to the presence of Al in the bifunctional catalyst that helps to improve the dispersion of copper. The metallic copper dispersion for CZZ-Si/Al-50 is 4.6 % and it is smaller than for CZZ probably because it has smaller content of copper and smaller than for CZZ-Si/Al-25 probably because it has smaller content of Al.

### 4.3.1.5 Thermal gravimetric analysis

**Thermal Gravimetric Analyzer (TGA)** was used to test the thermal stability of the catalysts and the TGA results for calcined CZZ and calcined bifunctional catalyst CZZ-Si/Al-25 are shown in Figure 4- 6.

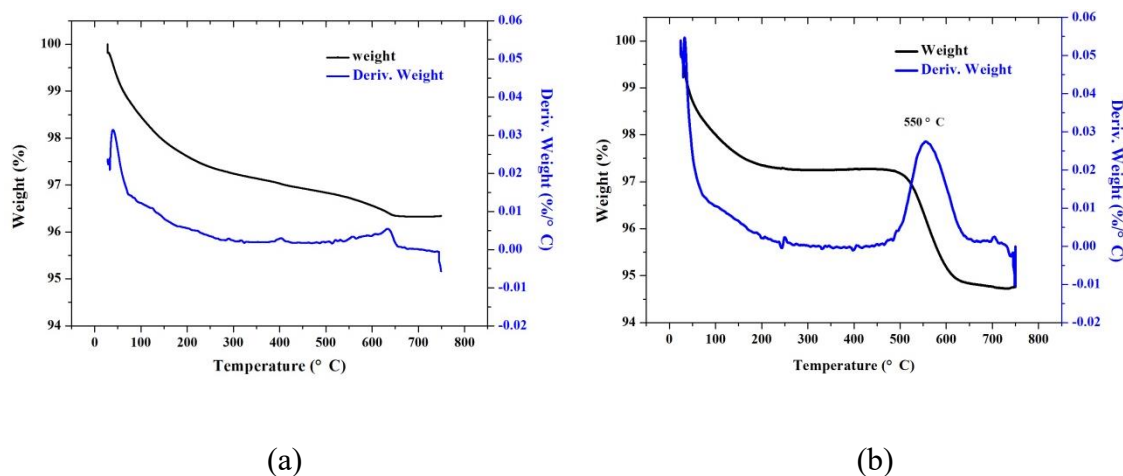


Figure 4- 6 TGA profiles of CZZ and of CZZ-Si/Al-25

The pure CZZ catalyst, consisting of CuO, ZnO and ZrO<sub>2</sub>, has black appearance while the calcined bifunctional catalysts are dark green, probably owing to the existence of carbonates (Cu,Zn)<sub>5</sub>(CO<sub>3</sub>)<sub>2</sub>(OH)<sub>6</sub> or (Cu,Zn)<sub>2</sub>(OH)<sub>2</sub>CO<sub>3</sub>, which are the precursors for copper and zinc based methanol synthesis catalysts[8].

The Al-TUD-1 (Si/Al-25) was calcined at 600 °C, so it is supposed that there will be no weight loss for it. It can be seen from Figure 4- 6 that there are two weight losses for the both catalysts. First weight loss is observed under around 100 °C and may be attributed to the loss of adsorbed water on the materials surface. The second weight loss is observed at the temperatures higher than the calcination temperature (400 °C). The pure CZZ catalyst has a very small weight loss around 620 °C that may correspond to the decomposition of carbonates at high temperatures. The bifunctional catalyst CZZ-Si/Al-25 shows a big weight loss peak around 550 °C with weight losing value ( $\Delta m$ ) of 2.6%. It can be attributed to the decomposition of high temperature carbonates [17], which are considered as a growth inhibitor for the oxide crystallites and they are beneficial for the

dispersion of copper [17, 18]. Malte Behrens regarded that the high temperature carbonates are trapped at the ZnO-CuO interface [19]. So the existence of high temperature carbonate is beneficial for the stability and the dispersion of copper.

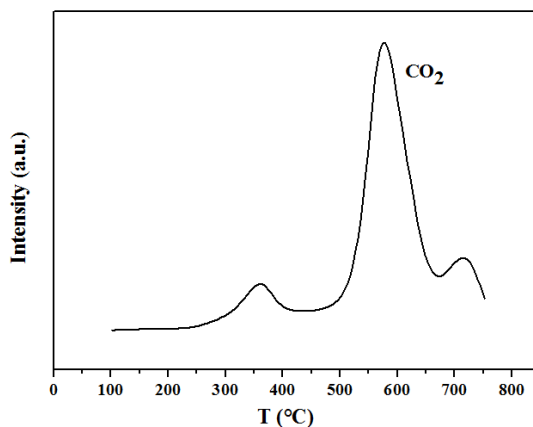


Figure 4- 7 CO<sub>2</sub> profile from CZZ-Si/Al-25 TGA analysis

In order to confirm that the weight loss peaks at high temperatures belong to the CO<sub>2</sub> coming from the decomposition of carbonates, the bifunctional catalyst CZZ-Si/Al-25 was heated to 750 °C in helium atmosphere with the temperature ramp of 10 °C/min and the gas in outlet was recorded by MS detector. The CO<sub>2</sub> profile in the outlet gas is shown in Figure 4- 7. It is clearly demonstrated that the CO<sub>2</sub> peaks appear at 350 °C, 550 °C and 720 °C, which is in line TGA. So the weight loss peak at 550 °C is attributed to the decomposition of carbonates which are still present in the catalysts' structure after calcination. A small peak at 350 °C could be also attributed to 'low temperature carbonates' but it was not observed by TGA due to the small precision. The quantity of the 'high temperature' carbonates is much bigger in the bifunctional catalyst CZZ-Si/Al-25 than in the pure CZZ catalyst resulting thus in the smaller copper crystallite size and higher metallic copper dispersion.

#### **4.3.1.6 Acid properties**

Acid sites are the active sites for methanol dehydration to DME [3, 20, 21], which is an very important function for the bifunctional catalysts working in direct DME synthesis reaction. The surface acid properties were determined by **temperature**

**programed desorption of NH<sub>3</sub> (NH<sub>3</sub>-TPD).** The NH<sub>3</sub> desorption profiles for bifunctional catalysts are shown in Figure 4- 8 and the NH<sub>3</sub> desorption amounts are summarized in Table 4- 6.

The profiles all display one asymmetric and broad NH<sub>3</sub> desorption peak from 150 °C to 600 °C, which shows the similar NH<sub>3</sub> desorption curves for the supports (chapter 3.3.3). It has been referred in chapter 3 that the strength of acid sites corresponds to the desorption temperature of NH<sub>3</sub>. Most of adsorbed NH<sub>3</sub> desorbs below 400 °C indicating that the most of the acid sites has weak and medium force, which is the exact active sites for methanol dehydration to DME.

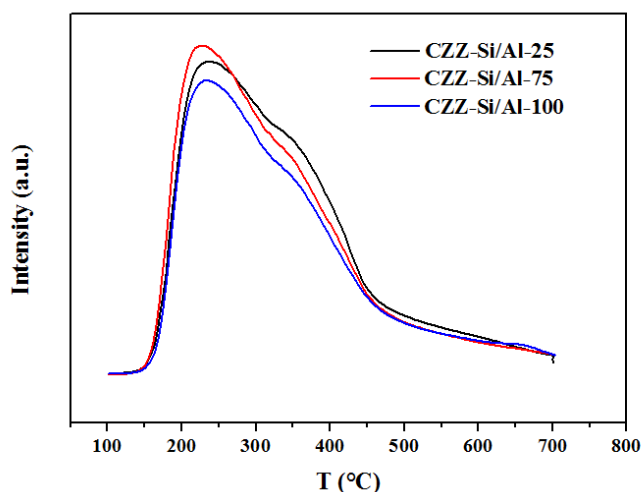


Figure 4- 8 NH<sub>3</sub>-TPD profiles of the bifunctional catalysts

Table 4- 6 Surface acid sites properties of bifunctional catalysts

Sample	mmol NH <sub>3</sub> /g
CZZ-Si/Al-25	0.338
CZZ-Si/Al-75	0.333
CZZ-Si/Al-100	0.308

From the Table 4- 6 it can be seen that the desorbed NH<sub>3</sub> amount doesn't change a lot for different bifunctional catalysts while still follows the trend, CZZ-Si/Al-25 > CZZ-Si/Al-75 > CZZ-Si/Al-100, which shows the same trend for Al-TUD-1 materials – the acidity increases slightly if the Si/Al ratio is decreased.

#### 4.3.1.7 Basic properties

The basic properties of the pure CZZ catalyst and the bifunctional catalyst CZZ-Si/Al-25 were measured by **temperature programmed desorption of CO<sub>2</sub> (CO<sub>2</sub>-TPD)** [22]. CO<sub>2</sub> has strong interaction with the basic sites, thus the strength of basic sites can be reflected by the desorption temperature of CO<sub>2</sub>, which follows the same principle as for NH<sub>3</sub>-TPD. The quantity of basic sites is correlated with the desorbed CO<sub>2</sub> amount [16, 23].

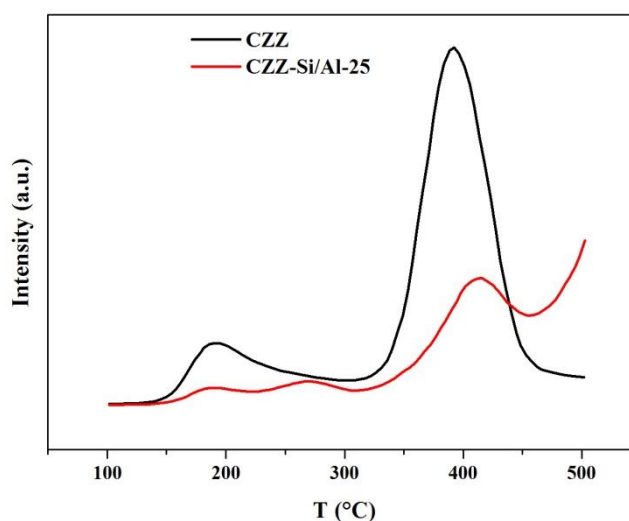


Figure 4- 9 CO<sub>2</sub>-TPD profiles for CZZ and CZZ-Si/Al-25

The CO<sub>2</sub> desorption profiles for CZZ and the bifunctional catalyst CZZ-Si/Al-25 are shown in Figure 4- 9. It is obviously observed that there are two big CO<sub>2</sub> desorption peaks for CZZ, one asymmetric peak – at 180 °C with a small shoulder, and one at 400 °C, which can be ascribed to weak basic sites and strong basic sites [16], respectively. For the bifunctional catalyst two small peaks are observed in the low temperature range under 300 °C that could correspond to the two different natures of the weak basic sites in the CZZ-Si/Al-25; the distribution of the weak basic sites is different for these catalysts, but the ratio between the quantity of weak and strong basic sites is similar for both catalysts – strong basicity is predominant. The total area of the CO<sub>2</sub> desorption peaks for bifunctional catalyst CZZ-Si/Al-25 is much smaller than for CZZ, which means that there are more basic sites on CZZ than on the bifunctional catalyst

CZZ-Si/Al-25. It can be concluded that after the CZZ was deposited on Al-TUD-1 (Si/Al-25) some basic sites on CZZ were lost.

#### 4.3.1.8 Morphology

The morphology of the catalysts was characterized by **transmission electron microscopy (TEM)**<sup>2</sup>. The TEM images of the calcined Al-TUD-1 (Si/Al-25), CZZ-Si/Al-25 and CZZ-Si/Al-100 are shown in Figure 4- 10.

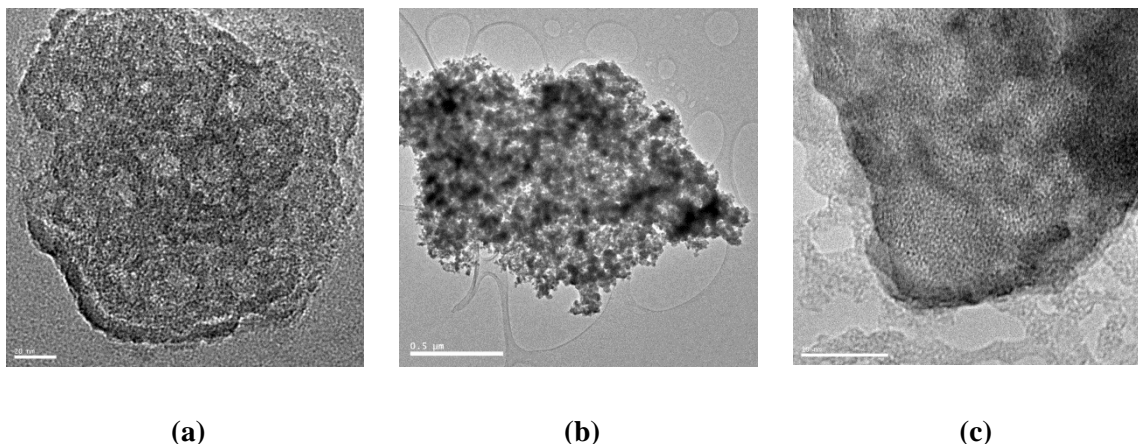


Figure 4- 10 The TEM images of the fresh Al-TUD-1 (a), CZZ-Si/Al-25 (b) and CZZ-Si/Al-100 (c)

The morphology of the pure Al-TUD-1 (Si/Al) is discussed in 3.3.1, from the TEM analysis (Figure 4- 10a) it can be seen that the material has an amorphous morphology with the presence of unordered worm-like pores. No crystallites were detected. The TEM image of CZZ-Si/Al-25 (Figure 4- 10b) was presented here with the scale of 0.5 μm. This material has an aerial aspect and seems to have large number of pores, it looks precisely as the Al-TUD-1 with the amorphous bulk structure and some dark areas that are coming probably from the CZZ deposited on the Si/Al support. When we go to the small scale of the TEM image for the bifunctional catalyst CZZ-Si/Al-100 (Figure 4- 10c), we found that there are no big particles observed and the amorphous morphology is still present. The bulk is amorphous Si/Al-25 with the worm-like pore structure. Some tiny crystalline domains were found on the border and on the surface, indicating that the metal oxides were well deposited and nicely dispersed on Al-TUD-1

<sup>2</sup>Acknowledgements to Corinne BOUILLET from IPCMS, Strasbourg, for the TEM characterization

support. The different metal oxides overlap with each other, supposing the intimate contact between CuO, ZnO, ZrO<sub>2</sub>. These results explain why no crystalline phase but one large and broadened peak was observed on the XRD patterns (Figure 4- 4a).

The TEM images of two reduced bifunctional catalysts are presented on Figure 4- 11.

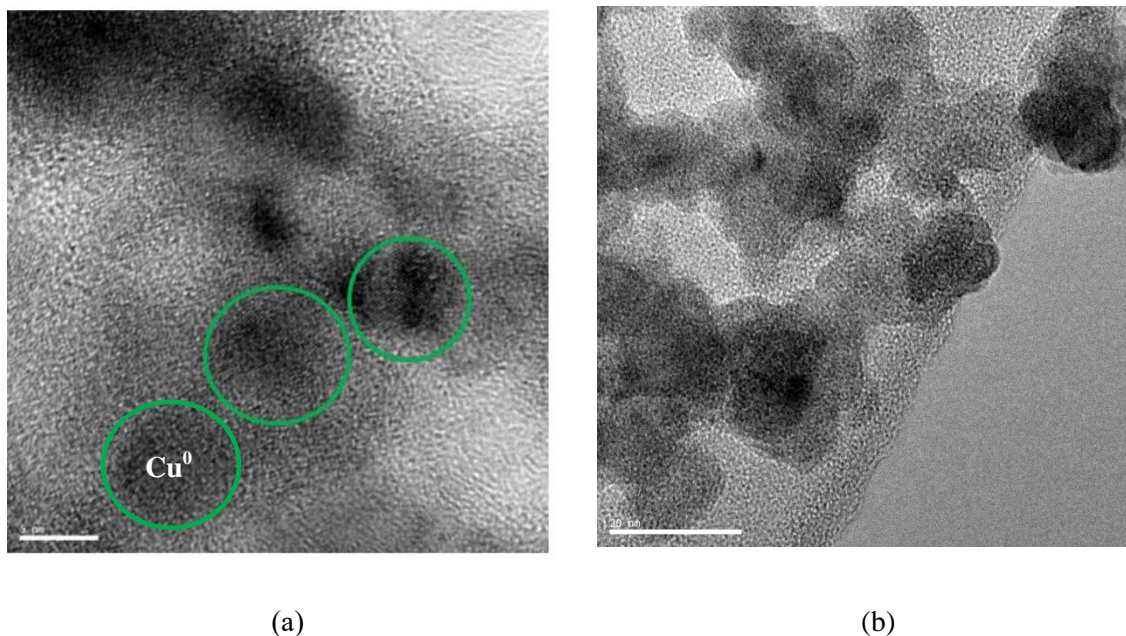


Figure 4- 11 TEM for the reduced CZZ-Si/Al-25 (a) and CZZ-Si/Al-50 (b)

For the reduced CZZ-Si/Al-25 (Figure 4- 11a) the microstructure of well dispersed metal oxides and metallic nanoparticles immobilized on the amorphous Al-TUD-1 (Si/Al-25) with worm-like pores was shown. The grain in the rings which is labeled by green (Figure 4- 11a) owns the lattice spacing of 2.0 Å, which is deduced to be the (1 1 1) surface of metallic copper with the d-spacing of 2.08Å. The particle size is around 5nm, which is consistent with the crystallite sizes calculated from XRD. The TEM image of the reduced CZZ-Si/Al-50 (Figure 4- 11b) demonstrates the overall porosity of the material and the dispersion of the copper based part on the amorphous Al-TUD-1.

#### **4.3.1.9 DFT modelling of the surface interaction with copper**

From the experimental results the co-precipitation method of the bifunctional catalysts synthesis is beneficial from several aspects: bigger specific surface area, nice dispersion of the copper based part, smaller metallic copper particles size were obtained. In the same time the reduction of copper is retarded and the acidity is partly lost after the deposition of the CZZ part. In order to investigate molecular level the interaction between the copper based part and the Al-TUD-1 part of the bifunctional materials the density functional theory was employed<sup>3</sup>.

In our work, metallic copper was simplified as one copper atom [24] to save the efficiency (Figure 4- 12). Pure silica was modeled as  $\alpha$ -SiO<sub>2</sub> [25] (Figure 4- 12), which was saturated with hydroxyl group on the surface (1 0 0) according to Zhuravlev model of the amorphous silica [26], with vacuum height of 10 Å to avoid the interaction between different periodic slabs [27]. Al-TUD-1 was modeled as Al doped silica (Figure 4- 12), namely that several tetravalent Si cations were replaced by trivalent Al cations [28]. In this study, the open source package-GPAW was employed for modelling. The adsorption properties of copper on pure silica and Al-doped silica were calculated respectively to study the interaction behaviors between copper and support and the influence of Al incorporation.

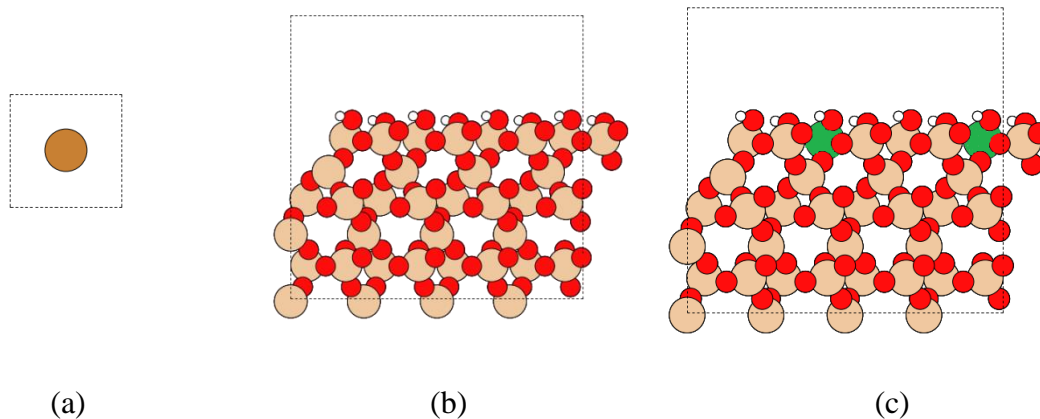


Figure 4- 12 Models for copper (a), pure SiO<sub>2</sub> (b) and Al doped SiO<sub>2</sub> (c)

<sup>3</sup>Acknowledgements for Thierry DINTZER from ICPEES, Strasbourg, for the DFT analysis

Three different adsorption sites were considered in the calculation: top site (on the top of one oxygen atom), bridge site (on the top of the O-O bridge) and hollow site (in the center of three oxygen atoms), which are shown in Figure 4- 13.

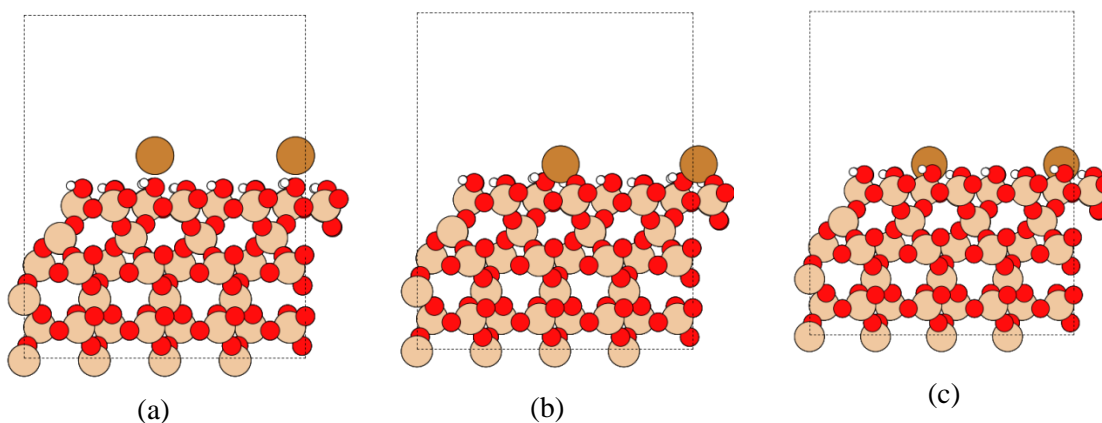


Figure 4- 13 Different adsorption sites of copper on SiO<sub>2</sub>, top site (a), bridge site (b) and hollow site (c)

The adsorption energies ( $E_{ads}$ ) are calculated as following:

$$E_{ads} = E_{SiO_2} + E_{copper} - E_{copper-SiO_2}$$

or

$$E_{ads} = E_{Al-SiO_2} + E_{copper} - E_{copper-Al-SiO_2}$$

The energies of different adsorption configurations were calculated, among which the three-order polynomial fitted curves for the energies of the top adsorption configurations on Cu-SiO<sub>2</sub> and Cu-Al doped SiO<sub>2</sub> are shown in Figure 4- 14.

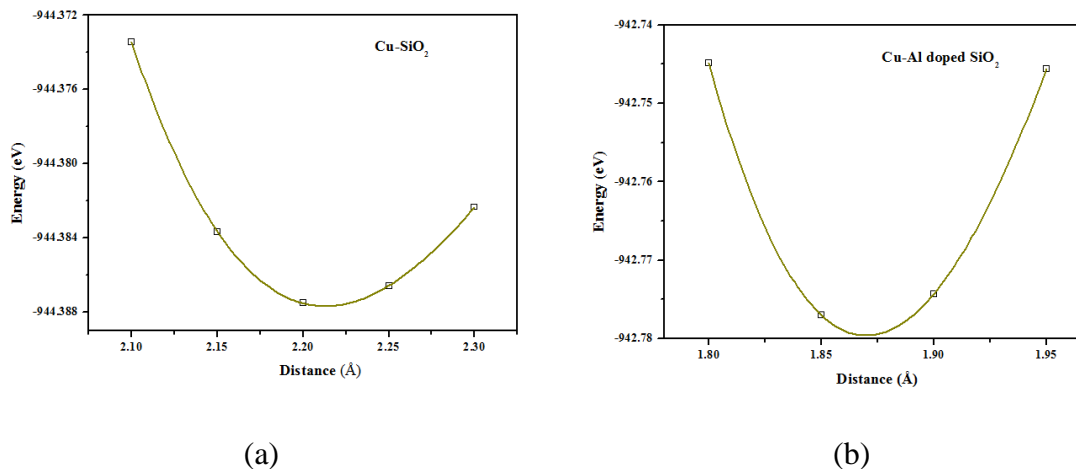


Figure 4- 14 Energies of Cu-SiO<sub>2</sub> (a) and Cu-Al-SiO<sub>2</sub> (b) with cutoff energy of 700 eV (top adsorption configurations)

The binding energy of copper is -0.0719 eV at the cutoff energy of 700 eV. The adsorption energies of the top site adsorption configuration on Cu-SiO<sub>2</sub> and Cu-Al-SiO<sub>2</sub> are summarized in Table 4- 7.

Table 4- 7 Adsorption energies for Cu-SiO<sub>2</sub> and Cu-Al-SiO<sub>2</sub> (Cu in top site)

Cu-SiO <sub>2</sub>		Cu-Al-SiO <sub>2</sub>	
distance/Å	Adsorption energy/eV	distance/Å	Adsorption energy/eV
2.1	-0.2477	1.8	-2.5690
2.15	-0.2579	1.85	-2.6012
2.2	-0.2617	1.9	-2.5984
2.25	-0.2608	1.95	-2.5698
2.3	-0.2566	-	-

From Figure 4- 14, it can be observed that the distances of Cu-O for the most stable Cu-SiO<sub>2</sub> and Cu-Al-SiO<sub>2</sub> adsorption configurations are around 2.21 and 1.87 Å. The distance between O atom and Cu atom is shorter, the interaction is stronger. Cu-Al-SiO<sub>2</sub> shows much higher adsorption energy by the factor of 10 than Cu-SiO<sub>2</sub> (Table 4- 7), which means the copper has stronger interaction with Al doped SiO<sub>2</sub> than with pure SiO<sub>2</sub>.

Other adsorption configurations of the bridge site and the hollow site were also calculated and the adsorption energies of copper on SiO<sub>2</sub> and Al doped SiO<sub>2</sub> is positive, which means they are not stable adsorption configurations.

The top site was demonstrated to be the most stable adsorption site. The adsorption energy of Cu on Al-doped SiO<sub>2</sub> (-2.6012 eV, top site) is higher than the one of Cu on SiO<sub>2</sub> (-0.2617 eV, top site), which means the interaction between copper and Al doped SiO<sub>2</sub> is stronger than the interaction between copper and pure SiO<sub>2</sub>.

The density functional theory results prove that the incorporation of Al can induce copper anchoring sites. It explains why the copper surface area increases with the Al content obtained from N<sub>2</sub>O-TPD results from the molecular level. The strong interaction between copper and the O atom connected with Al will lead to the coverage of the acid sites on the support.

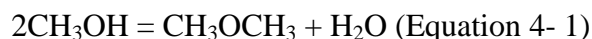
### 4.3.2 Catalytic tests

In this part, the bifunctional catalysts were tested in two reactions, the methanol dehydration to DME and the direct DME synthesis from CO<sub>2</sub>/H<sub>2</sub>.

#### 4.3.2.1 Methanol to DME

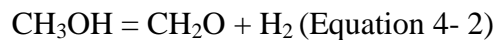
In order to understand the influence of CZZ component of the bifunctional catalysts on the activity in the methanol dehydration into DME reaction, the literature search of possible reactions was done. It has been indicated that the consumption of methanol was not only involved in methanol dehydration reaction (Equation 4- 1) but also occurred in methanol dehydrogenation reaction (Equation 4-2) which takes place on metallic copper surface [29, 30].

Methanol can dehydrate to DME on weak and moderate acid sites (Equation 4- 1). Depending on the strength of acid sites, the dehydration of methanol may continue till the formation of light hydrocarbons (methane and others) and olefins in the presence of zeolites or other strong solid acid materials [31, 32]. It is not expected in the case of our samples because our bifunctional materials possess only weak and moderate acid sites.



Methanol can dehydrogenate to formaldehyde on metallic copper active sites (Equation 5-5) [29, 30, 33-38]. This reaction is endothermic and thermodynamically

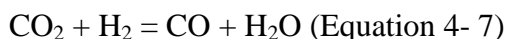
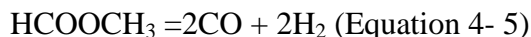
unfavorable below 400 °C, while it can proceed coupling with formaldehyde-consuming reaction which is favorable under 400 °C [34, 35].



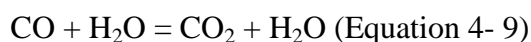
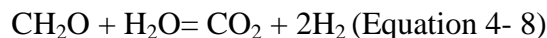
Different formaldehyde-consuming reactions have been reported. Methyl formate has been demonstrated as the main product in methanol dehydrogenation on copper containing catalyst. While the pathway for methyl formate formation is controversial. Some researchers hold the opinion that the methyl formate comes from the fast reaction between intermediate formaldehyde and the reactant methanol [29, 30] (Equation 4- 3). Other researchers thought that the methyl formate is formed from formaldehyde dimerization (Equation 4- 4) [35, 39, 40]. In our case, both of these reactions may happen but we will not focus on the pathways of the methyl formate production.



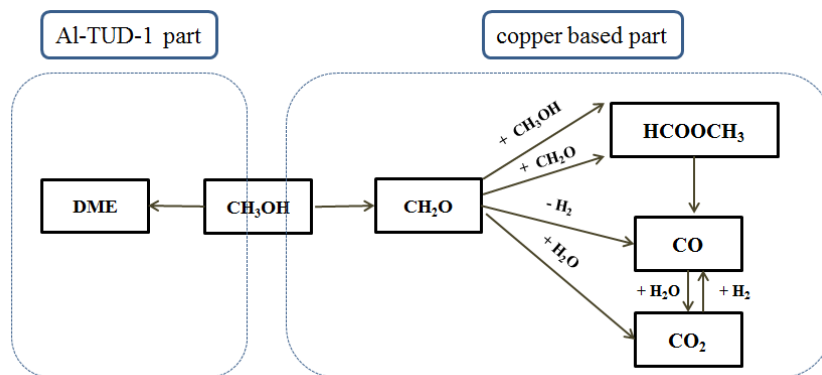
There are three kinds of explanations for CO formation, consecutive degradation of methyl formate [29, 30, 41] (Equation 4- 5) or the dehydrogenation of formaldehyde [35](Equation 4- 6). Another possible way is RWGS reaction (Equation 4- 7).



The pathway for CO<sub>2</sub> formation is also controversial. Some researchers thought that the water formed from methanol dehydration to DME reaction can easily react with the intermediate compound formaldehyde, resulting in the formation of CO<sub>2</sub> (Equation 4- 8) [29], while others thought that CO<sub>2</sub> comes from water gas shift reaction (Equation 4- 9) [34].



The schematic representation of the possible products and reaction pathways are shown in Scheme 4- 1.



Scheme 4- 1 Possible reaction pathways over the bifunctional catalysts

Firstly the pure copper based catalyst CZZ was tested in the methanol dehydration to DME. Then three bifunctional materials, CZZ-Si/Al-25, CZZ-Si/Al-75 and CZZ-Si/Al-100 with different ratio of Si/Al were tested as well. The catalytic tests were performed at 280 °C and atmospheric pressure. Methanol conversion will be followed. In the case of bifunctional catalysts H<sub>2</sub>, MF, CO and CO<sub>2</sub> were found as the reaction products together with the main product DME. CH<sub>2</sub>O was not observed in outgases. The discussion will be based on the following the formation of DME, MF and the mixture CO + CO<sub>2</sub>. H<sub>2</sub>O and H<sub>2</sub> were not detected by the GC column that was chosen.

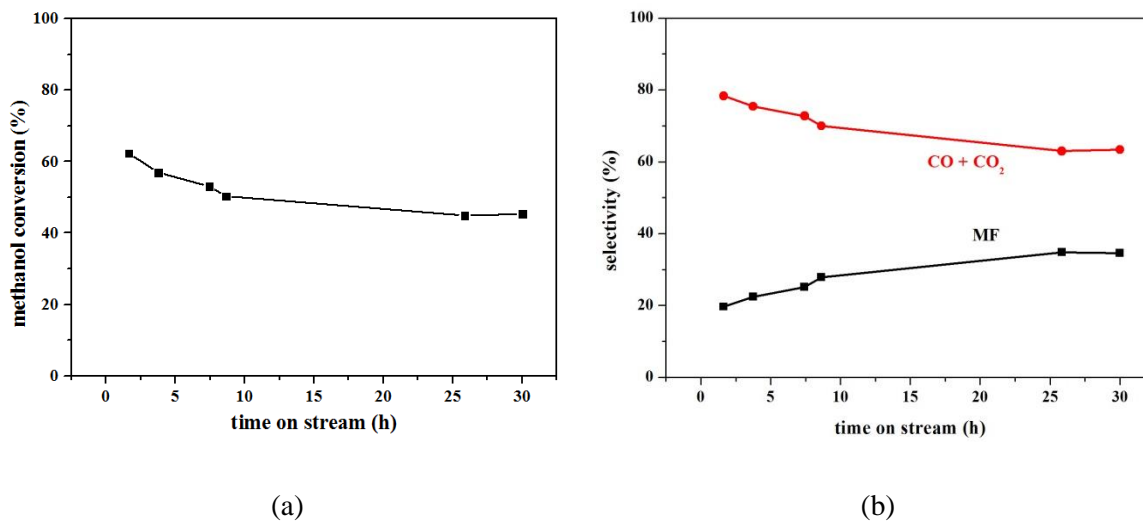


Figure 4- 15 Methanol conversion (a) and products selectivity (b) for CZZ catalyst

Figure 4- 15 presents the methanol conversion and selectivity of products formation in presence of the pure CZZ catalyst. Two main carbon-containing products are methyl formate and CO+CO<sub>2</sub>, no DME was detected. It can be observed that the methanol conversion decreases from 63% to 43% after 30h reaction. The selectivity of CO+CO<sub>2</sub> decreases from 80% to 64% and the selectivity of methyl formate increases from 20% to 35% after 30h reaction.

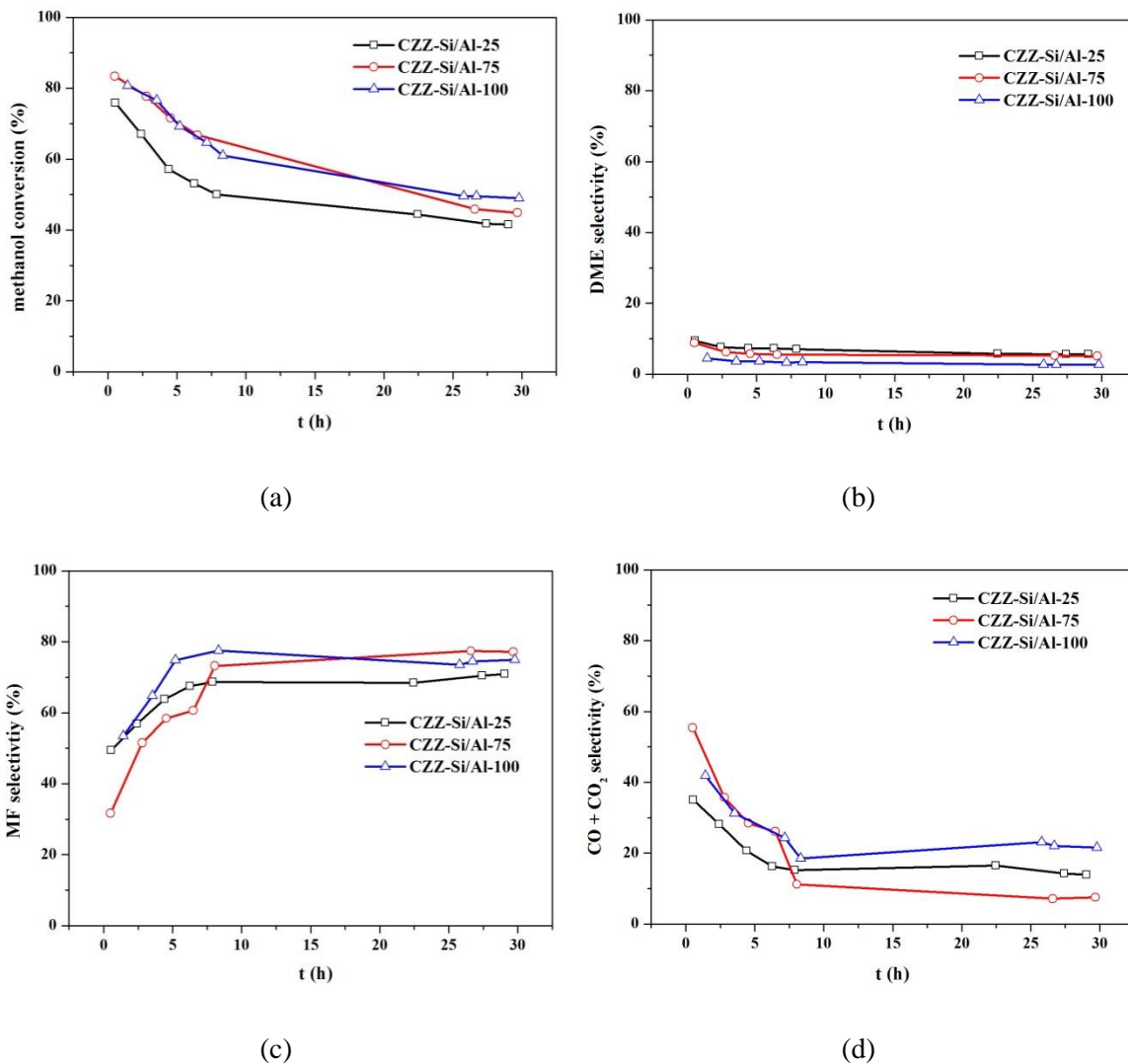


Figure 4- 16 Methanol conversion (a) and products selectivity (b, c, d) for bifunctional catalysts

Figure 4- 16 presents the methanol conversion and products selectivity for bifunctional catalysts. The methanol conversion decreases with time from 77-82% to 40-50%. In the beginning of the reaction it is slightly higher than for the pure CZZ catalyst probably due to the additional formation of DME (Figure 4- 16b). Three main carbon-containing products were observed: methyl formate, CO+CO<sub>2</sub> and DME. Methyl formate selectivity increases with time and CO selectivity decreases with time, those trends are opposite to what was observed for the pure CZZ catalyst. They become constant after 25h.

The more obvious decrease of the methanol conversion for bifunctional catalysts may due to some additional formation of water (Equation 4- 1) that has a negative effect on the catalytic performance. Apart from the methyl formate and carbon oxides the DME was obtained over the bifunctional catalysts. This is due to the existence of acid sites introduced by Al-TUD-1 support.

It has been reported that there are several factors which have influence on methyl formate decomposition to CO, such as contact time or basic properties [30, 41]. In this work, all the reactions were conducted with the GHSV of 10,000 h<sup>-1</sup>, so the basic property should be the main factor for the distribution of methyl formate and CO in the products. According to Yin et al's work [30], the catalyst with low quantity of basic sites favored the methanol dehydrogenation to methyl formate, while the catalysts with high amount of basic sites lead to the degradation of methyl formate to CO and H<sub>2</sub>. From the CO<sub>2</sub>-TPD results (chapter 4.3.1.7), it was found that CZZ owns more basic sites and has higher basicity than the bifunctional catalyst CZZ-Si/Al-25. It can be supposed that MF is decomposed on basic sites of CZZ and MF is accumulated in case of CZZ-Si/Al because of lack of basic sites. For all the catalysts the CO selectivity decreases and methyl formate selectivity increases with the time on stream. It may be supposed that a part of basic sites becomes inactive with the proceeding of the reaction.

The DME selectivity in the methanol dehydration reaction under atmospheric pressure for these three bi-functional catalysts was unexpectedly low – less than 10%. There was no visible trend of the activity in the function of the quantity of acid sites or

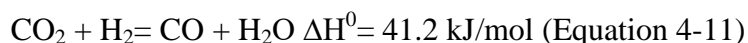
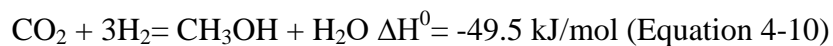
Si/Al ratio. The other products, carbon oxides and methyl formate, were observed. The selectivity of methyl formate formation over bifunctional catalysts is bigger than over the pure CZZ catalyst. On the contrary to methyl formate the selectivity of CO+CO<sub>2</sub> was much smaller for the bifunctional catalysts than for the CZZ catalyst. In the presence of pure CZZ catalyst methyl formate is rapidly decomposed to carbon oxides thanks to the presence of higher quantity of basic sites; as the CZZ catalyst does not contain acid sites there were no DME detected. The most probable reason of the low DME selectivity could be explained after DFT calculations explained in 4.3.1.9. It has been demonstrated that the copper shows the high adsorption energy (-2.6012 eV) on the Al modified SiO<sub>2</sub>. It implies that copper will probably occupy all the acid sites on the Al-TUD-1 support. Regarding the results obtained there is no expectation of a high DME selectivity in the direct DME synthesis under pressure.

#### **4.3.2.2 Direct DME synthesis**

Bifunctional catalysts prepared by co-precipitation deposition method were employed in direct DME synthesis reaction from CO<sub>2</sub>/H<sub>2</sub> mixture. The bifunctional catalyst with higher Al loading in the Al-TUD-1 (Si/Al) part is expected to be more active in the formation of methanol and DME as it owns bigger metallic copper surface area and slightly more acid sites.

#### *Thermodynamic simulation*

Thermodynamic simulation of the direct DME synthesis from CO<sub>2</sub>/H<sub>2</sub> mixture at was performed by ProSimPlus. The Gibbs reactor was used with the system based on the minimization of Gibbs energy. The thermodynamic simulation was done using the same reactants' flow composition as for catalytic tests: total flow 40 mL/min, H<sub>2</sub>/CO<sub>2</sub>/N<sub>2</sub> ratio equal to 3/1/0.16. The different reactions can happen in this system: methanol synthesis by CO<sub>2</sub> hydrogenation (Equation 4-10), methanol dehydration into DME (Equation 4-1) and Reverse Water Gas Shift reaction (Equation 4-11) [3, 42].



The products that could be formed are: DME, methanol, CO and water. The reactants and products together constitute the thermodynamic system. The temperature of the Gibbs reactor was varied from 200 to 320 °C, the pressure was fixed at 20 bars. The calculations of H<sub>2</sub> and CO<sub>2</sub> conversion, methanol, CO and DME selectivities were done. The results of the thermodynamic simulation of the direct DME synthesis from CO<sub>2</sub>/H<sub>2</sub> are shown in Figure 4- 17.

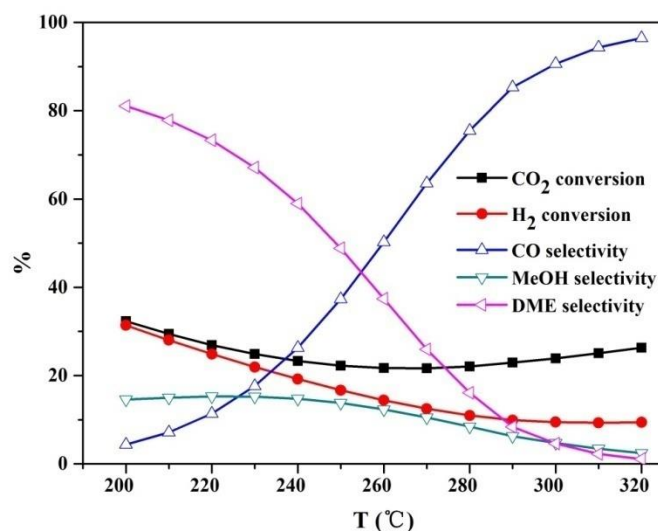


Figure 4- 17 Thermodynamic simulation results for direct DME synthesis from CO<sub>2</sub>/H<sub>2</sub>

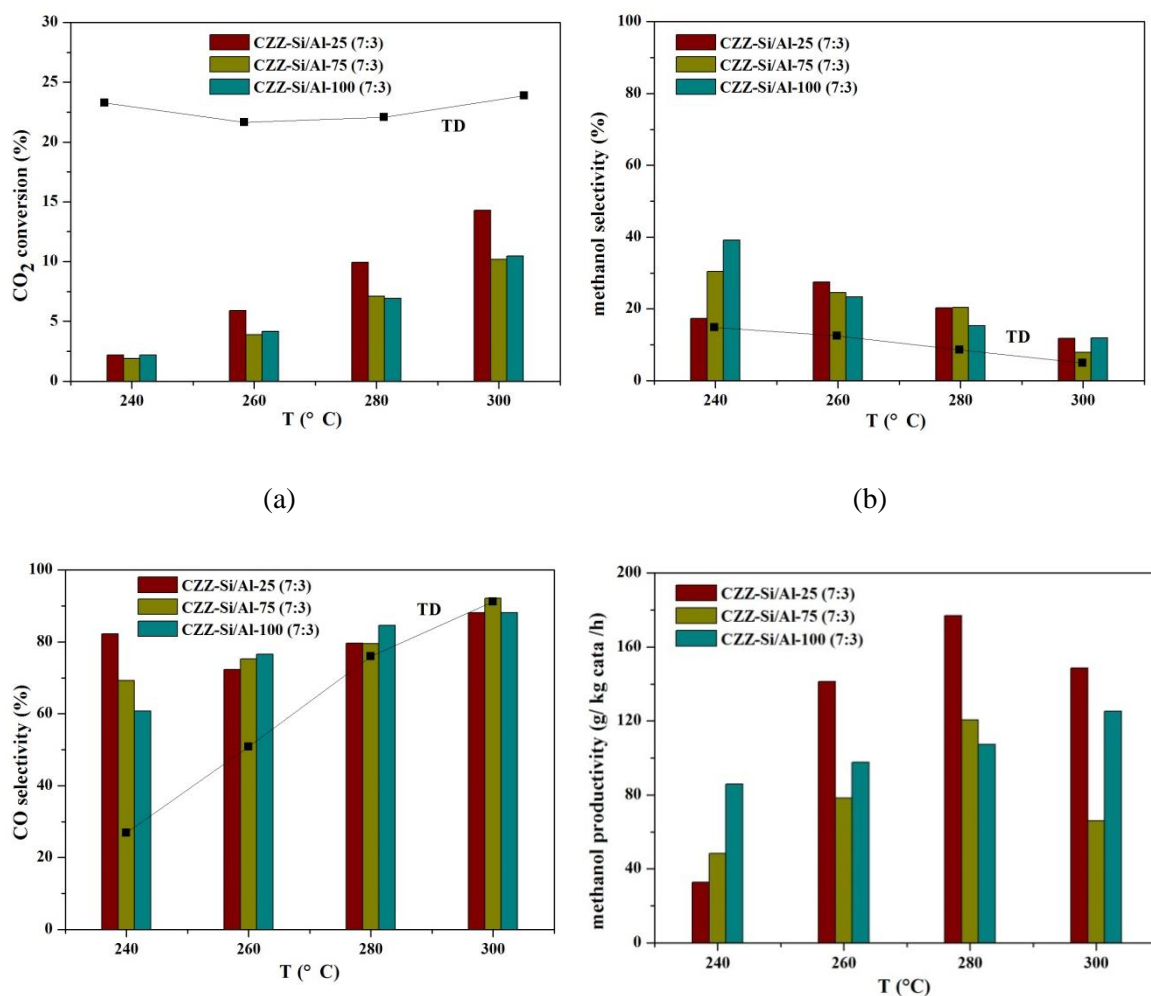
The CO<sub>2</sub> conversion and H<sub>2</sub> conversion are both 33% at 200 °C. Then CO<sub>2</sub> conversion decreases with the temperature and is observed with the minimum of 21% at 270 °C. The H<sub>2</sub> conversion decreases with temperature for all the temperatures studied and is around 11% at 320 °C. The methanol selectivity decreases with temperature from 15% at 200 °C to around 2% at 320 °C with slight slope. DME selectivity decreases with temperature from 81% at 200 °C to 0 at 320 °C and CO selectivity increases with temperature from 5% at 200 °C to 97% at 320 °C, which is due to the instinct of exothermic and endothermic reaction, respectively.

The results of thermodynamic simulations indicate clearly that the highest CO<sub>2</sub> and H<sub>2</sub> conversions as well as the highest DME selectivity could be obtained in the low temperatures range 200-220 °C according to the Le Chatelier law. However to obtain sufficient catalytic activity and thus to have sufficient reaction rates it is advised to work

at more elevated temperatures [43]. For the catalytic tests of the direct DME synthesis, following conditions were chosen: 240-300 °C and 20 bars. The influence of pressure was performed by L. Angelo [44] and it was shown that better methanol productivity could be obtained at higher pressures.

#### Catalytic results for the direct DME synthesis

The direct DME synthesis was performed in the presence of three bifunctional catalysts CZZ-Si/Al-25, CZZ-Si/Al-75 and CZZ-Si/Al-100. The tests were done at 240 °C, 260 °C, 280 °C and 300 °C at 20 bars. The catalytic results: CO<sub>2</sub> conversion, methanol and CO selectivity and methanol productivity as well as the TD values are shown in Figure 4- 18.



(c)

(d)

Figure 4- 18 Direct DME synthesis results of bifunctional catalysts

From the catalytic results of these three bifunctional catalysts, it can be seen that the CO<sub>2</sub> conversion increases with temperature and bifunctional catalysts CZZ-Si/Al-25 shows the highest CO<sub>2</sub> conversion at all the investigated temperatures. The CO selectivity increases with temperature and methanol selectivity decreases with temperature, which is in line with thermodynamic simulation and due to the endothermic and exothermic reaction instinct.

Among the three bifunctional catalysts, the methanol productivity for CZZ-Si/Al-25 increases from 240 °C to 280 °C and reaches the maximum at 280 °C with 180 g/ kg cata/ h. CZZ-Si/Al-75 also shows the highest methanol productivity at 280 °C with 120 g/ kg cata/ h. While for the catalyst CZZ-Si/Al-100, the methanol productivity increases with temperature and shows the highest value at 300 °C with also around 120 g/ kg cata/ h. The bifunctional catalyst CZZ-Si/Al-25 shows the highest methanol productivity probably due to the biggest metallic copper surface area (10.3 m<sup>2</sup>/g cata from N<sub>2</sub>O-TPD results), which is responsible for high methanol productivity from CO<sub>2</sub> hydrogenation reaction [13, 45].

The DME selectivity was found very low, less than 1% for all these bifunctional catalysts. It has been demonstrated that the water existence shows the negative effect on methanol dehydration to DME performance in chapter 3. For the direct DME synthesis from CO<sub>2</sub>/H<sub>2</sub>, water comes from CO<sub>2</sub> hydrogenation to methanol (Equation 4-10), RWGS (Equation 4-11) and methanol dehydration to DME reaction (Equation 4-1). All the reactions occurred in the reaction system produce water and there is no reaction that consumes it. So there is a high amount of water that exists in the reaction system and that may affect the formation of DME by its preferential adsorption on the acid sites of Al-TUD-1 (Si/Al) part and thus resulting in the decrease of a number of acid sites for methanol dehydration to DME.

Another reason of low DME selectivity was proved by DFT calculations in 4.3.1.9. It has been demonstrated that the copper shows the high adsorption energy (-2.6012 eV) on the top site of O atom connected with Al in the modified SiO<sub>2</sub>. It implies that copper would occupy all the acid sites on the Al-TUD-1 support. The molar ratio of Cu/Al in the catalyst CZZ-Si/Al-25 is equal to 17, so probably the increasing the Al amount in Al-TUD-1 and increasing the mass loading of Al-TUD-1 are the promising ways for optimization of the bifunctional catalyst.

Though the bifunctional catalysts have low DME selectivity, the methanol productivity was obtained as high as 180 g/ kg cata/ h at 280 °C over the catalyst CZZ-Si/Al-25. Additional catalytic tests at higher pressure were performed (50 bars) to compare the catalyst CZZ-Si/Al-25 to the pure copper based catalyst CZZ. The catalytic results are show in Table 4- 8.

Table 4- 8 Catalytic results of direct DME synthesis from CO<sub>2</sub>/H<sub>2</sub> over pure CZZ catalyst (50 bars) and bifunctional catalyst CZZ-Si/Al-25 (50 bars and 20 bars)

Sample	Temperature (°C)	Conversion (%)		Selectivity (%)		Methanol productivity (g/kg <sub>cata</sub> *h)	Methanol productivity (mg/m <sup>2</sup> <sub>Cu</sub> *h)	Methanol productivity (g/g <sub>Cu</sub> *h)
		CO <sub>2</sub>	H <sub>2</sub>	CO	MeOH			
CZZ 50 bars	260	17.4	7.5	57.5	42.5	347	33.0	1.16
	280	25.3	10.3	65.5	34.5	410	39.1	1.37
CZZ-Si/Al- 25 (7:3) 50 bars	260	10.6	4.7	55.3	44.7	330	32.0	1.57
	280	15.3	6.5	64.1	35.8	383	37.2	1.82
	300	18.2	7.4	73.3	26.7	338	32.9	1.61
CZZ-Si/Al- 25 (7:3) 20 bars	260	5.9	2.6	72.3	27.5	141	13.7	0.67
	280	10.0	3.9	79.6	20.3	177	17.2	0.84
	300	14.3	4.9	88.1	11.8	149	14.4	0.71

The CO<sub>2</sub> conversion and H<sub>2</sub> conversion are higher in the case of pure CZZ copper based catalyst probably due to higher content of basic sites that activate CO<sub>2</sub>. In the same time the selectivities of CO and methanol formation are approximately the same – it proves that the acid sites of Al-TUD-1 (Si/Al) part of the bifunctional catalyst are not working at all and seem to be completely blocked by copper based catalyst. The Al that should bring the weak-moderate acidity for the transformation of methanol to DME is serving actually as the copper dispersion agent. So the increasing of the Al amount in Al-TUD-1 or increasing of the mass loading of Al-TUD-1(Si/Al) part in the bifunctional catalysts are promising. Nevertheless thanks to the fact that the bifunctional catalyst

CZZ-Si/Al-25 (7:3) has lower loading of copper and its better dispersion and thus has bigger methanol productivity per g of copper per hour (Table 4- 8).

#### 4.4 The influence of weight ratio between CZZ and Al-TUD-1

In order to improve the DME selectivity and the DME productivity, two bifunctional catalysts with increased mass loading of Al-TUD-1 (Si/Al=25) part were prepared by co-precipitation-deposition method, with the CZZ to Al-TUD-1 (Si/Al=25) ratio 5:3 and 1:1. The prepared materials were characterized and tested in the direct DME synthesis at 20 bars.

##### 4.4.1 Characterization results

Three bifunctional catalysts CZZ-Si/Al-25 (7:3), CZZ-Si/Al-25 (5:3), CZZ-Si/Al-25 (1:1) were prepared as it was described in 4.2. Different characterization methods have been used for the analysis of these materials.

The isotherms and pore distributions measured by **N<sub>2</sub> adsorption/desorption method** are shown in Figure 4-19. The textural properties are shown in Table 4-9.

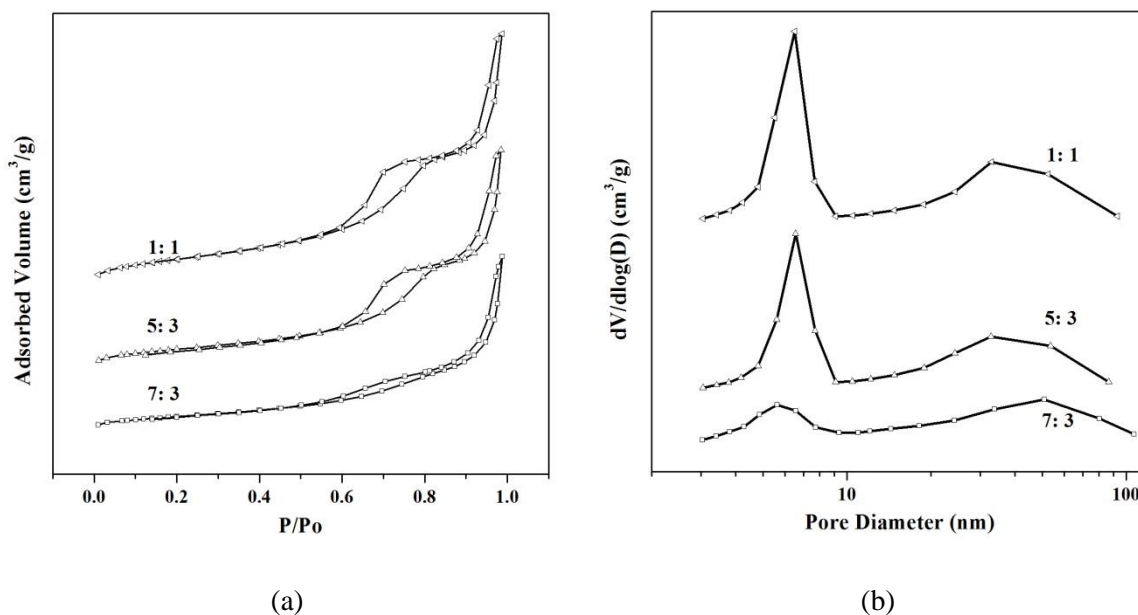


Figure 4-19 N<sub>2</sub> adsorption-desorption isotherms (a), and pore distribution (b) for bifunctional catalysts

The bifunctional catalysts own two kinds of pores, which can be reflected by isotherms with two hysteresis loops of H1 and H3-type, and by pore distribution with two different pore sizes (narrow pore distribution around 5 nm and broad pore distribution from 10 nm to 100 nm). The small pores around 5 nm owes to the Al-TUD-1 support and the big pores with broad distribution belong to the pore structure of CZZ. This has been detailed for the four bifunctional catalysts in 4.3.1.1.

Table 4-9 Physicochemical properties of catalysts

sample	S <sub>BET</sub> (m <sup>2</sup> g <sup>-1</sup> )	V <sub>pore</sub> (cm <sup>3</sup> g <sup>-1</sup> )	D <sub>p</sub> (nm)	Cu surface area (m <sup>2</sup> g <sub>cata</sub> <sup>-1</sup> )	Cu surface area (m <sup>2</sup> g <sub>copper</sub> <sup>-1</sup> )
CZZ-Si/Al-25 (7:3)	161	0.71	5.6, 50.9	10.3	49.3
CZZ-Si/Al-25 (5:3)	225	0.92	6.5, 32.9	6.1	32.5
CZZ-Si/Al-25 (1:1)	315	1.04	6.5, 32.9	Under limit	Under limit

With increasing the content of Al-TUD-1 (Si/Al) part, the fraction of small pores increased, which can be reflected by the size of hysteresis loop as well as the peak area (around 5 nm) in pore distribution [3]. The specific surface area is improved also and the total pore volume is increased (Table 4-9).

**Powder X-ray diffraction (XRD)** was employed for the characterization of the phase composition of the catalysts and the XRD patterns for the fresh and reduced bifunctional catalysts are shown in Figure 4-20.

It shows the amorphous XRD patterns for the calcined samples with two amorphous peaks, 10°-30° and 30°-40°, which due to amorphous SiO<sub>2</sub> from the XRD sampler and overlapping of broadened CuO and ZnO peaks, respectively. Peaks belonging to the metallic copper (Figure 4-20b) present in reduced bifunctional catalysts were analyzed to calculate the crystallite sizes, the results are shown in Table 4- 10. It can be observed that the metallic copper crystallite size decreases with the additional amount of Al-TUD-1 in the bifunctional catalysts, which means that metallic copper is better dispersed with higher Si/Al support content.

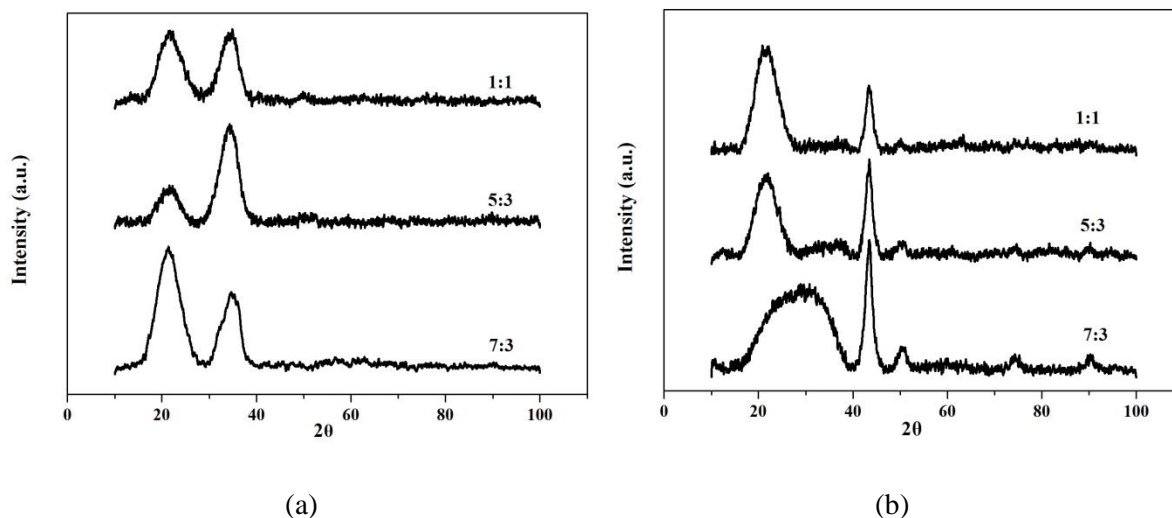


Figure 4-20 XRD patterns of calcined (a) and reduced (b) (280 °C, 1 °C/min, 50 mL/min 10% $H_2$ /Ar) bifunctional catalysts CZZ-Si/Al with different weight ratio between CZZ and Si-Al

Table 4- 10 Metallic copper crystallite size in the reduced bifunctional catalysts

sample	metallic copper particle size (nm)
CZZ-Si/Al-25 (7:3)	5.6
CZZ-Si/Al-25 (5:3)	5.4
CZZ-Si/Al-25 (1:1)	4.8

The metallic copper plays an important role in the  $CO_2$  hydrogenation to methanol, and big surface area with easy reducibility of CuO is responsible for a good methanol synthesis performance [46]. The reduction behavior and the interaction between copper and the support were studied by  **$H_2$  temperature programmed reduction ( $H_2$ -TPR)**. The interaction of copper crystallites with the support is also important for suppress of the copper particles aggregation during the reaction [46].

The reduction profiles of the bifunctional catalysts are shown in Figure 4- 21. All the catalysts present one broad asymmetric reduction curve. For example, CZZ-Si/Al-25 (7:3) possesses the main reduction peak at 263 °C with a tiny shoulder peak at 232 °C. CZZ-Si/Al-25 (5:3) presents two obvious reduction peaks with the peaks maxima at 247 °C and 273 °C. CZZ-Si/Al-25 (1:1) also shows two distinct reduction peaks at 252 °C and 287 °C, respectively. The asymmetric reduction peak with a shoulder peak

indicates that there is a strong interaction between copper and support, which is maybe owing to the successive reduction of copper,  $\text{Cu}^{2+} \rightarrow \text{Cu}^{1+} \rightarrow \text{Cu}^0$ . The reduction temperature increases with the content of Al-TUD-1 (Si/Al) part, which may be due to that more copper anchoring sites are introduced after improving the support content, leading to the stronger interaction between copper and support.

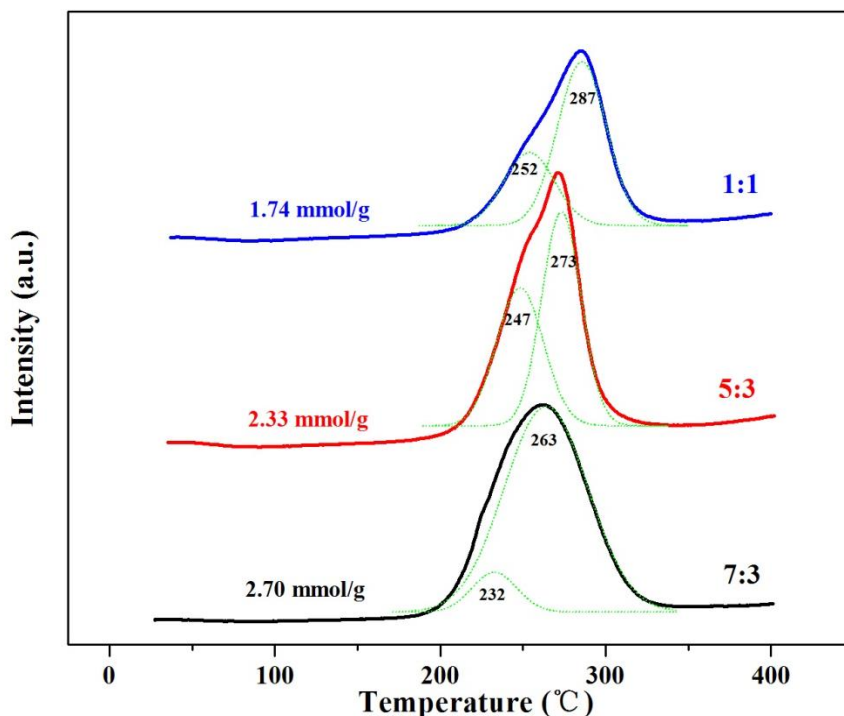


Figure 4- 21 TPR patterns for bifunctional catalysts

The  $\text{H}_2$  consumptions for CZZ-Si/Al-25 (7:3), CZZ-Si/Al-25 (5:3) and CZZ-Si/Al-25 (1:1) were found 2.70 mmol/g, 2.33mmol/g and 1.74 mmol/g, respectively. The decrease of  $\text{H}_2$  consumption was caused by the decreases of CZZ content.

The copper reducibility and the copper dispersion are shown in Table 4- 11. The reduction degree of copper was reflected by the reducibility calculated from the  $\text{H}_2$  consumption. The reducibility of these three bifunctional catalysts is 83% for CZZ-Si/Al-25 (7:3), 79% for CZZ-Si/Al-25 (5:3) and 72 % for CZZ-Si/Al-25 (1:1). It decreases with the support content, which is due to the stronger metal support interaction (SMSI) with lower copper content and improving aluminum content in the overall bifunctional material [30]. Some copper could be embedded in the pore structure of Al-

TUD-1 with increased pore volume after improving the support content and thus it is inaccessible for reduction.

Table 4- 11 copper reducibility, copper surface area and copper dispersion of bifunctional catalysts

sample	Reducibility (%)	Copper dispersion (%)
CZZ-Si/Al-25 (7:3)	83	9.2
CZZ-Si/Al-25 (5:3)	79	5.8
CZZ-Si/Al-25 (1:1)	72	-

The metallic copper surface was measured by N<sub>2</sub>O-TPD continuous method; the results are shown in Table 4-9. The metallic copper surface area for these catalysts follow the trend, CZZ-Si/Al-25 (7:3) > CZZ-Si/Al-25 (5:3) > CZZ-Si/Al-25 (1:1), which is due to the decrease of copper base part content. The copper dispersion was calculated by the combination of the results from N<sub>2</sub>O-TPD and H<sub>2</sub>-TPR. The copper dispersion is 9.2% for CZZ-Si/Al-25 (7:3) and 5.8% for CZZ-Si/Al-25 (5:3). It decreases with the decrease of the copper content.

#### 4.4.2 Direct DME synthesis

Bifunctional catalysts with different weight ratio between CZZ and Al-TUD-1 (Si/Al) prepared by co-precipitation deposition method were employed in the direct DME synthesis reaction from CO<sub>2</sub>/H<sub>2</sub> mixture. The bifunctional catalyst with higher Al-TUD-1 (Si/Al) part loading is expected to be more active in the formation of methanol and DME as it owns bigger metallic copper surface area and more acid sites.

The CO<sub>2</sub> conversion, methanol selectivity, CO selectivity and methanol productivity over the bifunctional catalysts CZZ-Si/Al-25 (7:3), CZZ-Si/Al-25 (5:3) and CZZ-Si/Al-25 (1:1) as well as the TD results are shown in Figure 4-22.

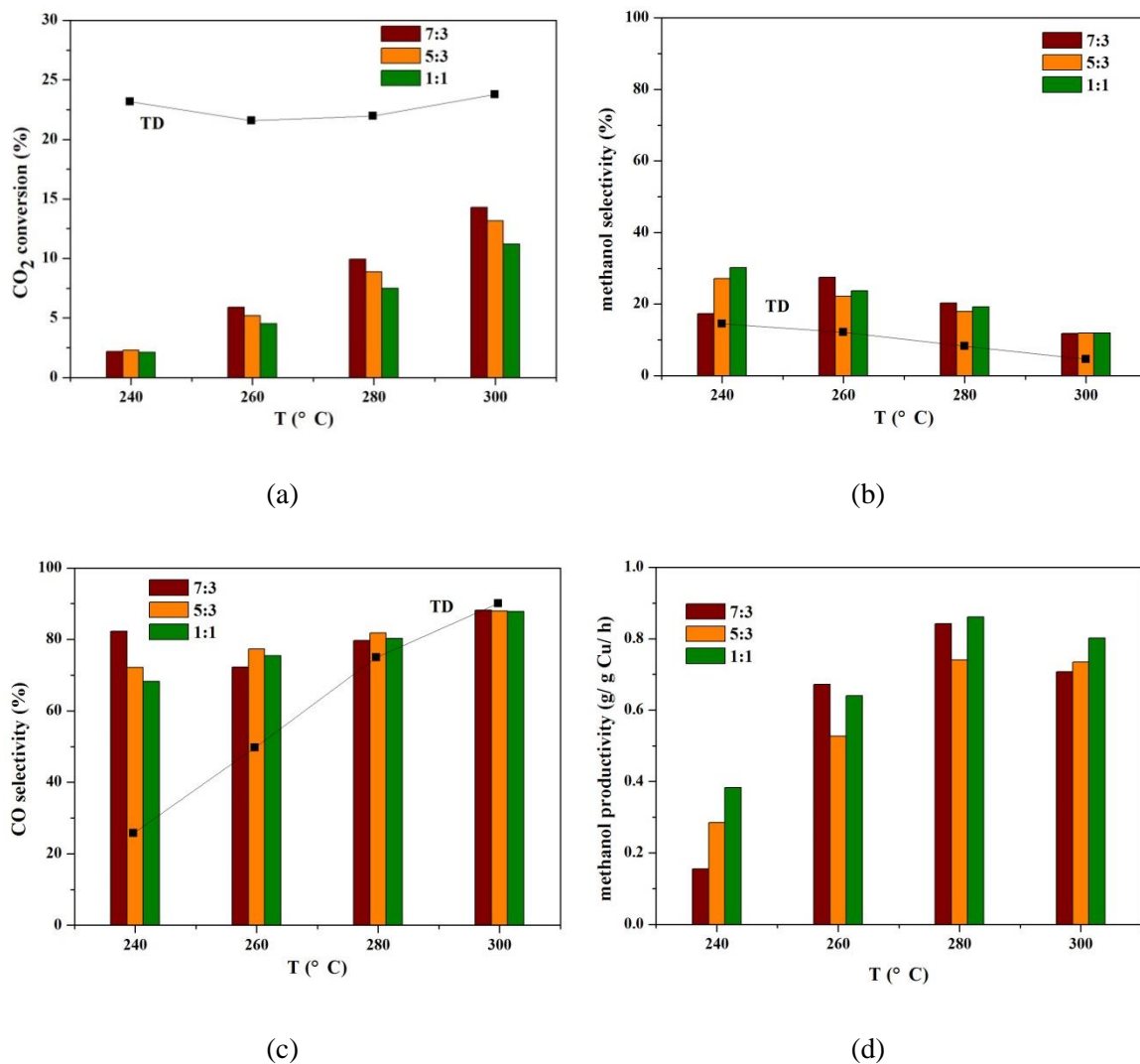


Figure 4-22 Direct DME synthesis results of bifunctional catalysts CZZ-Si/Al-25 (7:3), CZZ-Si/Al-25 (5:3) and CZZ-Si/Al-25 (1:1)

For all the three bifunctional catalysts, the CO<sub>2</sub> conversion increases with temperature. The main carbon-containing products were methanol and CO, very small selectivity of DME formation was observed (less than 1.6%). Methanol selectivity decreases with temperature and CO selectivity increases with temperature, which is owing to the intrinsic exothermic and endothermic reaction heat. There is no big difference of methanol selectivity and CO selectivity for all the three catalyst, showing around 80 % CO selectivity at 280 °C, which is consistent with thermodynamic simulation results. The methanol selectivity is bigger than the thermodynamic results. It is caused by the absence of DME in the products. Despite the similar catalytic activity of

these samples the copper content was not the same. The highest methanol productivity 0.86 g/ g Cu/ h was observed over the catalyst CZZ-Si/Al-25 (1:1) at 280 °C.

It can be found that the DME selectivity is not well improved by the increasing of Al-TUD-1 (Si/Al) part content. The main reason for the unpleasant results of the direct DME synthesis performance is insufficient content of acid sites in the catalyst. The molar ratio of Cu/Al in the catalyst CZZ-Si/Al-25 (1:1) is equal to 7, so probably the increasing the mass loading of Al-TUD-1 was not sufficient due to the blockage of acid sites by copper based part.

## 4.5 Conclusions and perspectives

The bifunctional catalysts CZZ-Si/Al prepared by co-precipitation deposition method show bigger specific surface area than the pure CZZ copper based catalyst. They possess an amorphous morphology similar to the Al-TUD-1 structure. This method of synthesis allows good copper dispersion over the Si/Al support with small metallic copper particles around 5 nm. The copper surface area increases with the decrease of Si/Al ratio. The bifunctional catalyst CZZ-Si/Al-25 shows the biggest copper surface area ( $10.3 \text{ m}^2/\text{g}_{\text{cata}}$ ) among all the investigated bifunctional catalysts. All the catalysts with different Si/Al ratio were tested in the direct DME synthesis. Low DME selectivity was observed for all the bifunctional catalysts, but nevertheless they were active in the methanol formation and the highest methanol productivity 180 g/ kg cata/ hat 280 °C was obtained for CZZ-Si/Al-25.

The density functional theory was employed to investigate the Al influence on the interaction behavior between copper and silica or Al doped silica. The adsorption energy of Cu on Al-doped  $\text{SiO}_2$  in the top site adsorption configuration (-2.6012 eV) is higher than the adsorption energy of Cu on pure  $\text{SiO}_2$  (-0.2617 eV), which means that the incorporation of Al can induce copper anchoring sites and this implies that copper occupies the acid sites on the support.

In addition two bifunctional catalysts with more Al-TUD-1 part in the bifunctional catalyst CZZ-Si/Al-25 were prepared in order to increase the quantity of acid

sites. The materials were tested in the direct DME synthesis. Still low DME selectivity was observed. It is assumed that the copper based part of the bifunctional catalysts blocks the acid sites of the Al-TUD-1 part.

The reasons for the observed low DME productivity are the insufficient quantity of acid sites; the blockage of acid sites by copper based parts and also the presence of water in the reaction system.

The possible way of the bifunctional catalyst optimization would be the increasing of the content of the Al-TUD-1 part but in this case the copper content will decrease and probably the catalytic activity of the samples in methanol formation from CO<sub>2</sub> hydrogenation will be lost. So it is interesting to find a way to expose the acid sites on the surface without their blockage by copper.

## 4.6 References

- [1] M. Behrens, D. Brennecke, F. Girgsdies, S. Kissner, A. Trunschke, N. Nasrudin, S. Zakaria, N.F. Idris, S.B. Abd Hamid, B. Kniep, R. Fischer, W. Busser, M. Muhler, R. Schlogl, Understanding the complexity of a catalyst synthesis: Co-precipitation of mixed Cu,Zn,Al hydroxycarbonate precursors for Cu/ZnO/Al<sub>2</sub>O<sub>3</sub> catalysts investigated by titration experiments, *Appl Catal A-Gen*, 392 (2011) 93-102.
- [2] K.S.W. Sing, D.H. Everett, R.A.W. Haul, L. Moscou, R.A. Pierotti, J. Rouquerol, T. Siemieniewska, Reporting Physisorption Data for Gas Solid Systems with Special Reference to the Determination of Surface-Area and Porosity (Recommendations 1984), *Pure Appl Chem*, 57 (1985) 603-619.
- [3] J.W. Bae, H.S. Potdar, S.H. Kang, K.W. Jun, Coproduction of methanol and dimethyl ether from biomass-derived syngas on a Cu-ZnO-Al<sub>2</sub>O<sub>3</sub>/  $\gamma$ -Al<sub>2</sub>O<sub>3</sub> hybrid catalyst, *Energy Fuel*, 22 (2008) 223-230.
- [4] M.S. Hamdy, G. Mul, W. Wei, R. Anand, U. Hanefeld, J.C. Jansen, J.A. Moulijn, Fe, Co and Cu-incorporated TUD-1: Synthesis, characterization and catalytic performance in N<sub>2</sub>O decomposition and cyclohexane oxidation, *Catal Today*, 110 (2005) 264-271.
- [5] A. Garcia-Trenco, A. Martinez, A simple and efficient approach to confine Cu/ZnO methanol synthesis catalysts in the ordered mesoporous SBA-15 silica, *Catal Today*, 215 (2013) 152-161.
- [6] M. Gentzen, W. Habicht, D.E. Doronkin, J.D. Grunwaldt, J. Sauer, S. Behrens, Bifunctional hybrid catalysts derived from Cu/Zn-based nanoparticles for single-step dimethyl ether synthesis, *Catal Sci Technol*, 6 (2016) 1054-1063.
- [7] K.F. Dong, H.H. Li, J.Y. Deng, Y.G. Peng, G. Ju, G.M. Chow, J.S. Chen, Crystalline ZrO<sub>2</sub> doping induced columnar structural FePt films with larger coercivity and high aspect ratio, *J Appl Phys*, 117 (2015).
- [8] C. Baltes, S. Vukojevic, F. Schuth, Correlations between synthesis, precursor, and catalyst structure and activity of a large set of CuO/ZnO/Al<sub>2</sub>O<sub>3</sub> catalysts for methanol synthesis, *J Catal*, 258 (2008) 334-344.
- [9] H. Gies, S. Grabowski, M. Bandyopadhyay, W. Grunert, O.P. Tkachenko, K.V. Klementiev, A. Birkner, Synthesis and characterization of silica MCM-48 as carrier of

size-confined nanocrystalline metal oxides particles inside the pore system, *Micropor Mesopor Mat*, 60 (2003) 31-42.

[10] O.P. Tkachenko, K.V. Klementiev, E. Loffler, I. Ritzkopf, F. Schuth, M. Bandyopadhyay, S. Grabowski, H. Gies, V. Hagen, M. Muhler, L.H. Lu, R.A. Fischer, W. Grunert, The structure of zinc and copper oxide species hosted in porous siliceous matrices, *Phys Chem Chem Phys*, 5 (2003) 4325-4334.

[11] C.J. Huang, S.Y. Chen, X.Y. Fei, D. Liu, Y.C. Zhang, Catalytic Hydrogenation of CO<sub>2</sub> to Methanol: Study of Synergistic Effect on Adsorption Properties of CO<sub>2</sub> and H<sub>2</sub> in CuO/ZnO/ZrO<sub>2</sub> System, *Catalysts*, 5 (2015) 1846-1861.

[12] F. Arena, K. Barbera, G. Italiano, G. Bonura, L. Spadaro, F. Frusteri, Synthesis, characterization and activity pattern of Cu-ZnO/ZrO<sub>2</sub> catalysts in the hydrogenation of carbon dioxide to methanol, *J Catal*, 249 (2007) 185-194.

[13] L. Angelo, M. Girleanu, O. Ersen, C. Serra, K. Parkhomenko, A.C. Roger, Catalyst synthesis by continuous coprecipitation under micro-fluidic conditions: Application to the preparation of catalysts for methanol synthesis from CO<sub>2</sub>/H<sub>2</sub>, *Catal Today*, 270 (2016) 59-67.

[14] G.C. Chinchin, C.M. Hay, H.D. Vandervell, K.C. Waugh, The Measurement of Copper Surface-Areas by Reactive Frontal Chromatography, *J Catal*, 103 (1987) 79-86.

[15] A.Y. Yin, X.Y. Guo, W.L. Dai, K.N. Fan, Effect of Si/Al Ratio of Mesoporous Support on the Structure Evolution and Catalytic Performance of the Cu/Al-HMS Catalyst, *J Phys Chem C*, 114 (2010) 8523-8532.

[16] W.J. Cai, P.R. de la Piscina, J. Toyir, N. Homs, CO<sub>2</sub> hydrogenation to methanol over CuZnGa catalysts prepared using microwave-assisted methods, *Catal Today*, 242 (2015) 193-199.

[17] M. Schur, B. Bems, A. Dassenoy, I. Kassatkine, J. Urban, H. Wilmes, O. Hinrichsen, M. Muhler, R. Schlogl, Continuous coprecipitation of catalysts in a micromixer: Nanostructured Cu/ZnO composite for the synthesis of methanol, *Angew Chem Int Edit*, 42 (2003) 3815-3817.

[18] B. Bems, M. Schur, A. Dassenoy, H. Junkes, D. Herein, R. Schlogl, Relations between synthesis and microstructural properties of copper/zinc hydroxycarbonates, *Chem-Eur J*, 9 (2003) 2039-2052.

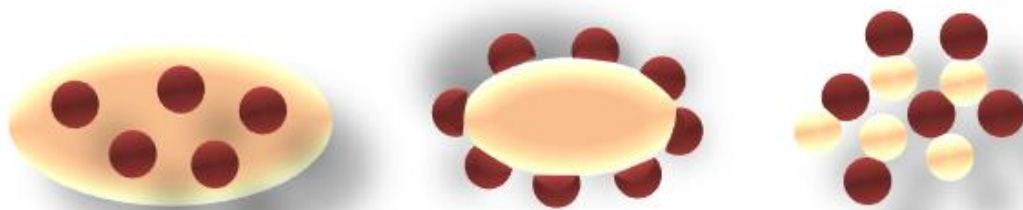
- [19] M. Behrens, F. Girgsdies, A. Trunschke, R. Schlögl, Minerals as Model Compounds for Cu/ZnO Catalyst Precursors: Structural and Thermal Properties and IR Spectra of Mineral and Synthetic (Zincian) Malachite, Rosasite and Aurichalcite and a Catalyst Precursor Mixture, *Eur J Inorg Chem*, (2009) 1347-1357.
- [20] S.H. Kang, J.W. Bae, K.W. Jun, H.S. Potdar, Dimethyl ether synthesis from syngas over the composite catalysts of Cu-ZnO-Al<sub>2</sub>O<sub>3</sub>/ Zr-modified zeolites, *Catal Commun*, 9 (2008) 2035-2039.
- [21] P.S.S. Prasad, J.W. Bae, S.H. Kang, Y.J. Lee, K.W. Jun, Single-step synthesis of DME from syngas on Cu-ZnO-Al<sub>2</sub>O<sub>3</sub>/ zeolite bifunctional catalysts: The superiority of ferrierite over the other zeolites, *Fuel Process Technol*, 89 (2008) 1281-1286.
- [22] H.J. Zhan, F. Li, P. Gao, N. Zhao, F.K. Xiao, W. Wei, L.S. Zhong, Y.H. Sun, Methanol synthesis from CO<sub>2</sub> hydrogenation over La-M-Cu-Zn-O (M = Y, Ce, Mg, Zr) catalysts derived from perovskite-type precursors, *J Power Sources*, 251 (2014) 113-121.
- [23] N. Supamathanon, J. Wittayakun, S. Prayoonpokarach, W. Supronowicz, F. Roessner, Basic Properties of Potassium Oxide Supported on Zeolite Y Studied by Pyrrole-Tpd and Catalytic Conversion of Methylbutynol, *Quim Nova*, 35 (2012) 1719-1723.
- [24] S.J. Sun, D.S. Zhang, C.Y. Li, Y.J. Wang, Q.S. Yang, Density functional theory study of mercury adsorption and oxidation on CuO(111) surface, *Chem Eng J*, 258 (2014) 128-135.
- [25] R.H. Miwa, T.M. Schmidt, W.L. Scopel, A. Fazzio, Doping of graphene adsorbed on the α-SiO<sub>2</sub> surface, *Appl Phys Lett*, 99 (2011).
- [26] L.T. Zhuravlev, The surface chemistry of amorphous silica. Zhuravlev model, *Colloid Surface A*, 173 (2000) 1-38.
- [27] X. Huang, W. Chu, W.J. Sun, C.F. Jiang, Y.Y. Feng, Y. Xue, Investigation of oxygen-containing group promotion effect on CO<sub>2</sub>-coal interaction by density functional theory, *Appl Surf Sci*, 299 (2014) 162-169.
- [28] M. Gerosa, C. Di Valentin, C.E. Bottani, G. Onida, G. Pacchioni, Communication: Hole localization in Al-doped quartz SiO<sub>2</sub> within ab initio hybrid-functional DFT, *J Chem Phys*, 143 (2015).

- [29] D.Z. Gao, H.B. Yin, Y.H. Feng, A.L. Wang, Coupling reaction between methanol dehydrogenation and maleic anhydride hydrogenation over zeolite-supported copper catalysts, *Can J Chem Eng*, 93 (2015) 1107-1118.
- [30] Z.P. Lu, D.Z. Gao, H.B. Yin, A.L. Wang, S.X. Liu, Methanol dehydrogenation to methyl formate catalyzed by SiO<sub>2</sub>-, hydroxyapatite-, and MgO-supported copper catalysts and reaction kinetics, *J Ind Eng Chem*, 31 (2015) 301-308.
- [31] G. Laugel, X. Nitsch, F. Ocampo, B. Louis, Methanol dehydration into dimethylether over ZSM-5 type zeolites: Raise in the operational temperature range, *Appl Catal A-Gen*, 402 (2011) 139-145.
- [32] E. Catizzone, A. Aloise, M. Migliori, G. Giordano, Dimethyl ether synthesis via methanol dehydration: Effect of zeolite structure, *Appl Catal A-Gen*, 502 (2015) 215-220.
- [33] K.D. Jung, O.S. Joo, Support effects of copper containing catalysts on methanol dehydrogenation, *B Korean Chem Soc*, 23 (2002) 1135-1138.
- [34] E.H. Shreiber, G.W. Roberts, Methanol dehydrogenation in a slurry reactor: evaluation of copper chromite and iron/titanium catalysts, *Appl Catal B-Environ*, 26 (2000) 119-129.
- [35] E.H. Shreiber, M.D. Rhodes, G.W. Roberts, Methanol dehydrogenation with Raney copper in a slurry reactor, *Appl Catal B-Environ*, 23 (1999) 9-24.
- [36] R. Zhang, Y.H. Sun, S.Y. Peng, In situ FTIR studies of methanol adsorption and dehydrogenation over Cu/SiO<sub>2</sub> catalyst, *Fuel*, 81 (2002) 1619-1624.
- [37] E.D. Guerreiro, O.F. Gorriiz, J.B. Rivarola, L.A. Arrua, Characterization of Cu/SiO<sub>2</sub> catalysts prepared by ion exchange for methanol dehydrogenation, *Appl Catal A-Gen*, 165 (1997) 259-271.
- [38] K.D. Jung, O.S. Joo, Preparation of Cu/ZnO/M<sub>2</sub>O<sub>3</sub> (M = Al, Cr) catalyst to stabilize Cu/ZnO catalyst in methanol dehydrogenation, *Catal Lett*, 84 (2002) 21-25.
- [39] H. Imai, T. Tagawa, K. Nakamura, Catalytic Activities of Hydrogen Storage Alloys for Decomposition of Alcohols, *Appl Catal*, 62 (1990) 348-352.
- [40] H. Imai, T. Tagawa, K. Nakamura, Dehydrogenation of Methanol to Formaldehyde over Titanium-Alloys, *React Kinet Catal L*, 43 (1991) 355-359.

- [41] T.P. Minyukova, I.I. Simentsova, A.V. Khasin, N.V. Shtertser, N.A. Baronskaya, A.A. Khassin, T.M. Yurieva, Dehydrogenation of methanol over copper-containing catalysts, *Appl Catal A-Gen*, 237 (2002) 171-180.
- [42] H.G. Ahn, H.G. Lee, M.C. Chung, K.P. Park, K.J. Kim, B.M. Kang, W.J. Jeong, S.C. Jung, D.J. Lee, Catalytic Activity of Nanosized CuO-ZnO Supported on Titanium Chips in Hydrogenation of Carbon Dioxide to Methyl Alcohol, *J Nanosci Nanotechno*, 16 (2016) 2024-2027.
- [43] L.X. Zhang, Y.C. Zhang, S.Y. Chen, Effect of promoter SiO<sub>2</sub>, TiO<sub>2</sub> or SiO<sub>2</sub>-TiO<sub>2</sub> on the performance of CuO-ZnO-Al<sub>2</sub>O<sub>3</sub> catalyst for methanol synthesis from CO<sub>2</sub> hydrogenation, *Appl Catal A-Gen*, 415 (2012) 118-123.
- [44] L. Angelo, Développement de catalyseurs pour la synthèse de méthanol produit par hydrogénation du dioxyde de carbone, Strasbourg, 2014.
- [45] L. Angelo, K. Kobl, L.M.M. Tejada, Y. Zimmermann, K. Parkhomenko, A.C. Roger, Study of CuZnMO<sub>x</sub> oxides (M = Al, Zr, Ce, CeZr) for the catalytic hydrogenation of CO<sub>2</sub> into methanol, *Cr Chim*, 18 (2015) 250-260.
- [46] H. Ham, J. Kim, S.J. Cho, J.H. Choi, D.J. Moon, J.W. Bae, Enhanced Stability of Spatially Confined Copper Nanoparticles in an Ordered Mesoporous Alumina for Dimethyl Ether Synthesis from Syngas, *Acs Catal*, 6 (2016) 5629-5640.



*Chapter 5: Optimization of the bifunctional catalysts*





## 5.1 Introduction

In chapter 4, the bifunctional catalysts prepared by co-precipitation deposition method have been investigated in the direct DME synthesis reaction. It has been found that the acid sites are blocked by the copper based part. In this chapter, it is proposed to prepare the bifunctional catalyst by core-shell method, where the copper based part will be placed in the core and the Al-TUD-1 part will be placed in the shell in order to prevent the blockage of the acid sites by copper. In addition, the bifunctional catalyst with the same composition will be prepared by physically mixing method. These two new materials will be compared to the CZZ-Si/Al-25 that was prepared by co-precipitation deposition method and described in chapter 4.

The prepared materials will be analyzed with the aid of different characterization methods, such as N<sub>2</sub> adsorption/desorption method, X-ray diffraction (XRD), H<sub>2</sub> temperature programmed reduction (H<sub>2</sub>-TPR) and temperature programmed desorption of NH<sub>3</sub> (NH<sub>3</sub>-TPD). The direct DME synthesis performance of these three bifunctional catalysts with the same composition will be tested. These three catalysts will be also employed in the methanol dehydration to DME reaction.

## 5.2 Catalysts preparation

All the catalysts use Al-TUD-1 with the Si/Al ratio of 25 as methanol dehydration catalyst and possess the same weight ratio between methanol synthesis catalyst (CZZ) and methanol dehydration catalyst ( $m_{CZZ} : m_{Si/Al-25} = 1:1$ ).

### Core shell method

Firstly, 0.2683 g aluminum isopropoxide (98%, Aldrich) was added into ethanol under stirring. After the aluminum isopropoxide was completely dissolved, 2g sieved CZZ (prepared in chapter 4) with the particle size of 50-100  $\mu\text{m}$  was added into the solution. Then 6.8421 g tetraethyl orthosilicate (TEOS, 98%, ACROS) was added. After stirring for a few minutes, the well mixed 4.8933 g triethanolamine (TEA, 98%, ACROS) and 3.7177 g distilled water was added drop by drop, followed by the addition of 4.0341 g tetraethyl ammonium hydroxide (TEAOH, 35 wt % in water, ACROS). Afterwards, it

was kept under stirring overnight and then left to age at room temperature until a gel formed. After that the gel was dried at 100 °C for 24h for the evaporation of H<sub>2</sub>O and ethanol, followed by hydrothermal treatment at 180 °C for 3h with ramp of 5 °C/min in an autoclave with a Teflon pocket and by calcination at 400 °C for 4h with ramp of 2 °C/min.

### Physically mixing method

Sieved CZZ (100-200 μm) and the Al-TUD-1 material (Si/Al-25) (100-200 μm) were physically mixed with the same weight ratio.

## 5.3 Characterizations and discussions

The bifunctional catalysts that will be investigated in this chapter are prepared by core-shell method, co-precipitation deposition method and physically mixing method, they are abbreviated as **cs**, **pd** and **m**, respectively. The schematic diagram for these catalysts is shown in Figure 5- 1.

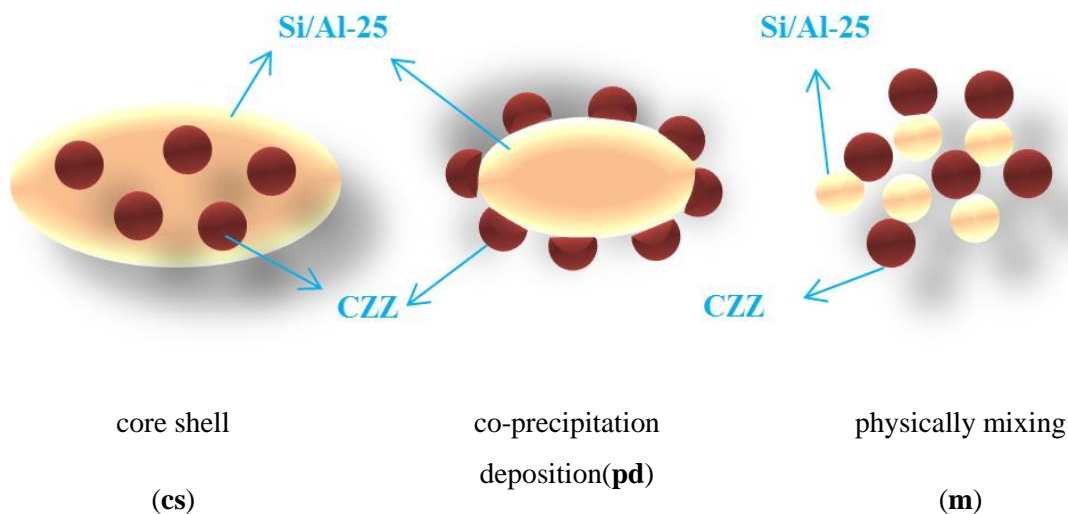


Figure 5- 1 Schematic diagram of bifunctional catalysts

### 5.3.1 Textural properties

The textural properties of these materials were analyzed by N<sub>2</sub> adsorption/desorption method. The N<sub>2</sub> adsorption/desorption isotherms and pore distribution for bifunctional catalysts prepared by three different methods are shown in Figure 5- 2.

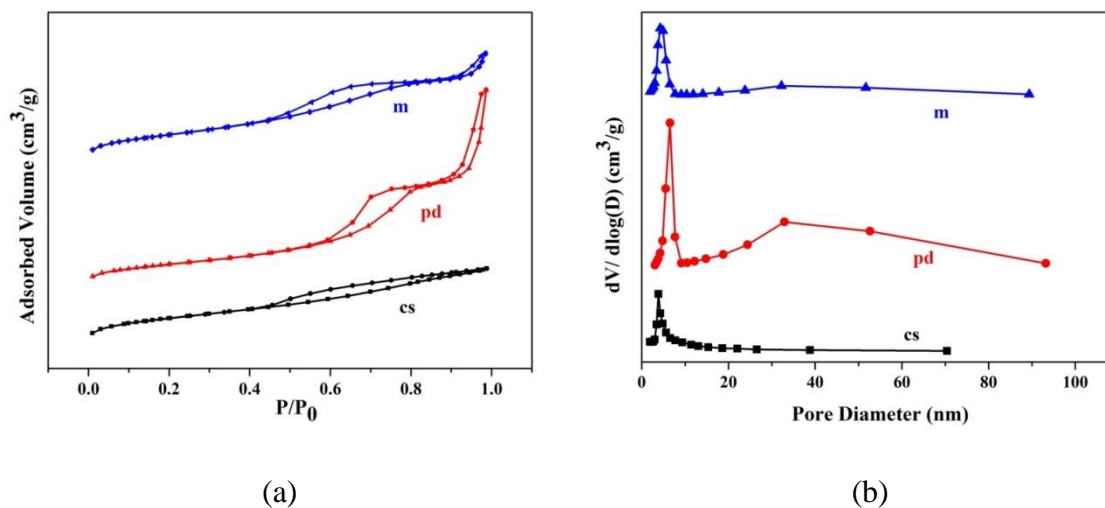


Figure 5- 2 N<sub>2</sub> adsorption/desorption isotherms (a) and pore distribution (b) for the bifunctional catalysts **cs**, **pd** and **m**.

From the isotherms, it can be seen that both the catalyst **pd** and catalyst **m** show two kinds of hysteresis loop, H1 and H3-type with “cylindrical” and “slit” shaped pore, respectively [1]. The former is introduced by Al-TUD-1 (Si/Al-25) and the latter arises from the intragrain porosity of CZZ [2]. The catalyst **cs** shows only one hysteresis loop with the H4 type associated with narrow slit-like pores [1]. During the core-shell synthesis procedure, some Al-TUD-1 synthesis solution enters the pores of the core catalyst CZZ. The aluminosilicate is formed after hydrothermal treatment and calcination and thus fills the pores of CZZ and forms the shell around each grain [3]. The presented pore distributions of these three bifunctional catalysts are consistent with the isotherms. They have two kinds of pores for bifunctional catalysts **pd** and **m**, and there is only one peak for the pore distribution of bifunctional catalyst **cs**.

The textural properties regarding specific surface area, pore volume and pore diameter of bifunctional catalysts prepared by different methods are shown in Table 5- 1. The bifunctional catalyst **cs** possesses the highest specific surface area 404 m<sup>2</sup>g<sup>-1</sup> with the pore size around 4nm. The catalyst **m** owns the specific surface area of 384 m<sup>2</sup>g<sup>-1</sup>, which is higher than the catalyst prepared by co-precipitation deposition method of 315 m<sup>2</sup>g<sup>-1</sup>. The pore volume estimated from the BJH method are 0.39 cm<sup>3</sup>g<sup>-1</sup> for catalyst **cs**, 1.04 cm<sup>3</sup>g<sup>-1</sup> for catalyst **pd** and 0.58 cm<sup>3</sup>g<sup>-1</sup> for catalyst **m**, respectively.

Table 5- 1 Textural properties of bifunctional catalysts

sample	$S_{\text{BET}}$ ( $\text{m}^2\text{g}^{-1}$ )	$V_{\text{pore}}$ ( $\text{cm}^3\text{g}^{-1}$ )	$D_p$ (nm)
<b>cs</b>	404	0.39	3.8
<b>pd</b>	315	1.04	6.5, 32.9
<b>m</b>	384	0.58	4.2, 32.2

### 5.3.2 Crystalline structure

The **XRD** patterns for pure CZZ and calcined bifunctional catalysts prepared by different methods are shown in Figure 5- 3.

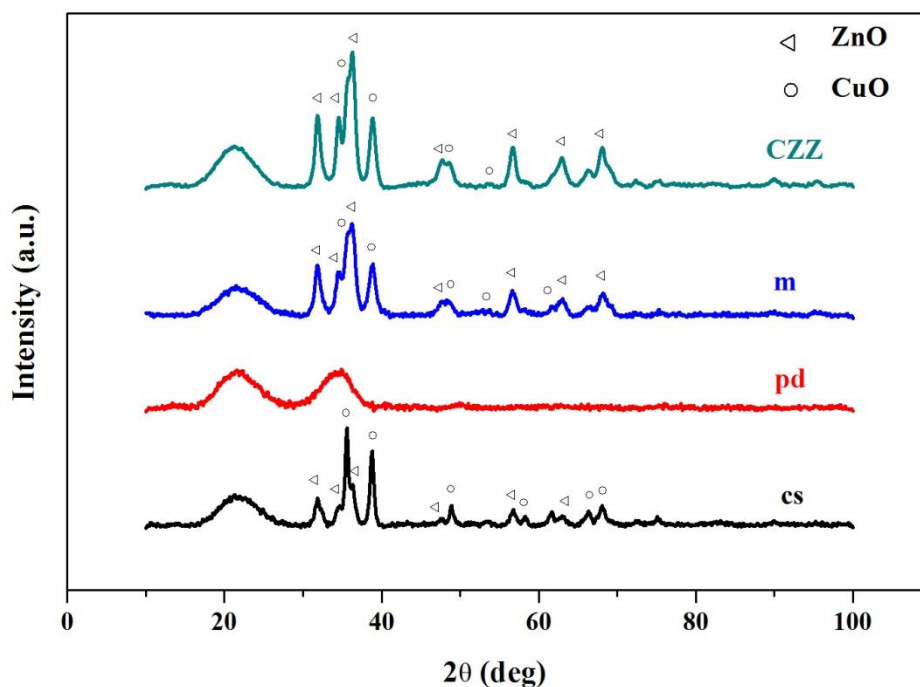


Figure 5- 3XRD patterns for CZZ and calcined bifunctional catalysts.

The first large peak at  $15^\circ$ - $25^\circ$   $2\theta$  is owing to the amorphous  $\text{SiO}_2$  [4, 5] coming probably from the glass sample support for XRD analysis. Among the XRD patterns for the calcined bifunctional catalysts, the catalyst **pd** shows the amorphous peaks at  $30^\circ$ - $40^\circ 2\theta$ . This peak is probably owing to the overlapping of broadened and not well crystallized CuO and ZnO signals [6], which has been explained in chapter 4. For all the catalysts, it is supposed that the  $\text{ZrO}_2$  is present in the amorphous form because of the

absence of characteristic crystalline peaks [6, 7]. The bifunctional catalysts **m** and **cs** possess crystalline CuO and ZnO peaks. The catalyst **m** shows similar XRD patterns as catalyst **CZZ**. In the catalyst **cs**, the intensity of ZnO peak at the position  $2\theta = 36.265^\circ$  is much smaller than the intensity of CuO peak at the position  $2\theta = 35.496^\circ$ , while in the catalyst **m**, the intensity of ZnO peak at the position  $2\theta = 36.265^\circ$  is bigger than the intensity of CuO peak at the position  $2\theta = 35.496^\circ$ .

The intensity of the strongest characteristic diffraction peak of ZnO ( $36.265^\circ$ ) and CuO ( $35.496^\circ$ ) are compared for different catalysts and the intensity ratios between them are shown in Table 5- 2 as well as the area ratio for independent ZnO ( $30.773^\circ$ ) and CuO ( $37.750^\circ$ ) peaks. The ratios of  $I_{\text{ZnO}}/I_{\text{CuO}}$  for the catalyst **m** and the catalyst **CZZ** is the same with the value of 1.2. The structure of **CZZ** is not changed during the preparation of the catalyst **m**. The  $I_{\text{ZnO}}/I_{\text{CuO}}$  ratio of the catalyst **cs** is 0.4. The area ratio for ZnO and CuO shows the similar value. So in the catalyst **cs**, the original structure of **CZZ** was changed. Supposingly a part of the core (**CZZ**) has reacted with TEOS during the preparation and Cu, Zn, Zr leach from the initial structure of the core. It can be supposed that the core of the catalyst **cs** could be a polymorph of different phases such as initial **CZZ**, Zn-TUD-1, Cu-TUD-1 and Zr-TUD-1 [4, 8-11]. The last three supposed substances are amorphous and probably exist in small quantities so they could not be visible on XRD patterns.

Table 5- 2 Ratio of intensities of characteristic peak of ZnO and CuO

	$I_{\text{ZnO}}/I_{\text{CuO}}$	$A_{\text{ZnO}}/A_{\text{CuO}}$
<b>cs</b>	0.4	0.6
<b>pd</b>	-	-
<b>m</b>	1.2	1.2
<b>CZZ</b>	1.2	1.2

The crystallite sizes of CuO and ZnO in calcined samples and the crystallite sizes of  $\text{Cu}^0$  and ZnO in reduced samples determined by Debye-Scherrer equation are shown in Table 5- 3. Attributed to the amorphous peak presented in the catalyst **pd**, the crystallite sizes of CuO and ZnO in the calcined sample cannot be calculated. The crystallite sizes of CuO and ZnO for calcined catalyst **cs** are 15.0 nm and 8.9 nm. They are 9.0 nm and 10.0 nm respectively for the calcined catalyst **m**. The CuO crystallite size of calcined

catalyst **m** is smaller than for the calcined catalyst **cs**. It may be due to the fact that the structure of the core catalyst **CZZ** was damaged during the synthesis procedures as it was already observed in [12].

Table 5- 3CuO and ZnO crystallite size of calcined bifunctional catalysts

sample	crystallite size of calcined samples (nm)		crystallite size of reduced samples (nm)		crystallite size after direct DME synthesis reaction (nm)	
	CuO	ZnO	Cu <sup>0</sup>	ZnO	Cu <sup>0</sup>	ZnO
<b>cs</b>	15.0	8.9	22.8	7.0	24.5	13.1
<b>pd</b>	-	-	4.8	-	-	-
<b>m</b>	9.0	10.0	14.0	13.5	20.7	18.5
<b>CZZ</b>	9.7	10.5	10.9	11.2	-	-

These catalysts were reduced at 280 °C for 1h with the temperature ramp of 1 °C/min. The XRD patterns for these reduced catalysts are shown in Figure 5- 4 . From Figure 5- 4, it can be observed that the reduced catalyst **cs** shows strong diffraction peaks belonging to metallic copper and very small ZnO peaks. ZnO peaks become smaller after reduction compared with the calcined **cs** probably owing to the interaction or the migration of ZnO to the shell structure [4]. The metallic copper crystallite size is 22.8 nm, which is much larger than the CuO crystalline size of calcined **cs**, which means that the copper agglomerates during the reduction process. It is probably due to the decrease of ZnO content in the core, which is the geometry spacer for copper, resulting in the agglomeration of copper.

The reduced catalyst **pd** shows only Cu<sup>0</sup> peak with the crystallite size of 4.8 nm, which means that the copper is well dispersed and anchored, probably owing to strong metal support interaction (SMSI) (chapter 4 conclusions).

The crystallite size of Cu<sup>0</sup> in the reduced catalyst **m** is 14.0 nm, which is bigger than the CuO crystallite size in the calcined sample of 9 nm. The ZnO crystallite size in the reduced sample **m** is also a little bigger than for the calcined sample. It means copper and ZnO agglomeration happened during the reduction.

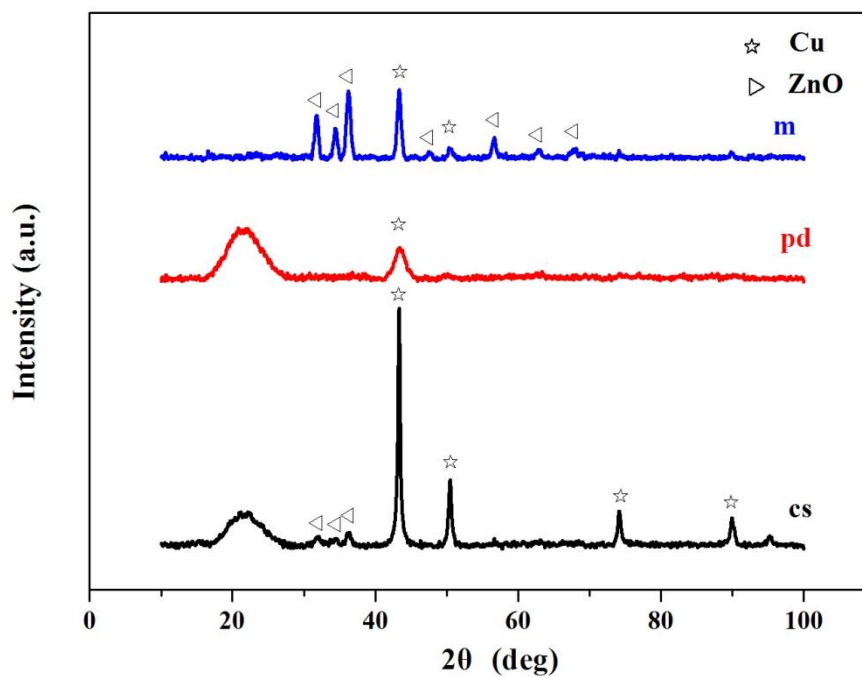
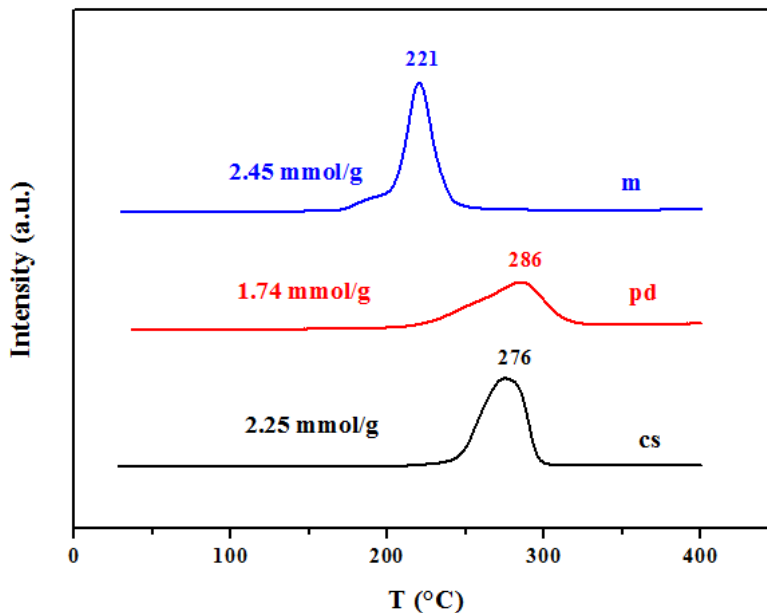


Figure 5- 4 XRD patterns for reduced bifunctional catalysts

### 5.3.3 Redox properties

The H<sub>2</sub>-TPR curves, the temperature of the reduction peak center and the H<sub>2</sub>consumption amount of the bifunctional catalysts prepared by different method are shown in Figure 5- 5. The reducibility of these catalysts is calculated by the H<sub>2</sub>consumption amount and the theoretical Cu content during the synthesis, which is presented in Table 5- 4.

Figure 5- 5 H<sub>2</sub>-TPR profiles

The catalyst **m** shows the lowest reduction temperature among these three catalysts. It presents the similar reduction peak shape as for the methanol synthesis catalyst **CZZ** (chapter 4), showing the main sharp reduction peak with a shoulder peak at lower temperature. It also owns the similar reduction temperature as **CZZ**, 221 °C for bifunctional catalyst **m** and 219 °C for **CZZ**. It means that the methanol dehydration part Al-TUD-1 (Si/Al-25) has no effect on the methanol synthesis part in the bifunctional catalyst prepared by physically mixing method. The copper reducibility of **m** is 104%, which means that the copper can be completely reduced before 250 °C.

The catalyst **cs** shows a broad reduction peak from 250 °C to 300 °C with the peak maximum of 276 °C, which is higher than for the catalyst **m**. It may be due to the bigger CuO crystallite size of **cs** (15.0 nm) than in **m** (9.0 nm) (XRD results) from one hand. From the other hand, since **CZZ** is located in the core of the catalyst, the diffusion of H<sub>2</sub> to the core is not very easy. The reducibility of catalyst **cs** is 95%, the tiny unreduced CuO part may be located in the pores of Si/Al-25, which is inaccessible to H<sub>2</sub>.

Catalyst **pd** presents a broad asymmetric reduction peak and the highest reduction temperature of 286 °C. It means the strongest interaction of Cu based part and the Si/Al-25 support among these three catalysts. It shows the reducibility of 72%, which may due

to the strong metal support interaction (SMSI) [13], in addition some copper was embedded in the pore structure of the Si/Al-25 support as described in chapter 4.

Table 5- 4 Reducibility of the bifunctional catalysts prepared by different methods

Sample	Reducibility
<b>cs</b>	95%
<b>pd</b>	72%
<b>m</b>	104%

### 5.3.4 Basic properties

The basic properties were studied by CO<sub>2</sub>-TPD. The CO<sub>2</sub>-TPD profiles for the catalysts are presented in Figure 5- 6.

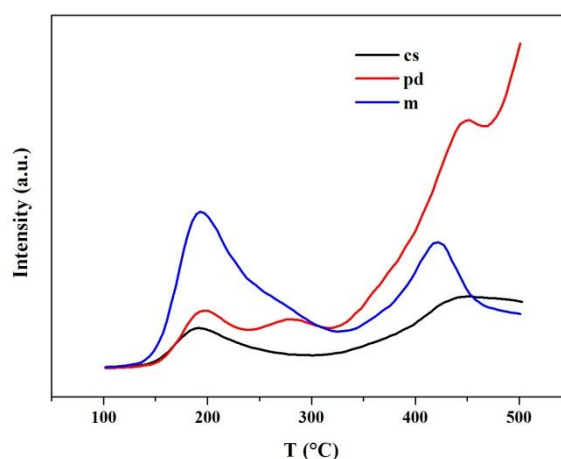


Figure 5- 6 CO<sub>2</sub>-TPD profiles for the catalysts **cs**, **pd** and **m**

The calcination temperature for the bifunctional catalysts is 400 °C. Below this temperature, only the weak basic sites could be discussed as they appear in low temperature range 100-350 °C. It can be seen that there are two temperature zones of CO<sub>2</sub> desorption for all catalysts, low temperature zone and high temperature zone. Weak basic sites in the range of 150-320 °C may be attributed to surface hydroxyl groups, metal oxygen pairs or unsaturated O<sup>2-</sup> ions induced by ZnO and ZrO<sub>2</sub> [14-16]. It can be observed that there are two CO<sub>2</sub> desorption peaks for catalyst **m**, around 200 °C and 420 °C. The catalyst **pd** shows CO<sub>2</sub> desorption peaks around 200 °C to 300 °C. Around

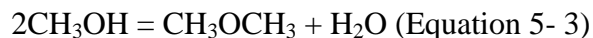
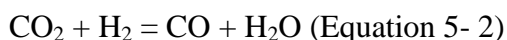
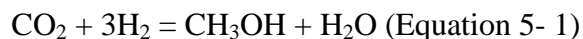
450 °C, another peak appears and the CO<sub>2</sub> desorption continues after that, which may be due to the CO<sub>2</sub> coming from the decomposition of high temperature carbonates (chapter 4). The catalyst **cs** shows one small peak around 200 °C and another broad peak at 450 °C.

Comparing the CO<sub>2</sub>-TPD profiles for these three catalysts, it can be concluded that the catalyst **m** owns more weak basic sites than other two catalysts. In catalysts **pd** and **cs**, some weak basic sites could be blocked due to the materials preparation, SMSI for catalyst **pd** and structural changes for catalyst **cs**.

## 5.4 Catalytic results

### 5.4.1 Direct DME synthesis

The direct DME synthesis reaction was conducted at 20 bars, GHSV of 10000 h<sup>-1</sup>, and different temperatures of 240 °C, 260 °C, 280 °C and 300 °C. Several reactions occurred in the direct DME synthesis from CO<sub>2</sub>/H<sub>2</sub> reaction: CO<sub>2</sub> hydrogenation to methanol (Equation 5- 1), reverse water gas shift reaction (Equation 5- 2) and methanol dehydration to DME reaction (Equation 5- 3).



In the presence of a bifunctional catalyst, the copper based part will convert CO<sub>2</sub>/H<sub>2</sub> to methanol (Equation 5- 1). Then it is expected that methanol will be transformed in DME (Equation 5- 3) on the acid sites of Al-TUD-1 (Si/Al-25) part of the catalyst. In addition, the RWGS reaction may occur in these conditions. It is catalyzed by Cu<sup>0</sup> sites and is in competition with methanol formation.

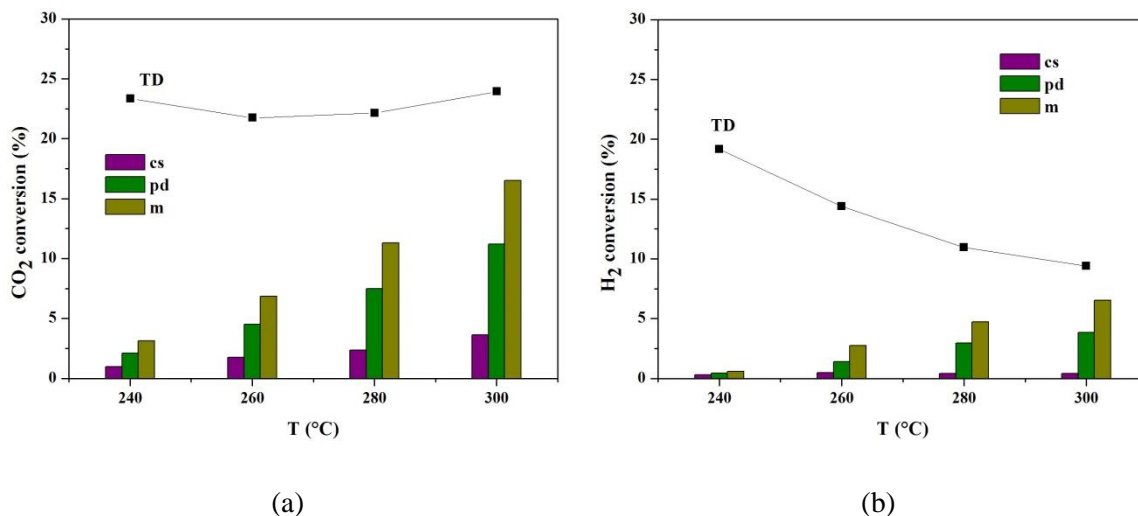


Figure 5- 7 CO<sub>2</sub> (a) and H<sub>2</sub> conversion (b)

The CO<sub>2</sub> and H<sub>2</sub> conversion for these three bifunctional catalysts as well as the values for thermodynamic (TD) results are presented in Figure 5- 7. The TD CO<sub>2</sub> conversion shows the slight decrease from 240 °C to 260 °C and then shows the increasing trend. The TD H<sub>2</sub> conversion decreases with temperature. The TD results were discussed in 4.3.2.2. The CO<sub>2</sub> and H<sub>2</sub> conversion for these three catalysts are lower than the TD results in all the studied temperatures, so the catalytic activity can be compared in the chosen conditions. Both the CO<sub>2</sub> and H<sub>2</sub> conversions increase with temperature, following the trend for all catalysts.

The catalyst **cs** shows the lowest CO<sub>2</sub> and H<sub>2</sub> conversions for all studied temperatures. It might be due to the fact that the copper based part is located in the core of the catalyst wrapped by the shell (Figure 5- 8). So CO<sub>2</sub> and H<sub>2</sub> can't reach the copper surface very easily compared to other two catalysts. Another reason is that the CZZ structure of the core has changed causing copper agglomeration.

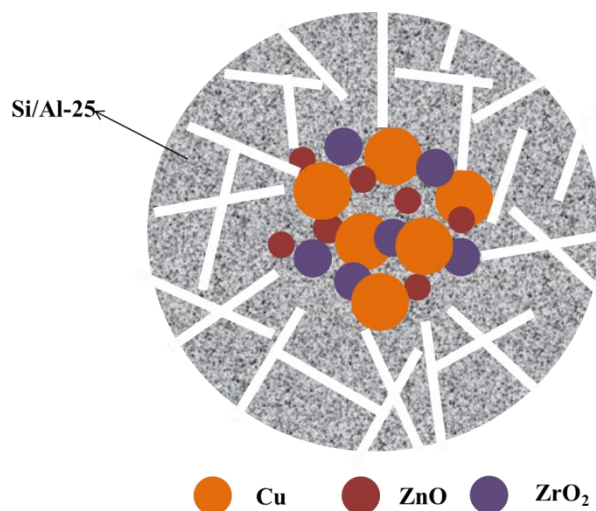


Figure 5- 8 Schematic diagram of the reduced catalyst **cs**

The schematic diagram of the reduced catalyst **cs** is presented in Figure 5- 8. The  $\text{Cu}^0$  crystallite size of the reduced catalyst is 22.8 nm. The pore diameter of Si/Al shell is just around 4 nm. So the reactant gases  $\text{CO}_2$  and  $\text{H}_2$  can only reach the metallic copper surface or  $\text{Cu}^0/\text{ZnO}$  interface responsible for methanol formation at the end of the pores of the shell. That explains the low  $\text{CO}_2$  and  $\text{H}_2$  conversions observed for the catalyst **cs**. The conversion of  $\text{CO}_2$  and  $\text{H}_2$  over the catalyst **pd** were higher than for catalyst **cs** and lower than for the catalyst **m** (Figure 5- 7).

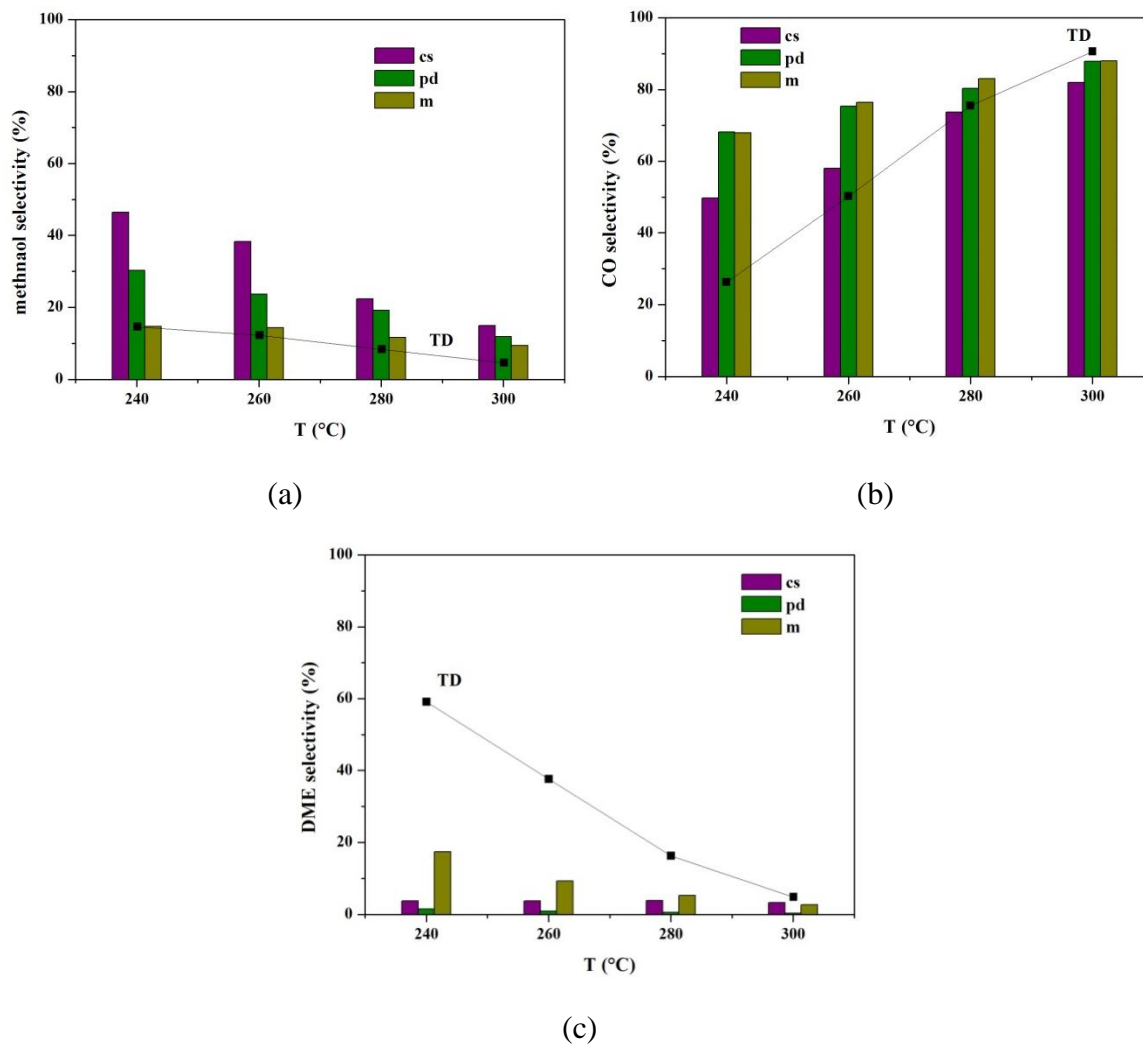


Figure 5-9Methanol (a), CO (b) and DME (c) selectivity

The selectivity of methanol, CO and DME formation for the catalysts **cs**, **pd** and **m** as well as the TD results are shown in Figure 5- 9. For the TD results, methanol and DME selectivity decrease with temperature and CO selectivity increases with temperature. Methanol, CO and DME selectivity for these three catalysts show the same trend as the TD results. The DME selectivity of these three catalysts is lower than the TD results and the methanol selectivity of these three catalysts is higher than the TD results. The TD results are calculated for multistep process, but in these experiments low DME productivity was observed. That explains why methanol can be seen in higher amount than presented TD limits, because most of it is not converted into DME. The CO selectivity of these three catalysts is higher than the TD results at 240 °C and 260 °C. It

may be due to the fact that the kinetic regime is prevailing at these temperatures for high GHSV values more than  $3000 \text{ h}^{-1}$  [17, 18]. At  $280 \text{ }^\circ\text{C}$  and  $300 \text{ }^\circ\text{C}$ , the CO selectivity for these three catalysts is close to TD limits.

It has been reported that the consumption of methanol in methanol dehydration reaction can break the chemical equilibrium in  $\text{CO}_2$  hydrogenation to methanol reaction and the reaction will go on to the right hand [12, 19-22]. Comparing the catalyst **pd** and **m**, the better DME selectivity of the catalyst **m** was observed than for the catalyst **pd** as well as the higher  $\text{CO}_2$  conversion.

Considering the products distribution, the catalyst **cs** shows the highest methanol and the lowest CO selectivities among three catalysts. Bifunctional catalysts **pd** and **m** possess higher CO selectivity and lower methanol selectivity than catalyst **cs**, but their difference is the formation of DME. The catalyst **pd** has lower DME selectivity than **m**, because the acid sites of **pd** were blocked by copper based part which leads to the unsuccessful methanol dehydration reaction. For the bifunctional catalyst **m**, methanol synthesis catalyst CZZ and methanol dehydration catalyst Si/Al-25 are physically mixed together, and both parts keep their individual properties.  $\text{CO}_2$  was hydrogenated on CZZ and then methanol was dehydrated on Si/Al-25, so it shows much higher DME selectivity than **pd**. It also confirms the thoughts that the low DME productivity of the catalyst prepared by the co-precipitation deposition method is due to the blocking of acidic sites by copper-based part because the catalysts have the same composition.

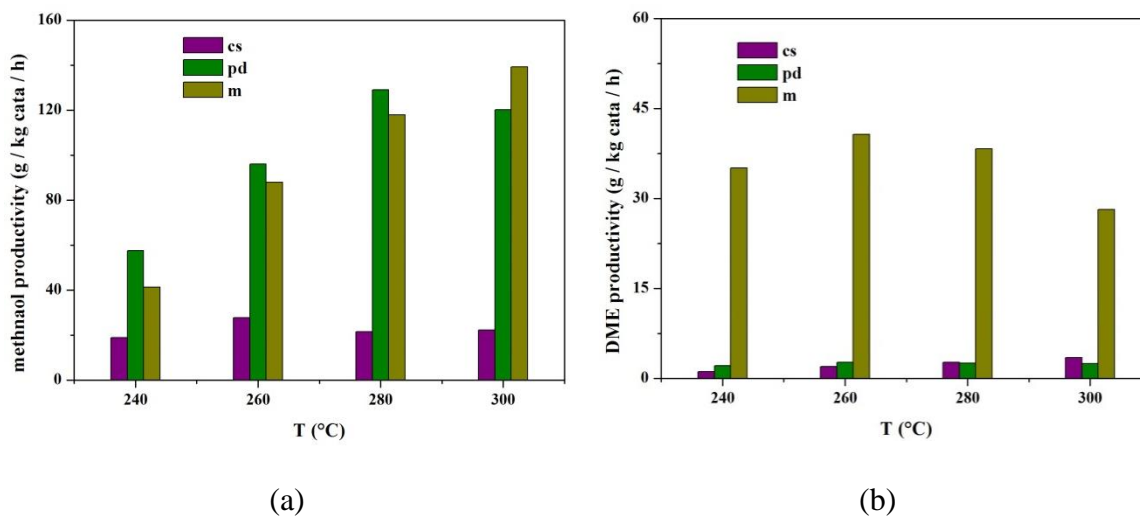


Figure 5- 10 Methanol (a) and DME (b) productivity

The productivity of methanol and DME are shown in Figure 5- 10. Catalyst **cs** shows highest methanol productivity of 27 g/ kgcata/ h at 260 °C among all the temperature investigated. Catalyst **pd** presents highest methanol productivity of 129 g/ kg cata/ h at 280 °C. While for catalyst **m** at the investigated temperatures, methanol productivity increases with temperature and shows the highest at 300 °C with 139 g/ kg cata/ h. DME productivity for **cs** and **pd** is less than 3.5 g/kg cata/ h for all the temperature investigated. The DME productivity for catalyst **m** is much higher than for other two catalysts. The highest DME productivity was found over the catalyst **m** and is about 41g/ kg cata/ h at 260 °C.

Comparing the crystallite size of reduced catalysts and the catalysts after direct DME synthesis reaction (Table 5- 3), it can be observed that the crystallite size of  $\text{Cu}^0$  didn't change a lot for catalyst **cs** (22.8 nm for the catalyst after reduction and 24.5 nm for the catalyst after reaction), while the  $\text{Cu}^0$  crystallite size increased from 14.0 nm (reduced catalyst) to 20.7 nm after reaction for catalyst **m**. It may due to that the Si/Al shell provides the channels for CZZ which prevents the excessive agglomeration of copper between particles during the reaction. The catalyst **pd** shows amorphous XRD patterns without the presence of characteristic peaks belonging to  $\text{Cu}^0$ . It means that the copper is still well dispersed and no agglomeration happened during the reaction.

The direct DME synthesis by CO<sub>2</sub> hydrogenation was also conducted by G. Bonura *et al* [18]. The authors obtained the methanol productivity of 430 g/ kg cata/ h (including methanol produced and methanol dehydrated to DME) at 240 °C and 30 bars, which is higher pressure than we used in this chapter. The CO<sub>2</sub> conversion is 16.1%, and the selectivity for DME, methanol and CO is 33.9%, 11.8% and 54.3 respectively. The catalyst they used is Cu–ZnO–ZrO<sub>2</sub>/ H-ZSM5 hybrid catalyst prepared by physically mixing method. The amount of the acid sites is 1.01 mmol/g measured by NH<sub>3</sub>-TPD. Comparing with our reaction, we have the same CO<sub>2</sub>/H<sub>2</sub> ratio (1/3) of the reactant and the same flow rate (40 ml/min). The catalyst they used owns more acid sites than ours, which is maybe the one of the reasons for the higher DME selectivity of their catalysts. Another reason is the operating conditions, they operated this reaction at higher pressure (30 bars) than us (20 bars). [17]. These results are the closest to our study, so it has reference value for us indicating the need of incorporating more acid sites in our bifunctional catalytic system.

The core-shell catalyst and the catalyst prepared by co-precipitation-deposition were compared to the known literature data (Table 5- 5). The main problem of the bifunctional catalytic materials is the selectivity, the DME formation was never observed without methanol and CO in the products. It could be overtaken only by equilibrium between three parameters – metallic copper surface area (copper dispersion and particle size), acidity and the basicity. For example, the catalysts with same composition but modified acidity and basicity could perform the same CO<sub>2</sub> conversion (lines 2 and 3, Table 5- 5). The strong acidity should be avoided, the compromise between Al content and synthesis method of the bifunctional catalytic material should be found. Bringing more Al could result in the formation of strong acidity and thus will switch the reaction to the olefins formation (side products in the direct DME synthesis) and decrease even more the selectivity of the DME formation. The catalysts prepared during this work faced the comparison to the materials with the same content of copper which is complicated. In this work the GHSV was higher (lines 5-8, Table 5- 5) than found in the literature, thus contact time was quite short. In addition the catalysts of this work were not diluted in SiC. That makes the chosen conditions rather severe and lets to the development and comparison of the catalysts in the conditions far from the thermodynamic limitations.

Table 5- 5 The comparison of reported and the bench-marking of obtained catalytic results

	Catalyst	Weight ratio (copper based part : acid part)	Copper content (%)	Copper surface area (m <sup>2</sup> /g)	Acid sites (m mol NH <sub>3</sub> /g cat)	Basic sites (m mol CO <sub>2</sub> /g cat)	T (°C)	P (bar)	V(CO <sub>2</sub> ): V(H <sub>2</sub> )	GHSV	X <sub>CO2</sub> (%)	S <sub>DME</sub> (%)	S <sub>methanol</sub> (%)	S <sub>CO</sub> (%)	Methanol productivity	DME productivity
1	CuZnZr-MFI (gel-oxalate co-precipitation [23])	9:1	40.8				240	30	1:3	10000 NL/ kg cat/h	15.9	38.5	9.9	51.6		
2	Cu–ZnO–ZrO <sub>2</sub> /H-ZSM5[22] NaHCO <sub>3</sub> as precipitation agent	1:1	17.2	10.2	0.067	0.0400	240	30	1:3	40mL/min, 0.25g catalyst + 0.25g SiC (9600 NL/ kg cat/h)	14.0	1	46	53		
3	Cu–ZnO–ZrO <sub>2</sub> /H-ZSM5 (NH <sub>4</sub> ) <sub>2</sub> CO <sub>3</sub> as precipitation agent [22]	1:1	16.7	9.3	0.379	0.0288	240	30	1:3	40mL/min, 0.25g catalyst + 0.25g SiC (9600 NL/ kg cat/h)	14.7	33	11	57	(157g/kg cat/h) (940g/kg copper/h)	225g DME/kg cat/h (1347 g/kg copper/h)
4	Cu–ZnO–ZrO <sub>2</sub> /HZSM-5[24] By physically mixing	1:1	16.5		1.01		220	30	1:3	36000NL/ kg cat/h 0.25g catalyst + 0.25g SiC	2.5	58	16	26		
							220	20	1:3	9000NL/ kg cat/h	7	40	18	42		
5	Cu–ZnO–ZrO <sub>2</sub> /Al-TUD-1 (physically mixing)	1:1	15.0				280	20	1:3	10000 h <sup>-1</sup> , 40ml/min (30000 NL/ kg cat/h)	11.3	5.3	11.7	83	119 g/kg cat/h (793 g/kg copper/h)	38.3 g/kg cat/h (255 g/kg copper/h)
6	Cu–ZnO–ZrO <sub>2</sub> /Al-TUD-1 co-precipitation deposition	1:1	15.0				280	20	1:3	10000 h <sup>-1</sup> , 40ml/min (30000 NL/ kg cat/h)	7.5	0.5	19.2	80.3	129 g/kg cat/h (860 g/kg copper/h )	2.5 g/kg cat/h (16.7 g/kg copper/h)
7	Cu–ZnO–ZrO <sub>2</sub> /Al-TUD-1 (co-precipitation deposition)	2.3:1	21	10.3			280	20	1:3	10000 h <sup>-1</sup> , 40ml/min (30000 NL/ kg cat/h)	10.0		20.3	79.6	177 g/kg cat/h (843 g/kg copper/h)	-
8	Cu–ZnO–ZrO <sub>2</sub> /Al-TUD-1 (core shell)	1:1	15.0				280	20	1:3	10000 h <sup>-1</sup> , 40ml/min (30000 NL/ kg cat/h)	2.3	3.9	22.4	73.7	21.5 g/kg cat/h (143 g/kg copper/h)	2.7 g/kg cat/h (18 g/kg copper/h)

### 5.4.2 Methanol dehydration to DME

The three bifunctional materials, **cs**, **pd** and **m**, were tested in methanol dehydration to DME reaction. Methanol conversion will be followed. H<sub>2</sub>, methyl formate, CO and CO<sub>2</sub> were found as the reaction products together with the main product DME. CH<sub>2</sub>O was not observed in outgases. The discussion will be based on the following the formation of DME, methyl formate and the mixture CO + CO<sub>2</sub>. H<sub>2</sub>O and H<sub>2</sub> were not detected by the GC column that was chosen.

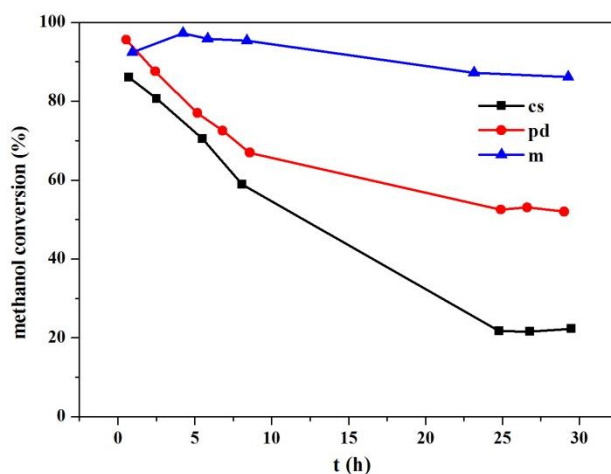


Figure 5- 11 Methanol conversion

The catalytic results of methanol conversion are presented in Figure 5- 11. The methanol conversion for catalyst **m** decreases slightly from 98% to 87% after 30h and the slope is not big. The catalyst seems to be rather stable. The methanol conversion of catalyst **pd** decreases from 97% to 52% after 30h. The methanol conversion of catalyst **cs** shows severe decrease from 87% to 22% after 30h.

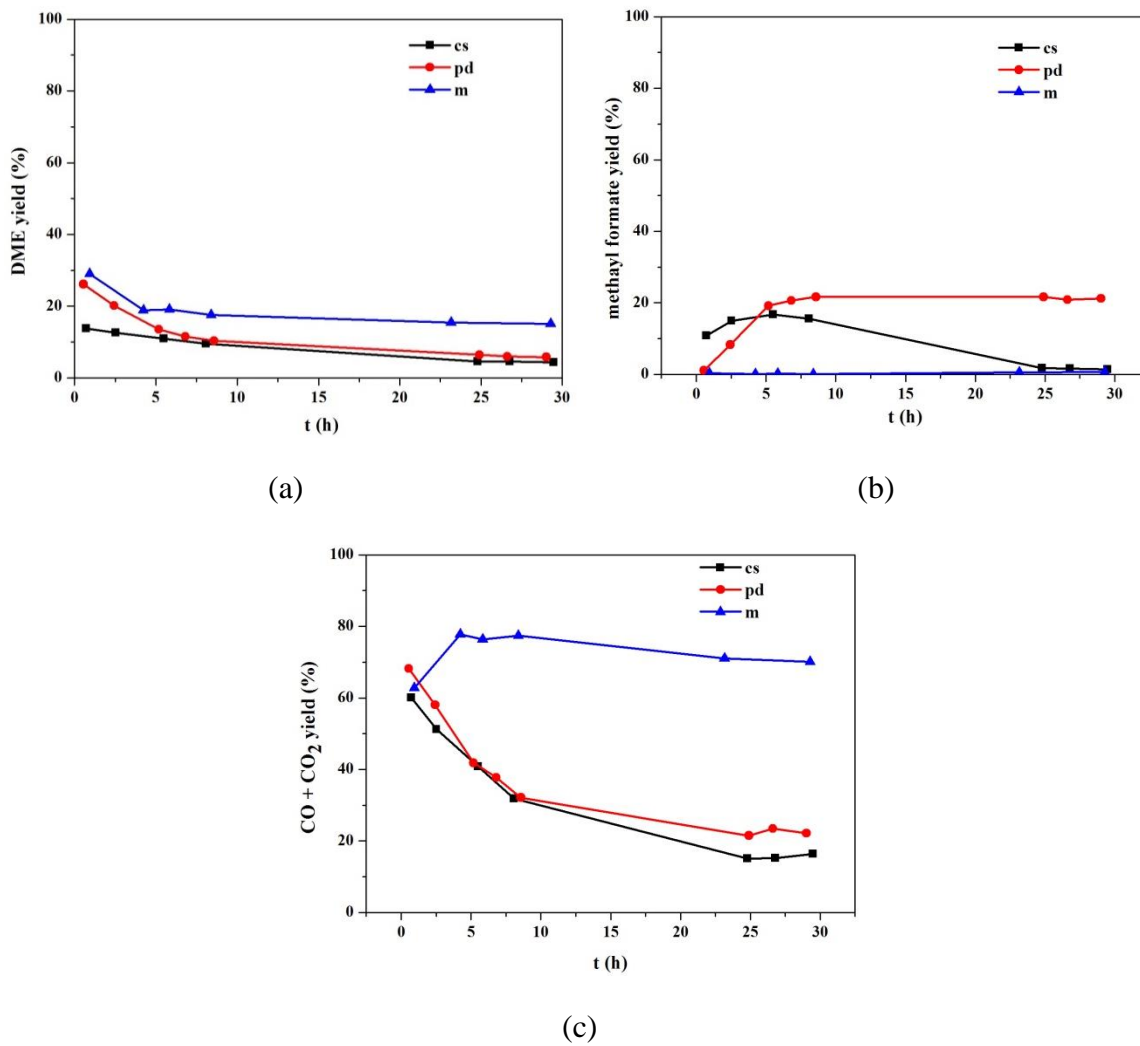


Figure 5- 12 DME yield (a), methyl formate yield (b) and CO + CO<sub>2</sub> yield (c) over the bifunctional catalysts **pd**, **m** and **cs**.

The C- containing products yield is presented in Figure 5- 12. The DME yield of catalysts **pd** and **m** was 26% and 30% at the beginning of the reaction and then decrease to 6% and 15% respectively after 30h. The DME yield of catalyst **cs** is lower than previous two at the beginning around 14% and then decrease to 4% after 30h of the reaction time. Apart from DME we found methyl formate and carbon oxides as by-products in this reaction.

The methyl formate yield of catalyst **pd** increases from around 1 to 21% and the CO + CO<sub>2</sub> mixture yield decreases from 68% to 22% after 30h. The methyl formate yield for catalyst **m** is around 0 during the reaction and the CO + CO<sub>2</sub> mixture yield is stable around 72%.

For catalyst **cs**, the methyl formate yield decreases from 11% at the beginning to almost 0% after 30h. The yields of CO + CO<sub>2</sub> mixture decreases and meets the curve of the **pd** catalyst.

The catalyst **cs** shows the lowest catalytic performance in methanol dehydration to DME reaction as well as in the direct DME synthesis reaction (5.4.1). It may be due to the insufficient access of reactants to the metallic copper embedded in the core of the core-shell structure which leads to the low methanol conversion. This phenomenon could be observed after 6h of the methanol dehydration to DME reaction when the catalyst **cs** stops producing methyl formate because of the blockage of its pores by reaction products. From the XRD patterns of the reduced catalyst **cs**, it can be found that the metallic copper particles aggregate and the ZnO particles become more dispersed after reduction (Figure 5- 3 and Figure 5- 4). It may be caused by the migration of ZnO to Al-TUD-1 (Si/Al-25) structure during the reduction. It has been reported that with the proceeding of methanol dehydrogenation reaction, the lattice oxygen of ZnO can be removed thus resulting in the reduction of zinc oxide, which is one of deactivation reasons for Cu/ZnO catalysts in methanol dehydrogenation reaction [25-27]. In our catalyst **cs**, the migrated ZnO was probably reduced with the proceeding of reaction and some O in ZnO disappears leading to the decrease of basic sites. Probably this catalyst's surface reconstruction (with possible ZnO reduction) continues during the first 6h of the reaction so methyl formate is still present. After 6h the yield of methyl formate starts to decrease so it can be supposed that methyl formate is not formed anymore and its decomposition occurs. The Al-TUD-1 (Si/Al-25) part is located in the shell of the catalyst, easily accessible for reactants, so the DME selectivity is almost stable during the reaction.

For the catalyst **pd**, with the proceeding of methanol dehydrogenation reaction, it can be supposed that some lattice oxygen of ZnO disappear resulting in the decrease of basic sites as it was observed for catalyst **cs**, this leads to the increase of methyl formate

yield with time. It has been demonstrated in chapter 4 that the acid sites are blocked by the copper based part for the bifunctional catalyst prepared by co-precipitation deposition method. The reduction of ZnO and the blockage of acid sites can explain the lower methanol conversion than for the catalyst **m**.

In the methanol dehydration to DME reaction, the methanol conversion over catalyst **cs** is the lowest after 30 h, which is consistent with the direct DME synthesis results with the lowest CO<sub>2</sub> conversion among the three catalysts and confirms the supposition that the insufficient access of the reactants and agglomeration of copper are the main reasons. For the catalyst **m**, the basic sites are attributed to the high CO + CO<sub>2</sub> selectivity, which is beneficial for the CO<sub>2</sub> adsorption thus resulting in the highest CO<sub>2</sub> conversion among the three catalysts in direct DME synthesis reaction. Additional acidity measurements by NH<sub>3</sub>-TPD are needed to be able to compare these three catalysts.

## 5.5 Conclusions and perspectives

In this chapter, two additional synthesis methods were employed for the catalyst composition CZZ-Si/Al-25 in order to overcome the problem of the blockage of the acid sites by copper based part in the bifunctional catalytic materials.

The core-shell method (**cs**) allowed placing the Al-TUD-1 part of the bifunctional catalyst outside the CZZ core thus hoping to get better accessibility of acid sites. During the synthesis of the catalyst **cs** the CZZ original structure has changed. After the reduction the agglomeration of copper was observed and the possible migration of Zn to the shell was supposed. The quantity of acid sites of the catalysts **pd**, **cs**, **m** are still under investigation, it will be compared with the pure CZZ catalyst that has ZrO<sub>2</sub> with acid-base character. The catalyst **pd** has more basic sites than the catalyst **cs**. Agglomerated copper in the core of the **cs** catalyst coupled with the insufficient access of reactants to the core of the catalyst leads to the low CO<sub>2</sub> conversion. Nevertheless the selectivity of methanol formation was much higher in the case of the catalyst **cs** than for the catalyst **pd**. The DME selectivity was observed higher for the catalysts **cs** than for the catalyst **pd**. That proves the concept of the core-shell synthesis and the improvement of acid sites accessibility for the methanol dehydration to DME was obtained.

Two prepared materials were compared to the catalyst prepared by physically mixing method (the catalyst **m**). The relatively independent existence of two catalytic functions in the catalyst **m** (the copper based part and the Al-TUD-1 (Si/Al-25) part) leads to the exposure of copper, basic sites and acid sites, devoting to the better H<sub>2</sub> and CO<sub>2</sub> conversion resulting in higher DME productivity than for other two catalysts, in the same time the catalyst **m** did not have an intimate contact between the two catalytic functions and thus was less selective in methanol than the catalyst **cs** and produced more CO at the same reaction temperatures.

It can be concluded that the catalyst **cs** might be a promising catalyst for the direct DME synthesis from CO<sub>2</sub>/ H<sub>2</sub> mixtures. Some optimization should be done, such as enhancing the reactants diffusion to the core by increasing the pores diameter in the shell; protecting the core structure by inducing a protecting inert layer which may be removed by simple calcination.

The compromise between the Al content and the synthesis method of the bifunctional catalytic materials should be found. Bringing more Al will result in the formation of strong acid sites and thus will switch the reaction to the olefins formation (side products in the direct DME synthesis).

The problem of water vapors production during the direct DME synthesis process could be solved by engineering, a membrane or micro/ nanoscale reactors.

## 5.6 References

- [1] K.S.W. Sing, D.H. Everett, R.A.W. Haul, L. Moscou, R.A. Pierotti, J. Rouquerol, T. Siemieniewska, Reporting Physisorption Data for Gas Solid Systems with Special Reference to the Determination of Surface-Area and Porosity (Recommendations 1984), *Pure Appl Chem*, 57 (1985) 603-619.
- [2] J.W. Bae, H.S. Potdar, S.H. Kang, K.W. Jun, Coproduction of methanol and dimethyl ether from biomass-derived syngas on a Cu-ZnO-Al<sub>2</sub>O<sub>3</sub>/  $\gamma$ -Al<sub>2</sub>O<sub>3</sub> hybrid catalyst, *Energy Fuel*, 22 (2008) 223-230.
- [3] G.H. Yang, M. Thongkam, T. Vitidsant, Y. Yoneyama, Y.S. Tan, N. Tsubaki, A double-shell capsule catalyst with core-shell-like structure for one-step exactly controlled synthesis of dimethyl ether from CO<sub>2</sub> containing syngas, *Catal Today*, 171 (2011) 229-235.
- [4] M.S. Hamdy, R. Amrollahi, I. Sinev, B. Mei, G. Mul, Strategies to Design Efficient Silica-Supported Photocatalysts for Reduction of CO<sub>2</sub>, *Journal of the American Chemical Society*, 136 (2014) 594-597.
- [5] F. Adam, T.S. Chew, J. Andas, A simple template-free sol-gel synthesis of spherical nanosilica from agricultural biomass, *J Sol-Gel Sci Techn*, 59 (2011) 580-583.
- [6] C. Baltes, S. Vukojevic, F. Schuth, Correlations between synthesis, precursor, and catalyst structure and activity of a large set of CuO/ZnO/Al<sub>2</sub>O<sub>3</sub> catalysts for methanol synthesis, *J Catal*, 258 (2008) 334-344.
- [7] K.F. Dong, H.H. Li, J.Y. Deng, Y.G. Peng, G. Ju, G.M. Chow, J.S. Chen, Crystalline ZrO<sub>2</sub> doping induced columnar structural FePt films with larger coercivity and high aspect ratio, *J Appl Phys*, 117 (2015).
- [8] S. Telalovic, U. Hanefeld, Noncovalent immobilization of chiral cyclopropanation catalysts on mesoporous TUD-1: Comparison of liquid-phase and gas-phase ion-exchange, *Appl Catal A-Gen*, 372 (2010) 217-223.
- [9] S. Telalovic, A. Ramanathan, G. Mul, U. Hanefeld, TUD-1: synthesis and application of a versatile catalyst, carrier, material ... *J Mater Chem*, 20 (2010) 642-658.

- [10] A. Ramanathan, D. Klomp, J.A. Peters, U. Hanefeld, Zr-TUD-1: A novel heterogeneous catalyst for the Meerwein-Ponndorf-Verley reaction, *J Mol Catal A-Chem*, 260 (2006) 62-69.
- [11] A. Ramanathan, M.C.C. Villalobos, C. Kwakernaak, S. Telalovic, U. Hanefeld, Zr-TUD-1: A lewis acidic, three-dimensional, mesoporous, zirconium-containing catalyst, *Chem-Eur J*, 14 (2008) 961-972.
- [12] G.H. Yang, N. Tsubaki, J. Shamoto, Y. Yoneyama, Y. Zhang, Confinement Effect and Synergistic Function of H-ZSM-5/ Cu-ZnO-Al<sub>2</sub>O<sub>3</sub> Capsule Catalyst for One-Step Controlled Synthesis, *Journal of the American Chemical Society*, 132 (2010) 8129-8136.
- [13] Z.P. Lu, D.Z. Gao, H.B. Yin, A.L. Wang, S.X. Liu, Methanol dehydrogenation to methyl formate catalyzed by SiO<sub>2</sub>-, hydroxyapatite-, and MgO-supported copper catalysts and reaction kinetics, *J Ind Eng Chem*, 31 (2015) 301-308.
- [14] P. Gao, F. Li, H.J. Zhan, N. Zhao, F.K. Xiao, W. Wei, L.S. Zhong, H. Wang, Y.H. Sun, Influence of Zr on the performance of Cu/Zn/Al/Zr catalysts via hydrotalcite-like precursors for CO<sub>2</sub> hydrogenation to methanol, *J Catal*, 298 (2013) 51-60.
- [15] G.D. Wu, X.L. Wang, W. Wei, Y.H. Sun, Fluorine-modified Mg-Al mixed oxides: A solid base with variable basic sites and tunable basicity, *Appl Catal A-Gen*, 377 (2010) 107-113.
- [16] Y.X. Liu, K.P. Sun, H.W. Ma, X.L. Xu, X.L. Wang, Cr, Zr-incorporated hydrotalcites and their application in the synthesis of isophorone, *Catal Commun*, 11 (2010) 880-883.
- [17] F. Arena, K. Barbera, G. Italiano, G. Bonura, L. Spadaro, F. Frusteri, Synthesis, characterization and activity pattern of Cu-ZnO/ZrO<sub>2</sub> catalysts in the hydrogenation of carbon dioxide to methanol, *J Catal*, 249 (2007) 185-194.
- [18] G. Bonura, M. Cordaro, L. Spadaro, C. Cannilla, F. Arena, F. Frusteri, Hybrid Cu-ZnO-ZrO<sub>2</sub>/ H-ZSM5 system for the direct synthesis of DME by CO<sub>2</sub> hydrogenation, *Appl Catal B-Environ*, 140 (2013) 16-24.
- [19] D.S. Mao, W.M. Yang, J.C. Xia, B. Zhang, Q.Y. Song, Q.L. Chen, Highly effective hybrid catalyst for the direct synthesis of dimethyl ether from syngas with magnesium oxide-modified HZSM-5 as a dehydration component, *J Catal*, 230 (2005) 140-149.

- [20] T. Witoon, T. Permsirivanich, N. Kanjanasontorn, C. Akkaraphataworn, A. Seubsai, K. Faungnawakij, C. Warakulwit, M. Chareonpanich, J. Limtrakul, Direct synthesis of dimethyl ether from CO<sub>2</sub> hydrogenation over Cu-ZnO-ZrO<sub>2</sub>/SO<sub>4</sub><sup>2-</sup>-ZrO<sub>2</sub> hybrid catalysts: effects of sulfur-to-zirconia ratios, *Catal Sci Technol*, 5 (2015) 2347-2357.
- [21] Y. Wang, W.L. Wang, Y.X. Chen, J.H. Ma, R.F. Li, Synthesis of dimethyl ether from syngas over core-shell structure catalyst CuO-ZnO-Al<sub>2</sub>O<sub>3</sub>@SiO<sub>2</sub>-Al<sub>2</sub>O<sub>3</sub>, *Chem Eng J*, 250 (2014) 248-256.
- [22] F. Frusteri, M. Cordaro, C. Cannilla, G. Bonura, Multifunctionality of Cu-ZnO-ZrO<sub>2</sub>/H-ZSM5 catalysts for the one-step CO<sub>2</sub>-to-DME hydrogenation reaction, *Appl Catal B-Environ*, 162 (2015) 57-65.
- [23] F. Frusteri, G. Bonura, C. Cannilla, G.D. Ferrante, A. Aloise, E. Catizzone, M. Migliori, G. Giordano, Stepwise tuning of metal-oxide and acid sites of CuZnZr-MFI hybrid catalysts for the direct DME synthesis by CO<sub>2</sub> hydrogenation, *Appl Catal B-Environ*, 176 (2015) 522-531.
- [24] G. Bonura, M. Cordaro, C. Cannilla, A. Mezzapica, L. Spadaro, F. Arena, F. Frusteri, Catalytic behaviour of a bifunctional system for the one step synthesis of DME by CO<sub>2</sub> hydrogenation, *Catal Today*, 228 (2014) 51-57.
- [23] K.D. Jung, O.S. Joo, Support effects of copper containing catalysts on methanol dehydrogenation, *B Korean Chem Soc*, 23 (2002) 1135-1138.
- [24] O.S. Joo, K.D. Jung, S.H. Han, S.J. Uhm, Synergistic Effects between Cu and ZnO in the Hydrogenation of Their Formates, *J Catal*, 157 (1995) 259-261.
- [25] K.D. Jung, O.S. Joo, S.H. Han, Structural change of Cu/ZnO by reduction of ZnO in Cu/ZnO with methanol, *Catal Lett*, 68 (2000) 49-54.



*Chapter 6: General conclusions and perspectives*





The main objective of the thesis was the development of bifunctional catalytic materials for the direct DME synthesis from  $\text{CO}_2/\text{H}_2$ . The bifunctional materials contain the copper based part for the methanol synthesis from  $\text{CO}_2/\text{H}_2$  and the acid part for catalyzing the methanol dehydration to DME. The  $\text{Cu}/\text{ZnO}/\text{ZrO}_2$  with the mass ratio of  $\text{CuO}:\text{ZnO}:\text{ZrO}_2 = 37.5:41:21.5$  (CZZ) was chosen as the copper based catalyst for the first step. It was combined with the mesoporous Al-TUD-1 material as the acid catalyst of the second step. The bifunctional materials were tested in the direct DME synthesis from  $\text{CO}_2/\text{H}_2$  under pressure. The influence of different factors on the direct DME synthesis was investigated.

In the beginning the pure Al-TUD-1 materials with different Si/Al ratios (25, 50, 75 and 100) were synthesized. They are sponge like mesoporous materials, with amorphous morphology, big surface area and narrow pore distribution. The amount of acid sites increases with the decrease of Si/Al ratio, following the trend  $\text{Si}/\text{Al}-25 > \text{Si}/\text{Al}-50 > \text{Si}/\text{Al}-75 > \text{Si}/\text{Al}-100$ . From the catalytic test of the second process step (methanol dehydration to DME), it can be concluded that the methanol conversion increases with the decrease of Si/Al ratio and the water existence shows the negative effect on methanol dehydration to DME performance. The best results were observed for Si/Al-25 which possesses higher Al content and thus higher acidity necessary for the methanol to DME reaction.

Secondly, the pure copper based catalyst was synthesized. Then the bifunctional catalytic materials containing both the copper based part CZZ and the acid part Al-TUD-1 (Si/Al) were prepared by co-precipitation deposition method and named CZZ-Si/Al. The bifunctional catalytic materials show bigger specific surface area than pure CZZ. They possess an amorphous morphology similar to the Al-TUD-1 structure. This method of synthesis allows a good copper dispersion over the Si/Al support with smaller metallic copper particles around 5 nm compared to the pure CZZ (around 11 nm). The copper surface area increases with the decrease of Si/Al ratio. The bifunctional catalyst CZZ-Si/Al-25 shows the biggest copper surface area ( $10.3 \text{ m}^2/\text{g}_{\text{cata}}$ ) among all the investigated bifunctional catalysts.

All the bifunctional catalytic materials with different Si/Al ratio were tested in the direct DME synthesis from  $\text{CO}_2/\text{H}_2$ . Low DME selectivity was observed, but nevertheless they were active in the methanol formation and the highest methanol productivity 180 g/ kg cata/ h at 280 °C was obtained for CZZ-Si/Al-25. These results indicate that the aluminum containing support helps the dispersion of metallic copper, more aluminum helps to get bigger metallic copper surface. In the same time the aluminum in the Al-TUD-1 loses the acid character when combined with the copper based catalyst. The density functional theory was employed to investigate the influence of Al. The adsorption energy of Cu on Al-doped  $\text{SiO}_2$  in the top site adsorption configuration (-2.6012 eV) is higher than the adsorption energy of Cu on the pure  $\text{SiO}_2$  (-0.2617 eV), which means that the incorporation of Al can induce copper anchoring sites and this implies that copper occupies the acid sites on the support.

The presence of water vapors that are produced during the direct DME synthesis process could be solved by engineering a membrane or micro/ nanoscale reactors. A possible membrane reactor for this process is presented on Figure 6- 1. In this work it was found that water presence declines slightly the conversion of methanol in the second step of the process (methanol dehydration to DME) but it could be beneficial for the suppressing the coke deposit.

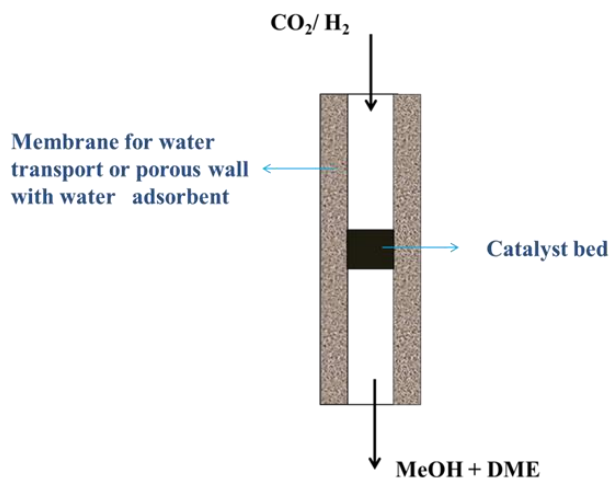


Figure 6- 1 Schematic diagram of a membrane reactor

Another possible way of the bifunctional catalyst optimization would be the increasing of the content of the Al-TUD-1 part but in this case the copper content will decrease and probably the catalytic activity of the samples in methanol formation from CO<sub>2</sub> hydrogenation will be lost.

Another method was employed to expose the acid sites of Al-TUD-1 part on the surface without their blockage by copper - the core-shell preparation method. It allowed placing the Al-TUD-1 part of the bi-functional catalyst outside the CZZ core. During the synthesis of the core-shell catalyst the CZZ original structure has changed. After the reduction the agglomeration of copper was observed and the possible migration of Zn to the shell was supposed. The quantity of acid sites of the catalysts prepared by the core-shell and the co-precipitation-deposition methods are still under investigation. The basicity of both catalysts was compared: core-shell catalyst has less basic sites. Agglomerated copper in the core of the core-shell catalyst coupled with the insufficient access of reactants to the core of the catalyst leads to the low CO<sub>2</sub> conversion. Nevertheless the selectivity of methanol and DME formation was much higher than in the case of the catalyst prepared by co-precipitation-deposition. That proves the concept of the core-shell synthesis as a way of the bifunctional catalyst optimization and the improvement of acid sites accessibility.

Two prepared materials were compared to the catalyst prepared by physically mixing method. The relatively independent existence of two catalytic functions in this catalyst (the copper based part and the Al-TUD-1 (Si/Al-25) part) leads to the exposure of copper, basic sites and acid sites, devoting to the better H<sub>2</sub> and CO<sub>2</sub> conversion resulting in higher DME productivity than for other two catalysts, in the same time the catalyst prepared by physically mixing did not have an intimate contact between the two catalytic functions and thus was less selective in methanol and produced more CO. In addition the investigation of the spent catalyst prepared by physically mixing shows the intensive growth of the metallic copper particles while the core-shell catalyst shows very stable metallic copper particles size.

It can be concluded that the core-shell catalyst might be a promising catalyst for the direct DME synthesis from CO<sub>2</sub>/H<sub>2</sub> mixtures. Some optimization should be done, such as enhancing the reactants diffusion to the CZZ core by increasing the pores diameter in the shell. Another improvement could be the protecting of the core structure by inducing an inert layer between the core and the shell which may be removed by simple calcination – in order to suppress the structural changes of CZZ core and the possible migration of its components to the shell.

# Qian JIANG

## Synthèse directe de diméthyl éther à partir de CO<sub>2</sub>/H<sub>2</sub>

### Résumé

DME est un carburant propre qui contribue à diminuer les émissions de gaz à effet de serre; il est aussi une molécule plate-forme pour le stockage d'énergie. L'objectif de la thèse est le développement de matériaux catalytiques bifonctionnels pour la synthèse directe de DME à partir de CO<sub>2</sub>/H<sub>2</sub> à partir de Cu/ZnO/ZrO<sub>2</sub> comme le catalyseur de la synthèse de méthanol à partir de CO<sub>2</sub>/H<sub>2</sub> et Al-TUD-1 comme le catalyseur de déshydratation du méthanol en DME. Dans cette thèse, Al-TUD-1 a été étudiée comme un catalyseur de la déshydratation du méthanol en DME pour la première fois. Son activité en déshydratation du méthanol en DME augmente avec la diminution du rapport Si/Al. Les catalyseurs bifonctionnels ont été préparés par un procédé de dépôt par co-précipitation. Le SMSI a été démontré et était bénéfique pour la dispersion de cuivre métallique, la surface de cuivre métallique augmente avec le rapport Si/Al. Dans le même temps, on a observé le blocage des sites acides d'Al-TUD-1 par le cuivre. Afin d'exposer les sites acides d'Al-TUD-1, la méthode de « core-shell » a été adoptée pour préparer le catalyseur bifonctionnel. Elle aide à libérer la fonction acide en empêchant son blocage par le cuivre. Cette méthode de synthèse a été bénéfique pour la stabilité des particules de cuivre métalliques, mais des faibles conversions de CO<sub>2</sub>/H<sub>2</sub> ont été observées en raison de l'inaccessibilité du noyau. Un autre catalyseur bifonctionnel a été préparé par une méthode de mélange physique pour comparaison. L'optimisation du catalyseur bifonctionnel Cu/ZnO/ZrO<sub>2</sub>@Al-TUD-1 pour la synthèse directe de DME à partir de CO<sub>2</sub>/H<sub>2</sub> a permis d'éclairer les principaux paramètres affectant le contact intime de deux fonctions catalytiques: surface et dispersion du cuivre, les propriétés acide et basique, la présence d'eau et l'accessibilité des sites actifs pour les réactifs.

Mots-clés: DME, hydrogénation du CO<sub>2</sub>, déshydratation du méthanol, Al-TUD-1

### Résumé en anglais

DME is a clean fuel that helps to diminish the emissions of green house gases; it is as well a platform molecule for the energy storage. The objective of the thesis is the development of bifunctional catalytic materials for the direct DME synthesis from CO<sub>2</sub>/H<sub>2</sub> based on Cu/ZnO/ZrO<sub>2</sub> as the methanol synthesis from CO<sub>2</sub>/H<sub>2</sub> catalyst and Al-TUD-1 as the methanol dehydration to DME catalyst. In this thesis, Al-TUD-1 was investigated as the methanol dehydration to DME catalyst for the first time. The methanol dehydration to DME performance increases with the decrease of Si/Al ratio. The bifunctional catalysts were prepared by co-precipitation deposition method. The SMSI was demonstrated and was beneficial for the metallic copper dispersion, the metallic copper surface area increases with the Si/Al ratio. In the same time the blockage of acid sites of Al-TUD-1 by copper was observed. In order to expose the acid sites of Al-TUD-1, the core shell method was adopted to prepare the bifunctional catalyst. It helps to free the acid function preventing its blockage by copper. This method of synthesis was beneficial for the stability of metallic copper particles, but performed low conversions of CO<sub>2</sub>/H<sub>2</sub> due to the inaccessibility of the core. Another bifunctional catalyst was prepared by physically mixing method for comparison. The optimization of the bifunctional Cu/ZnO/ZrO<sub>2</sub>@Al-TUD-1 catalyst for the direct DME synthesis from CO<sub>2</sub>/H<sub>2</sub> allowed enlightening the main parameters that affect the intimate contact of two catalytic functions: copper surface area and dispersion, acid and basic properties, water presence and the accessibility of the active sites for the reactants.

Keywords : DME, CO<sub>2</sub> hydrogenation, methanol dehydration, Al-TUD-1